Chaos: Classical and Quantum

Part II: Semiclassical Chaos

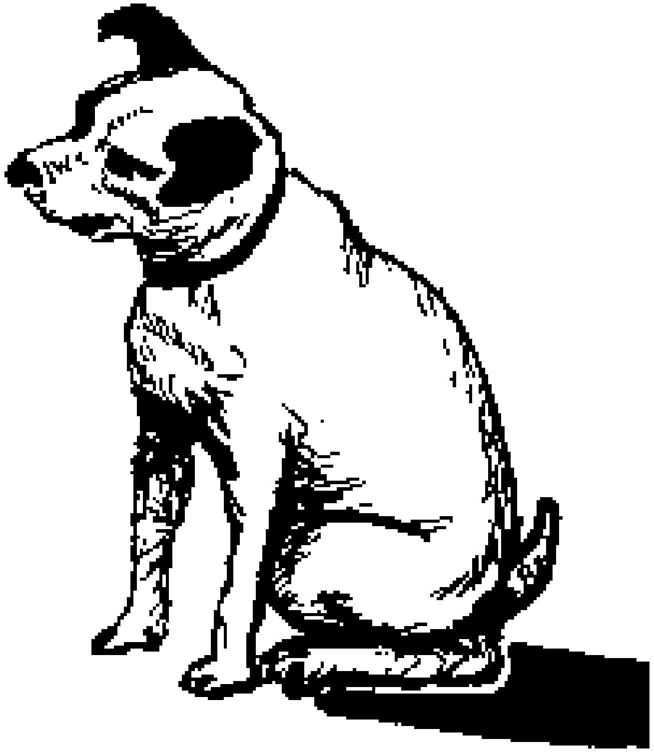

Predrag Cvitanović – Roberto Artuso – Per Dahlqvist – Ronnie Mainieri – Gregor Tanner – Gábor Vattay – Niall Whelan – Andreas Wirzba

ChaosBook.org version11.9.6, May 27 2008 printed June 22, 2008
ChaosBook.org comments to: predrag@nbi.dk

Chapter 28

Prologue

> Anyone who uses words "quantum" and "chaos" in the same sentence should be hung by his thumbs on a tree in the park behind the Niels Bohr Institute.
> —Joseph Ford

(G. Vattay, G. Tanner and P. Cvitanović)

You have read the first volume of this book. So far, so good – anyone can play a game of classical pinball, and a skilled neuroscientist can poke rat brains. We learned that information about chaotic dynamics can be obtained by calculating spectra of linear operators such as the evolution operator of sect. 15.2 or the associated partial differential equations such as the Liouville equation (14.37). The spectra of these operators can be expressed in terms of periodic orbits of the deterministic dynamics by means of trace formulas and cycle expansions.

But what happens quantum mechanically, i.e., if we scatter waves rather than point-like pinballs? Can we turn the problem round and study linear PDE's in terms of the underlying deterministic dynamics? And, is there a link between structures in the spectrum or the eigenfunctions of a PDE and the dynamical properties of the underlying classical flow? The answer is yes, but ... things are becoming somewhat more complicated when studying 2nd or higher order linear PDE's. We can find classical dynamics associated with a linear PDE, just take geometric optics as a familiar example. Propagation of light follows a second order wave equation but may in certain limits be well described in terms of geometric rays. A theory in terms of properties of the classical dynamics alone, referred to here as the *semiclassical theory*, will not be exact, in contrast to the classical periodic orbit formulas obtained so far. Waves exhibit new phenomena, such as interference, diffraction, and higher $\hbar$ corrections which will only be partially incorporated into the periodic orbit theory.

☞ chapter 36

28.1 Quantum pinball

chapter 31

In what follows, we will restrict the discussion to the non-relativistic Schrödinger equation. The approach will be very much in the spirit of the early days of quantum mechanics, before its wave character has been fully uncovered by Schrödinger in the mid 1920's. Indeed, were physicists of the period as familiar with classical chaos as we are today, this theory could have been developed 80 years ago. It was the discrete nature of the hydrogen spectrum which inspired the Bohr - de Broglie picture of the old quantum theory: one places a wave instead of a particle on a Keplerian orbit around the hydrogen nucleus. The quantization condition is that only those orbits contribute for which this wave is stationary; from this followed the Balmer spectrum and the Bohr-Sommerfeld quantization which eventually led to the more sophisticated theory of Heisenberg, Schrödinger and others. Today we are very aware of the fact that elliptic orbits are an idiosyncracy of the Kepler problem, and that chaos is the rule; so can the Bohr quantization be generalized to chaotic systems?

The question was answered affirmatively by M. Gutzwiller, as late as 1971: a chaotic system can indeed be quantized by placing a wave on each of the *infinity* of unstable periodic orbits. Due to the instability of the orbits the wave does not stay localized but leaks into neighborhoods of other periodic orbits. Contributions of different periodic orbits interfere and the quantization condition can no longer be attributed to a single periodic orbit: A coherent summation over the infinity of periodic orbit contributions gives the desired spectrum.

☞ chapter 17

The pleasant surprise is that the zeros of the dynamical zeta function (1.9) derived in the context of classical chaotic dynamics,

$$1/\zeta(z) = \prod_p (1 - t_p)\,,$$

also yield excellent estimates of *quantum* resonances, with the quantum amplitude associated with a given cycle approximated semiclassically by the weight

$$t_p = \frac{1}{|\Lambda_p|^{\frac{1}{2}}} e^{\frac{i}{\hbar}S_p - i\pi m_p/2}\,, \qquad (28.1)$$

whose magnitude is the square root of the classical weight (17.10)

$$t_p = \frac{1}{|\Lambda_p|} e^{\beta\cdot A_p - sT_p}\,,$$

and the phase is given by the Bohr-Sommerfeld action integral S_p, together with an additional topological phase m_p, the number of caustics along the periodic trajectory, points where the naive semiclassical approximation fails.

In this approach, the quantal spectra of classically chaotic dynamical systems are determined from the zeros of dynamical zeta functions, defined by cycle expansions of infinite products of form

$$1/\zeta = \prod_p (1 - t_p) = 1 - \sum_f t_f - \sum_k c_k \qquad (28.2)$$

with weight t_p associated to every prime (non-repeating) periodic orbit (or *cycle*) p.

The key observation is that the chaotic dynamics is often organized around a few *fundamental* cycles. These short cycles capture the skeletal topology of the motion in the sense that any long orbit can approximately be pieced together from the fundamental cycles. In chapter 18 it was shown that for this reason the cycle expansion (28.2) is a highly convergent expansion dominated by short cycles grouped into *fundamental* contributions, with longer cycles contributing rapidly decreasing *curvature* corrections. Computations with dynamical zeta functions are rather straightforward; typically one determines lengths and stabilities of a finite number of shortest periodic orbits, substitutes them into (28.2), and estimates the zeros of $1/\zeta$ from such polynomial approximations.

From the vantage point of the dynamical systems theory, the trace formulas (both the exact Selberg and the semiclassical Gutzwiller trace formula) fit into a general framework of replacing phase space averages by sums over periodic orbits. For classical hyperbolic systems this is possible since the invariant density can be represented by sum over all periodic orbits, with weights related to their instability. The semiclassical periodic orbit sums differ from the classical ones only in phase factors and stability weights; such differences may be traced back to the fact that in quantum mechanics the amplitudes rather than the probabilities are added.

☞ chapter 32

The type of dynamics has a strong influence on the convergence of cycle expansions and the properties of quantal spectra; this necessitates development of different approaches for different types of dynamical behavior such as, on one hand, the strongly hyperbolic and, on the other hand, the intermittent dynamics of chapters 18 and 22. For generic nonhyperbolic systems (which we shall not discuss here), with mixed phase space and marginally stable orbits, periodic orbit summations are hard to control, and it is still not clear that the periodic orbit sums should necessarily be the computational method of choice.

Where is all this taking us? The goal of this part of the book is to demonstrate that the cycle expansions, developed so far in classical settings, are also a powerful tool for evaluation of *quantum* resonances of classically chaotic systems.

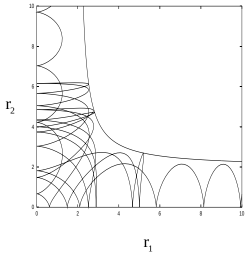

Figure 28.1: A typical collinear helium trajectory in the $r_1 - r_2$ plane; the trajectory enters along the r_1 axis and escapes to infinity along the r_2 axis.

First, we shall warm up playing our game of pinball, this time in a quantum version. Were the game of pinball a closed system, quantum mechanically one would determine its stationary eigenfunctions and eigenenergies. For open systems one seeks instead complex resonances, where the imaginary part of the eigenenergy describes the rate at which the quantum wave function leaks out of the central scattering region. This will turn out to work well, except who truly wants to know accurately the resonances of a quantum pinball?

☞ chapter 33

28.2 Quantization of helium

Once we have derived the semiclassical weight associated with the periodic orbit p (28.1), we will finally be in position to accomplish something altogether remarkable. We are now able to put together all ingredients that make the game of pinball unpredictable, and compute a “chaotic” part of the helium spectrum to shocking accuracy. From the classical dynamics point of view, helium is an example of Poincaré’s dreaded and intractable 3-body problem. Undaunted, we forge ahead and consider the *collinear* helium, with zero total angular momentum, and the two electrons on the opposite sides of the nucleus.

☞ chapter 35

We set the electron mass to 1, the nucleus mass to ∞, the helium nucleus charge to 2, the electron charges to -1. The Hamiltonian is

$$H = \frac{1}{2}p_1^2 + \frac{1}{2}p_2^2 - \frac{2}{r_1} - \frac{2}{r_2} + \frac{1}{r_1 + r_2}\,. \tag{28.3}$$

Due to the energy conservation, only three of the phase space coordinates (r_1, r_2, p_1, p_2) are independent. The dynamics can be visualized as a motion in the (r_1, r_2), $r_i \geq 0$ quadrant, figure 28.1, or, better still, by a well chosen 2-dimensional Poincaré section.

The motion in the (r_1, r_2) plane is topologically similar to the pinball motion in a 3-disk system, except that the motion is not free, but in the Coulomb potential. The classical collinear helium is also a repeller; almost all of the classical trajectories escape. Miraculously, the symbolic dynamics for the survivors turns out to be binary, just as in the 3-disk game of pinball, so we know what cycles need to be computed for the cycle expansion (1.10). A set of shortest cycles up to a given symbol string length then yields an estimate of the helium spectrum. This simple calculation yields surprisingly accurate eigenvalues; even though the cycle expansion was based on the *semiclassical approximation* (28.1) which is expected to be good only in the classical large energy limit, the eigenenergies are good to 1% all the way down to the ground state.

☞ chapter 35

Before we can get to this point, we first have to recapitulate some basic notions of quantum mechanics; after having defined the main quantum objects of interest, the quantum propagator and the Green’s function, we will relate the quantum propagation to the classical flow of the underlying dynamical system. We will then proceed to construct semiclassical approximations to the quantum propagator and the Green’s function. A rederivation of classical Hamiltonian dynamics starting from the Hamilton-Jacobi equation will be offered along the way. The derivation of the Gutzwiller trace formula and the semiclassical zeta function as a sum and as a product over periodic orbits will be given in chapter 32. In subsequent chapters we buttress our case by applying and extending the theory: a cycle expansion calculation of scattering resonances in a 3-disk billiard in chapter 33, the spectrum of helium in chapter 35, and the incorporation of diffraction effects in chapter 36.

Guide to literature

A key prerequisite to developing any theory of “quantum chaos” is solid understanding of Hamiltonian mechanics. For that, Arnol’d monograph [1.35] is the essential reference. Ozorio de Almeida’s monograph [7.11] offers a compact introduction to the aspects of Hamiltonian dynamics required for the quantization of integrable and nearly integrable systems, with emphasis on periodic orbits, normal forms, catastrophy theory and torus quantization. The book by Brack and Bhaduri [28.1] is an excellent introduction to the semiclassical methods. Gutzwiller’s monograph [28.2] is an advanced introduction focusing on chaotic dynamics both in classical Hamiltonian settings and in the semiclassical quantization. This book is worth browsing through for its many insights and erudite comments on quantum and celestial mechanics even if one is not working on problems of quantum chaos. More suitable as a graduate course text is Reichl’s exposition [28.3].

This book does not discuss the random matrix theory approach to chaos in quantal spectra; no randomness assumptions are made here, rather the goal is to milk the deterministic chaotic dynamics for its full worth. The book concentrates on the periodic orbit theory. For an introduction to "quantum chaos" that focuses on the random matrix theory the reader is referred to the excellent monograph by Haake [28.4], among others.

References

[28.1] M. Brack and R.K. Bhaduri, *Semiclassical Physics* (Addison-Wesley, New York 1997).

[28.2] M.C. Gutzwiller, *Chaos in Classical and Quantum Mechanics* (Springer, New York 1990).

[28.3] L.E. Reichl, *The Transition to Chaos in Conservative Classical Systems: Quantum Manifestations* (Springer-Verlag, New York 1992).

[28.4] F. Haake, *Quantum Signatures of Chaos*, 2. edition (Springer-Verlag, New York 2001).

Chapter 29

Quantum mechanics, briefly

We start with a review of standard quantum mechanical concepts prerequisite to the derivation of the semiclassical trace formula.

In coordinate representation the time evolution of a quantum mechanical wave function is governed by the Schrödinger equation

$$i\hbar\frac{\partial}{\partial t}\psi(q,t) = \hat{H}(q,\frac{\hbar}{i}\frac{\partial}{\partial q})\psi(q,t), \tag{29.1}$$

where the Hamilton operator $\hat{H}(q,-i\hbar\partial_q)$ is obtained from the classical Hamiltonian by substitution $p \to -i\hbar\partial_q$. Most of the Hamiltonians we shall consider here are of form

$$H(q,p) = T(p) + V(q)\,, \qquad T(p) = p^2/2m\,, \tag{29.2}$$

describing dynamics of a particle in a D-dimensional potential $V(q)$. For time independent Hamiltonians we are interested in finding stationary solutions of the Schrödinger equation of the form

$$\psi_n(q,t) = e^{-iE_nt/\hbar}\phi_n(q), \tag{29.3}$$

where E_n are the eigenenergies of the time-independent Schrödinger equation

$$\hat{H}\phi(q) = E\phi(q)\,. \tag{29.4}$$

If the kinetic term can be separated out as in (29.2), the time-independent Schrödinger equation

$$-\frac{\hbar^2}{2m}\partial^2\phi(q) + V(q)\phi(q) = E\phi(q) \tag{29.5}$$

can be rewritten in terms of a local wavenumber

$$(\partial^2 + k^2(q))\phi = 0\,, \qquad \hbar^2 k(q) = \sqrt{2m(E - V(q))}\,. \tag{29.6}$$

For bound systems the spectrum is discrete and the eigenfunctions form an orthonormal,

$$\int dq\, \phi_n(q)\phi_m^*(q) = \delta_{nm}\,, \tag{29.7}$$

and complete,

$$\sum_n \phi_n(q)\phi_n^*(q') = \delta(q - q')\,, \tag{29.8}$$

set of functions in a Hilbert space. Here and throughout the text,

$$\int dq = \int dq_1 dq_2 ... dq_D. \tag{29.9}$$

☞ chapter 33

For simplicity we will assume that the system is bound, although most of the results will be applicable to open systems, where one has complex resonances instead of real energies, and the spectrum has continuous components.

A given wave function can be expanded in the energy eigenbasis

$$\psi(q, t) = \sum_n c_n e^{-iE_n t/\hbar}\phi_n(q)\,, \tag{29.10}$$

where the expansion coefficient c_n is given by the projection of the initial wave function $\psi(q, 0)$ onto the nth eigenstate

$$c_n = \int dq\, \phi_n^*(q)\psi(q, 0). \tag{29.11}$$

By substituting (29.11) into (29.10), we can cast the evolution of a wave function into a multiplicative form

$$\psi(q, t) = \int dq' K(q, q', t)\psi(q', 0)\,,$$

with the kernel

$$K(q, q', t) = \sum_n \phi_n(q)\, e^{-iE_n t/\hbar}\phi_n^*(q') \tag{29.12}$$

called the quantum evolution operator, or the *propagator*. Applied twice, first for time t_1 and then for time t_2, it propagates the initial wave function from q' to q'', and then from q'' to q

$$K(q, q', t_1 + t_2) = \int dq''\, K(q, q'', t_2)K(q'', q', t_1) \tag{29.13}$$

forward in time, hence the name "propagator". In non-relativistic quantum mechanics the range of q'' is infinite, meaning that the wave can propagate at any speed; in relativistic quantum mechanics this is rectified by restricting the propagation to the forward light cone.

Since the propagator is a linear combination of the eigenfunctions of the Schrödinger equation, it also satisfies the Schrödinger equation

$$i\hbar\frac{\partial}{\partial t}K(q, q', t) = \hat{H}(q, \frac{i}{\hbar}\frac{\partial}{\partial q})K(q, q', t)\,, \tag{29.14}$$

and is thus a wave function defined for $t \geq 0$; from the completeness relation (29.8) we obtain the boundary condition at $t = 0$:

$$\lim_{t\to 0_+} K(q, q', t) = \delta(q - q')\,. \tag{29.15}$$

The propagator thus represents the time evolution of a wave packet which starts out as a configuration space delta-function localized in the point q' at the initial time $t = 0$.

For time independent Hamiltonians the time dependence of the wave functions is known as soon as the eigenenergies E_n and eigenfunctions ϕ_n have been determined. With time dependence rendered "trivial", it makes sense to focus on the *Green's function*, the Laplace transformation of the propagator

$$G(q, q', E+i\epsilon) = \frac{1}{i\hbar}\int_0^\infty dt\, e^{\frac{i}{\hbar}Et - \frac{\epsilon}{\hbar}t}K(q, q', t) = \sum_n \frac{\phi_n(q)\phi_n^*(q')}{E - E_n + i\epsilon}\,. \tag{29.16}$$

Here ϵ is a small positive number, ensuring the existence of the integral. The eigenenergies show up as poles in the Green's function with residues corresponding to the wave function amplitudes. If one is only interested in the spectrum, one may restrict the considerations to the (formal) trace of the Green's function,

$$\mathrm{tr}\, G(q, q', E) = \int dq\, G(q, q, E) = \sum_n \frac{1}{E - E_n}\,, \tag{29.17}$$

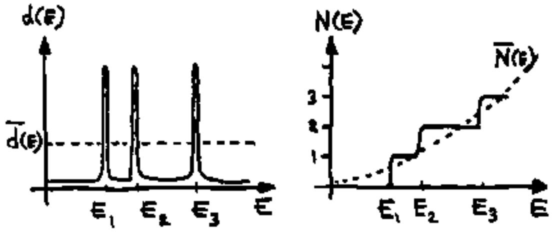

Figure 29.1: Schematic picture of **a)** the density of states $d(E)$, and **b)** the spectral staircase function $N(E)$. The dashed lines denote the mean density of states $\bar{d}(E)$ and the average number of states $\bar{N}(E)$ discussed in more detail in sect. 32.1.1.

where E is complex, with a positive imaginary part, and we have used the eigenfunction orthonormality (29.7). This trace is formal, since as it stands, the sum in (29.17) is often divergent. We shall return to this point in sects. 32.1.1 and 32.1.2.

A useful characterization of the set of eigenvalues is given in terms of the *density of states*, with a delta function peak at each eigenenergy, figure 29.1 (a),

$$d(E) = \sum_n \delta(E - E_n). \tag{29.18}$$

29.1
page 552

Using the identity

$$\delta(E - E_n) = -\lim_{\epsilon\to+0} \frac{1}{\pi} \mathrm{Im} \frac{1}{\mathrm{E} - \mathrm{E_n} + \mathrm{i}\epsilon} \tag{29.19}$$

we can express the density of states in terms of the trace of the Green's function, that is

$$d(E) = \sum_n \delta(E - E_n) = -\lim_{\epsilon\to 0} \frac{1}{\pi} \mathrm{Im\,tr\,G(q, q', E + i\epsilon)}. \tag{29.20}$$

sect. 32.1.1

As we shall see after "some" work, a semiclassical formula for right hand side of this relation will yield the quantum spectrum in terms of periodic orbits.

The density of states can be written as the derivative $d(E) = \mathrm{d}N(E)/\mathrm{d}E$ of the *spectral staircase* function

$$N(E) = \sum_n \Theta(E - E_n) \tag{29.21}$$

which counts the number of eigenenergies below E, figure 29.1 (b). Here Θ is the Heaviside function

$$\Theta(x) = 1 \quad \text{if } x > 0; \quad \Theta(x) = 0 \quad \text{if } x < 0\,. \tag{29.22}$$

The spectral staircase is a useful quantity in many contexts, both experimental and theoretical. This completes our lightning review of quantum mechanics.

Exercises

Exercise 29.1 **Dirac delta function, Lorentzian representation.** *Derive the representation (29.19)*

$$\delta(E - E_n) = -\lim_{\epsilon\to+0}\frac{1}{\pi}\mathrm{Im}\frac{1}{\mathrm{E}-\mathrm{E_n}+\mathrm{i}\epsilon}$$

of a delta function as imaginary part of $1/x$.

(Hint: read up on principal parts, positive and negative frequency part of the delta function, the Cauchy theorem in a good quantum mechanics textbook).

Exercise 29.2 **Green's function.** *Verify Green's function Laplace transform (29.16),*

$$\begin{aligned} G(q,q',E+i\varepsilon) &= \frac{1}{i\hbar}\int_0^\infty dt\, e^{\frac{i}{\hbar}Et-\frac{\varepsilon}{\hbar}t}K(q,q',t) \\ &= \sum\frac{\phi_n(q)\phi_n^*(q')}{E-E_n+i\varepsilon} \end{aligned}$$

argue that positive ϵ *is needed (hint: read a good quantum mechanics textbook).*

Chapter 30

WKB quantization

The wave function for a particle of energy E moving in a constant potential V is

$$\psi = Ae^{\frac{i}{\hbar}pq} \tag{30.1}$$

with a constant amplitude A, and constant wavelength $\lambda = 2\pi/k$, $k = p/\hbar$, and $p = \pm\sqrt{2m(E-V)}$ is the momentum. Here we generalize this solution to the case where the potential varies slowly over many wavelengths. This semiclassical (or WKB) approximate solution of the Schrödinger equation fails at classical turning points, configuration space points where the particle momentum vanishes. In such neighborhoods, where the semiclassical approximation fails, one needs to solve locally the exact quantum problem, in order to compute connection coefficients which patch up semiclassical segments into an approximate global wave function.

Two lessons follow. First, semiclassical methods can be very powerful - classical mechanics computations yield suprisingly accurate estimates of quantal spectra, without solving the Schrödinger equation. Second, semiclassical quantization does depend on a purely wave-mechanical phenomena, the coherent addition of phases accrued by all fixed energy phase space trajectories that connect pairs of coordinate points, and the topological phase loss at every turning point, a topological property of the classical flow that plays no role in classical mechanics.

30.1 WKB ansatz

Consider a time-independent Schrödinger equation in 1 spatial dimension:

$$-\frac{\hbar^2}{2m}\psi''(q) + V(q)\psi(q) = E\psi(q)\,, \tag{30.2}$$

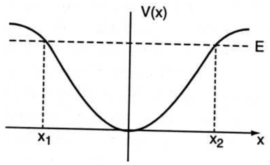

Figure 30.1: A 1-dimensional potential, location of the two turning points at fixed energy E.

with potential $V(q)$ growing sufficiently fast as $q \to \pm\infty$ so that the classical particle motion is confined for any E. Define the local momentum $p(q)$ and the local wavenumber $k(q)$ by

$$p(q) = \pm\sqrt{2m(E - V(q))}, \quad p(q) = \hbar k(q)\,. \tag{30.3}$$

The variable wavenumber form of the Schrödinger equation

$$\psi'' + k^2(q)\psi = 0 \tag{30.4}$$

sugests that the wave function be written as $\psi = Ae^{\frac{i}{\hbar}S}$, A and S real functions of q. Substitution yields two equations, one for the real and other for the imaginary part:

$$(S')^2 = p^2 + \hbar^2 \frac{A''}{A} \tag{30.5}$$

$$S''A + 2S'A' = \frac{1}{A}\frac{d}{dq}(S'A^2) = 0\,. \tag{30.6}$$

The Wentzel-Kramers-Brillouin *(WKB)* or *semiclassical* approximation consists of dropping the $\hbar^2$ term in (30.5). Recalling that $p = \hbar k$, this amounts to assuming that $k^2 \gg \frac{A''}{A}$, which in turn implies that the phase of the wave function is changing much faster than its overall amplitude. So the WKB approximation can interpreted either as a short wavelength/high frequency approximation to a wave-mechanical problem, or as the semiclassical, $\hbar \ll 1$ approximation to quantum mechanics.

Setting $\hbar = 0$ and integrating (30.5) we obtain the phase increment of a wave function initially at q, at energy E

$$S(q, q', E) = \int_{q'}^{q} dq'' p(q'')\,. \tag{30.7}$$

This integral over a particle trajectory of constant energy, called the *action*, will play a key role in all that follows. The integration of (30.6) is even easier

$$A(q) = \frac{C}{|p(q)|^{\frac{1}{2}}}, \qquad C = |p(q')|^{\frac{1}{2}}\psi(q')\,, \tag{30.8}$$

where the integration constant C is fixed by the value of the wave function at the initial point q'. The *WKB* (or *semiclassical*) *ansatz* wave function is given by

$$\psi_{sc}(q, q', E) = \frac{C}{|p(q)|^{\frac{1}{2}}} e^{\frac{i}{\hbar}S(q,q',E)}\,. \tag{30.9}$$

In what follows we shall supress dependence on the initial point and energy in such formulas, $(q, q', E) \to (q)$.

The WKB ansatz generalizes the free motion wave function (30.1), with the probability density $|A(q)|^2$ for finding a particle at q now inversely proportional to the velocity at that point, and the phase $\frac{1}{\hbar}q\,p$ replaced by $\frac{1}{\hbar}\int dq\,p(q)$, the integrated action along the trajectory. This is fine, except at any turning point q_0, figure 30.1, where all energy is potential, and

$$p(q) \to 0 \quad \text{as} \quad q \to q_0\,, \tag{30.10}$$

so that the assumption that $k^2 \gg \frac{A''}{A}$ fails. What can one do in this case?

For the task at hand, a simple physical picture, due to Maslov, does the job. In the q coordinate, the turning points are defined by the zero kinetic energy condition (see figure 30.1), and the motion appears singular. This is not so in the full phase space: the trajectory in a smooth confining 1-dimensional potential is always a smooth loop, with the "special" role of the turning points q_L, q_R seen to be an artifact of a particular choice of the (q, p) coordinate frame. Maslov's idea was to proceed from the initial point (q', p') to a point (q_A, p_A) preceeding the turning point in the $\psi(q)$ representation, then switch to the momentum representation

$$\widetilde{\psi}(p) = \frac{1}{\sqrt{2\pi\hbar}} \int dq\, e^{-\frac{i}{\hbar}qp}\psi(q)\,, \tag{30.11}$$

continue from (q_A, p_A) to (q_B, p_B), switch back to the coordinate representation,

$$\psi(q) = \frac{1}{\sqrt{2\pi\hbar}} \int dp\, e^{\frac{i}{\hbar}qp}\,\widetilde{\psi}(p)\,, \tag{30.12}$$

and so on.

The only rub is that one usually cannot evaluate these transforms exactly. But, as the WKB wave function (30.9) is approximate anyway, it suffices to estimate these transforms to leading order in $\hbar$ accuracy. This is accomplished by the method of stationary phase.

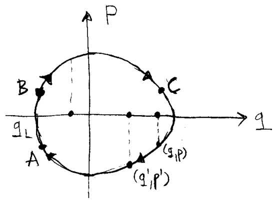

Figure 30.2: A 1-dof phase space trajectory of a particle moving in a bound potential.

30.2 Method of stationary phase

All "semiclassical" approximations are based on saddlepoint evaluations of integrals of the type

$$I = \int dx\, A(x)\, e^{is\Phi(x)}\,, \qquad x, \Phi(x) \in \mathbb{R}\,, \tag{30.13}$$

where s is assumed to be a large, real parameter, and $\Phi(x)$ is a real-valued function. In our applications $s = 1/\hbar$ will always be assumed large.

For large s, the phase oscillates rapidly and "averages to zero" everywhere except at the *extremal points* $\Phi'(x_0) = 0$. The method of approximating an integral by its values at extremal points is called the *method of stationary phase*. Consider first the case of a 1-dimensional integral, and expand $\Phi(x_0 + \delta x)$ around x_0 to second order in δx,

$$I = \int dx\, A(x)\, e^{is(\Phi(x_0)+\frac{1}{2}\Phi''(x_0)\delta x^2+\dots)}\,. \tag{30.14}$$

Assume (for time being) that $\Phi''(x_0) \neq 0$, with either sign, $\mathrm{sgn}[\Phi''] = \Phi''/|\Phi''| = \pm 1$. If in the neighborhood of x_0 the amplitude $A(x)$ varies slowly over many oscillations of the exponential function, we may retain the leading term in the Taylor expansion of the amplitude, and approximate the integral up to quadratic terms in the phase by

$$I \approx A(x_0) e^{is\Phi(x_0)} \int dx\, e^{\frac{1}{2}is\Phi''(x_0)(x-x_0)^2}\,. \tag{30.15}$$

30.1 page 563

Using the *Fresnel integral formula*

$$\frac{1}{\sqrt{2\pi}} \int_{-\infty}^{\infty} dx\, e^{-\frac{x^2}{2ia}} = \sqrt{ia} = |a|^{1/2}\, e^{i\frac{\pi}{4}\frac{a}{|a|}} \tag{30.16}$$

we obtain

$$I \approx A(x_0) \left| \frac{2\pi}{s\Phi''(x_0)} \right|^{1/2} e^{is\Phi(x_0)\pm i\frac{\pi}{4}}\,, \tag{30.17}$$

where $\pm$ corresponds to the positive/negative sign of $s\Phi''(x_0)$.

30.3 WKB quantization

We can now evaluate the Fourier transforms (30.11), (30.12) to the same order in $\hbar$ as the WKB wave function using the stationary phase method,

$$\begin{aligned} \widetilde{\psi}_{sc}(p) &= \frac{C}{\sqrt{2\pi\hbar}} \int \frac{dq}{|p(q)|^{\frac{1}{2}}}\, e^{\frac{i}{\hbar}(S(q)-qp)} \\ &\approx \frac{C}{\sqrt{2\pi\hbar}} \frac{e^{\frac{i}{\hbar}(S(q^*)-q^*p)}}{|p(q^*)|^{\frac{1}{2}}} \int dq\, e^{\frac{i}{2\hbar}S''(q^*)(q-q^*)^2}\,, \end{aligned} \tag{30.18}$$

where q^* is given implicitly by the stationary phase condition

$$0 = S'(q^*) - p = p(q^*) - p$$

and the sign of $S''(q^*) = p'(q^*)$ determines the phase of the Fresnel integral (30.16)

$$\widetilde{\psi}_{sc}(p) = \frac{C}{|p(q^*)p'(q^*)|^{\frac{1}{2}}} e^{\frac{i}{\hbar}[S(q^*)-q^*p]+\frac{i\pi}{4}\mathrm{sgn}[S''(q^*)]}\,. \tag{30.19}$$

As we continue from (q_A, p_A) to (q_B, p_B), nothing problematic occurrs - $p(q^*)$ is finite, and so is the acceleration $p'(q^*)$. Otherwise, the trajectory would take infinitely long to get across. We recognize the exponent as the Legendre transform

$$\tilde{S}(p) = S(q(p)) - q(p)p$$

which can be used to expresses everything in terms of the p variable,

$$q^* = q(p), \quad \frac{d}{dq}q = 1 = \frac{dp}{dq}\frac{dq(p)}{dp} = q'(p)p'(q^*)\,. \tag{30.20}$$

As the classical trajectory crosses q_L, the weight in (30.19),

$$\frac{d}{dq}p^2(q_L) = 2p(q_L)p'(q_L) = -2mV'(q)\,, \tag{30.21}$$

is finite, and $S''(q^*) = p'(q^*) < 0$ for any point in the lower left quadrant, including (q_A, p_A). Hence, the phase loss in (30.19) is $-\frac{\pi}{4}$. To go back from the p to the q representation, just turn figure 30.2 90^o anticlockwise. Everything is the same if you replace $(q,p) \to (-p,q)$; so, without much ado we get the semiclassical wave function at the point (q_B, p_B),

$$\psi_{sc}(q) = \frac{e^{\frac{i}{\hbar}(\tilde{S}(p^*)+qp^*)-\frac{i\pi}{4}}}{|q^*(p^*)|^{\frac{1}{2}}}\, \widetilde{\psi}_{sc}(p^*) = \frac{C}{|p(q)|^{\frac{1}{2}}} e^{\frac{i}{\hbar}S(q)-\frac{i\pi}{2}}\,. \tag{30.22}$$

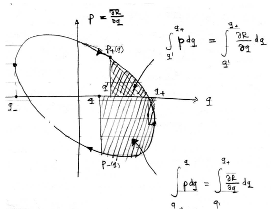

Figure 30.3: $S_p(E)$, the action of a periodic orbit p at energy E, equals the area in the phase space traced out by the 1-dof trajectory.

The extra $|p'(q^*)|^{1/2}$ weight in (30.19) is cancelled by the $|q'(p^*)|^{1/2}$ term, by the Legendre relation (30.20).

The message is that going through a smooth potential turning point the WKB wave function phase slips by $-\frac{\pi}{2}$. This is equally true for the right and the left turning points, as can be seen by rotating figure 30.2 by 180^o, and flipping coordinates $(q, p) \to (-q, -p)$. While a turning point is not an invariant concept (for a sufficiently short trajectory segment, it can be undone by a 45^o turn), for a complete period $(q, p) = (q', p')$ the total phase slip is always $-2 \cdot \pi/2$, as a loop always has $m = 2$ turning points.

The *WKB quantization condition* follows by demanding that the wave function computed after a complete period be single-valued. With the normalization (30.8), we obtain

$$\psi(q') = \psi(q) = \left|\frac{p(q')}{p(q)}\right|^{\frac{1}{2}} e^{i(\frac{1}{\hbar}\oint p(q)dq - \pi)}\psi(q') \,.$$

The prefactor is 1 by the periodic orbit condition $q = q'$, so the phase must be a multiple of 2π,

$$\frac{1}{\hbar}\oint p(q)dq = 2\pi\left(n + \frac{m}{4}\right) , \qquad (30.23)$$

where m is the number of turning points along the trajectory - for this 1-dof problem, $m = 2$.

The action integral in (30.23) is the area (see figure 30.3) enclosed by the classical phase space loop of figure 30.2, and the quantization condition says that eigenenergies correspond to loops whose action is an integer multiple of the unit quantum of action, Planck's constant $\hbar$. The extra topological phase, which, although it had been discovered many times in centuries past, had to wait for its most recent quantum chaotic (re)birth until the 1970's. Despite its derivation in a noninvariant coordinate frame, the final result involves only canonically invariant classical quantities, the periodic orbit action S, and the topological index m.

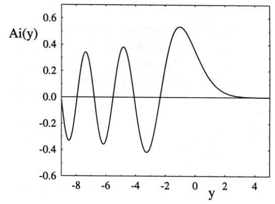

Figure 30.4: Airy function $Ai(q)$.

30.3.1 Harmonic oscillator quantization

Let us check the WKB quantization for one case (the only case?) whose quantum mechanics we fully understand: the harmonic oscillator

$$E = \frac{1}{2m}\left(p^2 + (m\omega q)^2\right) .$$

The loop in figure 30.2 is now a circle in the $(m\omega q, p)$ plane, the action is its area $S = 2\pi E/\omega$, and the spectrum in the WKB approximation

$$E_n = \hbar\omega(n + 1/2) \qquad (30.24)$$

turns out to be the *exact* harmonic oscillator spectrum. The stationary phase condition (30.18) keeps $V(q)$ accurate to order q^2, which in this case is the whole answer (but we were simply lucky, really). For many 1-dof problems the WKB spectrum turns out to be very accurate all the way down to the ground state. Surprisingly accurate, if one interprets dropping the $\hbar^2$ term in (30.5) as a short wavelength approximation.

30.4 Beyond the quadratic saddle point

We showed, with a bit of Fresnel/Maslov voodoo, that in a smoothly varying potential the phase of the WKB wave function slips by a $\pi/2$ for each turning point. This $\pi/2$ came from a $\sqrt{i}$ in the Fresnel integral (30.16), one such factor for every time we switched representation from the configuration space to the momentum space, or back. Good, but what does this mean?

The stationary phase approximation (30.14) fails whenever $\Phi''(x) = 0$, or, in our the WKB ansatz (30.18), whenever the momentum $p'(q) = S''(q)$ vanishes. In that case we have to go beyond the quadratic approximation (30.15) to the first nonvanishing term in the Taylor expansion of the exponent. If $\Phi'''(x_0) \neq 0$, then

$$I \approx A(x_0)e^{is\Phi(x_0)}\int_{-\infty}^{\infty} dx\, e^{is\Phi'''(x_0)\frac{(x-x_0)^3}{6}} \,. \qquad (30.25)$$

Airy functions can be represented by integrals of the form

$$Ai(x) = \frac{1}{2\pi}\int_{-\infty}^{+\infty} dy\, e^{i(xy-\frac{y^3}{3})}\,. \tag{30.26}$$

Derivations of the WKB quantization condition given in standard quantum mechanics textbooks rely on expanding the potential close to the turning point

$$V(q) = V(q_0) + (q-q_0)V'(q_0) + \cdots\,,$$

solving the Airy equation

$$\psi'' = q\psi\,, \tag{30.27}$$

and matching the oscillatory and the exponentially decaying "forbidden" region wave function pieces by means of the *WKB connection formulas*. That requires staring at Airy functions and learning about their asymptotics - a challenge that we will have to eventually overcome, in order to incorporate diffraction phenomena into semiclassical quantization.

2) what does the wave function look like?

3) generically useful when Gaussian approximations fail

The physical origin of the topological phase is illustrated by the shape of the Airy function, figure 30.4. For a potential with a finite slope $V'(q)$ the wave function pentrates into the forbidden region, and accomodates a bit more of a stationary wavelength then what one would expect from the classical trajectory alone. For infinite walls (i.e., billiards) a different argument applies: the wave function must vanish at the wall, and the phase slip due to a specular reflection is $-\pi$, rather than $-\pi/2$.

Commentary

Remark 30.1 Airy function. The stationary phase approximation is all that is needed for the semiclassical approximation, with the proviso that D in (31.36) has no zero eigenvalues. The zero eigenvalue case would require going beyond the Gaussian saddle-point approximation, which typically leads to approximations of the integrals in terms of Airy functions [30.10].

30.4 page 563

Remark 30.2 Bohr-Sommerfeld quantization. Bohr-Sommerfeld quantization condition was the key result of the old quantum theory, in which the electron trajectories were purely classical. They were lucky - the symmetries of the Kepler problem work out in such a way that the total topological index $m = 4$ amount effectively to numbering the energy levels starting with $n = 1$. They were unlucky - because the hydrogen $m = 4$ masked the topological index, they could never get the helium spectrum right - the semiclassical calculation had to wait for until 1980, when Leopold and Percival [**?**] added the topological indices.

Résumé

The WKB ansatz wave function for 1-degree of freedom problems fails at the turning points of the classical trajectory. While in the q-representation the WKB ansatz a turning point is singular, along the p direction the classical trajectory in the same neighborhood is smooth, as for any smooth bound potential the classical motion is topologically a circle around the origin in the (q, p) space. The simplest way to deal with such singularities is as follows; follow the classical trajectory in q-space until the WKB approximation fails close to the turning point; then insert $\int dp|p\rangle\langle p|$ and follow the classical trajectory in the p-space until you encounter the next p-space turning point; go back to the q-space representation, an so on. Each matching involves a Fresnel integral, yielding an extra $e^{-i\pi/4}$ phase shift, for a total of $e^{-i\pi}$ phase shift for a full period of a semiclassical particle moving in a soft potential. The condition that the wave-function be single-valued then leads to the 1-dimensional WKB quantization, and its lucky cousin, the Bohr-Sommerfeld quantization.

Alternatively, one can linearize the potential around the turning point a, $V(q) = V(a) + (q-a)V'(a) + \cdots$, and solve the quantum mechanical constant linear potential $V(q) = qF$ problem exactly, in terms of an Airy function. An approximate wave function is then patched together from an Airy function at each turning point, and the WKB ansatz wave-function segments inbetween via the WKB connection formulas. The single-valuedness condition again yields the 1-dimensional WKB quantization. This a bit more work than tracking the classical trajectory in the full phase space, but it gives us a better feeling for shapes of quantum eigenfunctions, and exemplifies the general strategy for dealing with other singularities, such as wedges, bifurcation points, creeping and tunneling: patch together the WKB segments by means of exact QM solutions to local approximations to singular points.

References

[30.1] D. J. Griffiths, *Introduction to Quantum Mechanics* (Prentice-Hall, Englewood Cliffs, New Jersey, 1994).

[30.2] J.W.S. Rayleigh, *The Theory of Sound* (Macmillan, London 1896; reprinted by Dover, New York 1945).

[30.3] J.B. Keller, *Ann. Phys. (N.Y.)* **4**, 180 (1958).

[30.4] J.B. Keller and S.I. Rubinow, *Ann. Phys. (N.Y.)* **9**, 24 (1960).

[30.5] J.B. Keller, "A geometrical theory of diffraction", in *Calculus of variations and its applications*, *Proc. of Symposia in appl. math.* **8**, (McGraw-Hill, New York, 1958).

[30.6] J.B. Keller, *Calculus of Variations* **27**, (1958).

[30.7] V.P. Maslov, *Théorie des Perturbations et Métodes Asymptotiques* (Dunod, Paris, 1972).

[30.8] V.P. Maslov and M.V. Fedoriuk, *Semi-Classical Approximation in Quantum Mechanics* (Reidel, Boston 1981).

[30.9] V.I. Arnold, *Functional Anal. Appl.* **1**, 1 (1967).

[30.10] N. Bleistein and R.A. Handelsman, *Asymptotic Expansions of Integrals* (Dover, New York 1986).

[30.11] I.C. Percival, *Adv. Chem. Phys.* **36**, 1 (1977).

Exercises

Exercise 30.1 WKB ansatz. *Try to show that no other ansatz other than (31.1) gives a meaningful definition of the momentum in the $\hbar \to 0$ limit.*

Exercise 30.2 Fresnel integral. *Derive the Fresnel integral*

$$\frac{1}{\sqrt{2\pi}} \int_{-\infty}^{\infty} dx \, e^{-\frac{x^2}{2ia}} = \sqrt{ia} = |a|^{1/2} e^{i\frac{\pi}{4}\frac{a}{|a|}} .$$

Exercise 30.3 Sterling formula for $n!$. *Compute an approximate value of $n!$ for large n using the stationary phase approximation. Hint: $n! = \int_0^\infty dt\, t^n e^{-t}$.*

Exercise 30.4 Airy function for large arguments. *Important contributions as stationary phase points may arise from extremal points where the first non-zero term in a Taylor expansion of the phase is of third or higher order. Such situations occur, for example, at bifurcation points or in diffraction effects, (such as waves near sharp corners, waves creeping around obstacles, etc.). In such calculations, one meets Airy functions integrals of the form*

$$Ai(x) = \frac{1}{2\pi} \int_{-\infty}^{+\infty} dy \, e^{i(xy - \frac{y^3}{3})} . \tag{30.28}$$

Calculate the Airy function $Ai(x)$ using the stationary phase approximation. What happens when considering the limit $x \to 0$. Estimate for which value of x the stationary phase approximation breaks down.

Chapter 31

Semiclassical evolution

> William Rowan Hamilton was born in 1805. At three he could read English; by four he began to read Latin, Greek and Hebrew, by ten he read Sanskrit, Persian, Arabic, Chaldee, Syrian and sundry Indian dialects. At age seventeen he began to think about optics, and worked out his great principle of "Characteristic Function".
>
> — Turnbull, *Lives of Mathematicians*

(G. Vattay, G. Tanner and P. Cvitanović)

Semiclassical approximations to quantum mechanics are valid in the regime where the de Broglie wavelength $\lambda \sim \hbar/p$ of a particle with momentum p is much shorter than the length scales across which the potential of the system changes significantly. In the short wavelength approximation the particle is a point-like object bouncing off potential walls, the same way it does in the classical mechanics. The novelty of quantum mechanics is the interference of the point-like particle with other versions of itself traveling along different classical trajectories, a feat impossible in classical mechanics. The short wavelength – or semiclassical – formalism is developed by formally taking the limit $\hbar \to 0$ in quantum mechanics in such a way that quantum quantities go to their classical counterparts. ☞ remark 31.1

31.1 Hamilton-Jacobi theory

We saw in chapter 30 that for a 1-dof particle moving in a slowly varying potential, it makes sense to generalize the free particle wave function (30.1) to a wave function

$$\psi(q,t) = A(q,t)e^{iR(q,t)/\hbar}\,, \tag{31.1}$$

with slowly varying (real) amplitude $A(q,t)$ and rapidly varying (real) phase $R(q,t)$. its phase and magnitude. The time evolution of the phase and 30.1 page 563

the magnitude of ψ follows from the Schrödinger equation (29.1)

$$\left(i\hbar\frac{\partial}{\partial t}+\frac{\hbar^2}{2m}\frac{\partial^2}{\partial q^2}-V(q)\right)\psi(q,t)=0\,. \tag{31.2}$$

Assume $A \neq 0$, and separate out the real and the imaginary parts. We get two equations: The real part governs the time evolution of the phase

$$\frac{\partial R}{\partial t}+\frac{1}{2m}\left(\frac{\partial R}{\partial q}\right)^2+V(q)-\frac{\hbar^2}{2m}\frac{1}{A}\frac{\partial^2}{\partial q^2}A=0\,, \tag{31.3}$$

and the imaginary part the time evolution of the amplitude

31.8 page 587
31.9 page 587
31.10 page 587

$$\frac{\partial A}{\partial t}+\frac{1}{m}\sum_{i=1}^{D}\frac{\partial A}{\partial q_i}\frac{\partial R}{\partial q_i}+\frac{1}{2m}A\frac{\partial^2 R}{\partial q^2}=0\,. \tag{31.4}$$

In this way a linear PDE for a complex wave function is converted into a set of coupled non-linear PDE's for real-valued functions R and A. The coupling term in (31.3) is, however, of order $\hbar^2$ and thus small in the semiclassical limit $\hbar \to 0$.

Now we generalize the *Wentzel-Kramers-Brillouin* (WKB) *ansatz* for 1-dof dynamics to the Van Vleck *ansatz* in arbitrary dimension: we assume the magnitude $A(q,t)$ varies slowly compared to the phase $R(q,t)/\hbar$, so we drop the $\hbar$-dependent term. In this approximation the phase $R(q,t)$ and the corresponding "momentum field" $\frac{\partial R}{\partial q}(q,t)$ can be determined from the amplitude independent equation

$$\frac{\partial R}{\partial t}+H\left(q,\frac{\partial R}{\partial q}\right)=0\,. \tag{31.5}$$

In classical mechanics this equation is known as the *Hamilton-Jacobi equation*. We will refer to this step (as well as all leading order in $\hbar$ approximations to follow) as the *semiclassical approximation* to wave mechanics, and from now on work only within this approximation.

31.1.1 Hamilton's equations

We now solve the nonlinear partial differential equation (31.5) in a way the 17 year old Hamilton might have solved it. The main step is the step leading from the nonlinear PDE (31.9) to Hamilton's ODEs (31.10). If you already understand the Hamilton-Jacobi theory, you can safely skip this section.

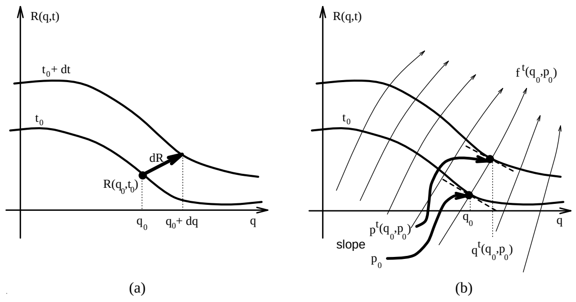

Figure 31.1: (a) A phase $R(q,t)$ plotted as a function of the position q for two infinitesimally close times. (b) The phase $R(q,t)$ transported by a swarm of "particles"; The Hamilton's equations (31.10) construct $R(q,t)$ by transporting $q_0 \to q(t)$ and the slope of $R(q_0,t_0)$, that is $p_0 \to p(t)$.

fast track:
sect. 31.1.3, p. 570

The wave equation (29.1) describes how the wave function ψ evolves with time, and if you think of ψ as an (infinite dimensional) vector, position q plays a role of an index. In one spatial dimension the phase R plotted as a function of the position q for two different times looks something like figure 31.1 (a): The phase $R(q,t_0)$ deforms smoothly with time into the phase $R(q,t)$ at time t. Hamilton's idea was to let a swarm of particles transport R and its slope $\partial R/\partial q$ at q at initial time $t=t_0$ to a corresponding $R(q,t)$ and its slope at time t, figure 31.1 (b). For notational convenience, define

$$p_i=p_i(q,t):=\frac{\partial R}{\partial q_i}\,,\quad i=1,2,\ldots,D\,. \tag{31.6}$$

We saw earlier that (31.3) reduces in the semiclassical approximation to the Hamilton-Jacobi equation (31.5). To make life simple, we shall assume throughout this chapter that the Hamilton's function $H(q,p)$ does not depend explicitly on time t, i.e., the energy is conserved.

To start with, we also assume that the function $R(q,t)$ is smooth and well defined for every q at the initial time t. This is true for sufficiently short times; as we will see later, R develops folds and becomes multi-valued as t progresses. Consider now the variation of the function $R(q,t)$ with respect to independent infinitesimal variations of the time and space coordinates dt and dq, figure 31.1 (a)

$$dR=\frac{\partial R}{\partial t}dt+\frac{\partial R}{\partial q}dq\,. \tag{31.7}$$

Dividing through by dt and substituting (31.5) we obtain the total derivative of $R(q,t)$ with respect to time *along the as yet arbitrary direction* $\dot{q}$, that is,

$$\frac{dR}{dt}(q,\dot{q},t) = -H(q,p) + \dot{q}\cdot p\,. \tag{31.8}$$

Note that the "momentum" $p = \partial R/\partial q$ is a well defined function of q and t. In order to integrate $R(q,t)$ with the help of (31.8) we also need to know how $p = \partial R/\partial q$ changes along $\dot{q}$. Varying p with respect to independent infinitesimal variations dt and dq and substituting the Hamilton-Jacobi equation (31.5) yields

$$d\frac{\partial R}{\partial q} = \frac{\partial^2 R}{\partial q \partial t}dt + \frac{\partial^2 R}{\partial q^2}dq = -\left(\frac{\partial H}{\partial q} + \frac{\partial H}{\partial p}\frac{\partial p}{\partial q}\right)dt + \frac{\partial p}{\partial q}dq\,.$$

Note that $H(q,p)$ depends on q also through $p(q,t) = \partial R/\partial q$, hence the $\frac{\partial H}{\partial p}$ term in the above equation. Dividing again through by dt we get the time derivative of $\partial R/\partial q$, that is,

$$\dot{p}(q,\dot{q},t) + \frac{\partial H}{\partial q} = \left(\dot{q} - \frac{\partial H}{\partial p}\right)\frac{\partial p}{\partial q}\,. \tag{31.9}$$

Time variation of p depends not only on the yet unknown $\dot{q}$, but also on the second derivatives of R with respect to q with yet unknown time dependence. However, if we *choose* $\dot{q}$ (which was arbitrary, so far) such that the right hand side of the above equation vanishes, we can calculate the function $R(q,t)$ along a specific trajectory $(q(t),p(t))$ given by integrating the ordinary differential equations

$$\dot{q} = \frac{\partial H(q,p)}{\partial p}, \qquad \dot{p} = -\frac{\partial H(q,p)}{\partial q} \tag{31.10}$$

with initial conditions

$$q(t_0) = q', \qquad p(t_0) = p' = \frac{\partial R}{\partial q}(q',t_0). \tag{31.11}$$

☞ sect. 6.1

We recognize (31.10) as Hamilton's equations of motion of classical mechanics. The miracle happens in the step leading from (31.5) to (31.9) – if you missed it, you have missed the point. Hamilton derived his equations contemplating optics - it took him three more years to realize that all of Newtonian dynamics can be profitably recast in this form.

$\dot{q}$ is no longer an independent function, and the phase $R(q,t)$ can now be computed by integrating equation (31.8) along the trajectory $(q(t),p(t))$

$$\begin{aligned} R(q,t) &= R(q',t_0) + R(q,t;q',t_0) \\ R(q,t;q',t_0) &= \int_{t_0}^{t} d\tau\,[\dot{q}(\tau)\cdot p(\tau) - H(q(\tau),p(\tau))]\,, \end{aligned} \tag{31.12}$$

with the initial conditions (31.11). In this way the Hamilton-Jacobi *partial* differential equation (31.3) is solved by integrating a set of *ordinary* differential equations, Hamilton's equations. In order to determine $R(q,t)$ for arbitrary q and t we have to find a q' such that the trajectory starting in $(q', p' = \partial_q R(q',t_0))$ reaches q in time t and then compute R along this trajectory, see figure 31.1 (b). The integrand of (31.12) is known as the *Lagrangian*,

$$L(q,\dot{q},t) = \dot{q}\cdot p - H(q,p,t)\,. \tag{31.13}$$

A variational principle lurks here, but we shall not make much fuss about it as yet.

Throughout this chapter we assume that the energy is conserved, and that the only time dependence of $H(q,p)$ is through $(q(\tau),p(\tau))$, so the value of $R(q,t;q',t_0)$ does not depend on t_0, but only on the elapsed time $t-t_0$. To simplify notation we will set $t_0 = 0$ and write

$$R(q,q',t) = R(q,t;q',0)\,.$$

The initial momentum of the particle must coincide with the initial momentum of the trajectory connecting q' and q:

$$p' = \frac{\partial}{\partial q'}R(q',0) = -\frac{\partial}{\partial q'}R(q,q',t). \tag{31.14}$$

The function $R(q,q',t)$ is known as *Hamilton's principal function.*

31.7 page 587
31.11 page 587

To summarize: Hamilton's achievement was to trade in the Hamilton-Jacobi *partial* differential equation (31.5) describing the evolution of a wave front for a finite number of *ordinary* differential equations of motion, with the initial phase $R(q,0)$ incremented by the integral (31.12) evaluated along the phase space trajectory $(q(\tau),p(\tau))$.

31.1.2 Action

Before proceeding, we note in passing a few facts about Hamiltonian dynamics that will be needed for the construction of semiclassical Green's functions. If the energy is conserved, the $\int H(q,p)d\tau$ integral in (31.12) is simply Et. The first term, or the *action*

$$S(q,q',E) = \int_0^t d\tau\,\dot{q}(\tau)\cdot p(\tau) = \int_{q'}^{q} dq\cdot p \tag{31.15}$$

is integrated along a trajectory from q' to q with a fixed energy E. By (31.12) the action is a Legendre transform of Hamilton's principal function

$$S(q,q',E) = R(q,q',t) + Et\,. \tag{31.16}$$

The time of flight t along the trajectory connecting $q' \to q$ with fixed energy E is given by

$$\frac{\partial}{\partial E} S(q, q', E) = t \,. \tag{31.17}$$

The way to think about the formula (31.16) for action is that the time of flight is a function of the energy, $t = t(q, q', E)$. The left hand side is explicitly a function of E; the right hand side is an implicit function of E through energy dependence of the flight time t.

Going in the opposite direction, the energy of a trajectory $E = E(q, q', t)$ connecting $q' \to q$ with a given time of flight t is given by the derivative of Hamilton's principal function

$$\frac{\partial}{\partial t} R(q, q', t) = -E \,, \tag{31.18}$$

and the second variations of R and S are related in the standard way of Legendre transforms:

$$\frac{\partial^2}{\partial t^2} R(q, q', t) \frac{\partial^2}{\partial E^2} S(q, q', E) = -1 \,. \tag{31.19}$$

sect. 31.1.4

A geometric visualization of what the phase evolution looks like is very helpful in understanding the origin of topological indices to be introduced in what follows. Given an initial phase $R(q, t_0)$, the gradient $\partial_q R$ defines a D-dimensional *Lagrangian manifold* $(q,\, p = \partial_q R(q))$ in the full $2d$ dimensional phase space (q, p). The defining property of this manifold is that any contractible loop γ in it has zero action,

$$0 = \oint_\gamma dq \cdot p,$$

a fact that follows from the definition of p as a gradient, and the Stokes theorem. Hamilton's equations of motion preserve this property and map a Lagrangian manifold into a Lagrangian manifold at a later time. t

Returning back to the main line of our argument: so far we have determined the wave function phase $R(q, t)$. Next we show that the velocity field given by the Hamilton's equations together with the continuity equation determines the amplitude of the wave function.

31.1.3 Density evolution

To obtain the full solution of the Schrödinger equation (29.1), we also have to integrate (31.4).

$$\rho(q, t) := A^2 = \psi^* \psi$$

plays the role of a density. To the leding order in $\hbar$, the gradient of R may be interpreted as the semiclassical momentum density

$$\psi(q, t)^* (-i\hbar \frac{\partial}{\partial q}) \psi(q, t) \;=\; -i\hbar A \frac{\partial A}{\partial q} + \rho \frac{\partial R}{\partial q} \,.$$

Evaluated along the trajectory $(q(t), p(t))$, the amplitude equation (31.4) is equivalent to the continuity equation (14.36) after multiplying (31.4) by $2A$, that is

$$\frac{\partial \rho}{\partial t} + \frac{\partial}{\partial q_i} (\rho v_i) = 0 \,. \tag{31.20}$$

Here, $v_i = \dot{q}_i = p_i/m$ denotes a velocity field, which is in turn determined by the gradient of $R(q, t)$, or the *Lagrangian manifold* $(q(t), p(t) = \partial_q R(q, t))$,

$$v = \frac{1}{m} \frac{\partial}{\partial q} R(q, t).$$

As we already know how to solve the Hamilton-Jacobi equation (31.5), we can also solve for the density evolution as follows:

The density $\rho(q)$ can be visualized as the density of a configuration space flow $q(t)$ of a swarm of hypothetical particles; the trajectories $q(t)$ are solutions of Hamilton's equations with initial conditions given by $(q(0) = q', p(0) = p' = \partial_q R(q', 0))$.

If we take a small configuration space volume $d^D q$ around some point q at time t, then the number of particles in it is $\rho(q, t) d^D dq$. They started initially in a small volume $d^D q'$ around the point q' of the configuration space. For the moment, we assume that there is only one solution, the case of several paths will be considered below. The number of particles at time t in the volume is the same as the number of particles in the initial volume at $t = 0$,

$$\rho(q(t), t) d^D q = \rho(q', 0) d^D q' \,,$$

see figure 31.2. The ratio of the initial and the final volumes can be expressed as

$$\rho(q(t), t) = \left| \det \frac{\partial q'}{\partial q} \right| \rho(q', 0) \,. \tag{31.21}$$

sect. 14.2

As we know how to compute trajectories $(q(t), p(t))$, we know how to compute this Jacobian and, by (31.21), the density $\rho(q(t), t)$ at time t.

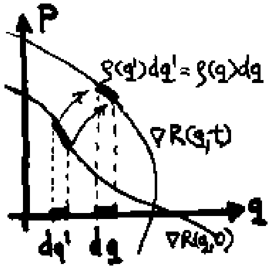

Figure 31.2: Density evolution of an initial surface $(q', p' = \partial_q R(q', 0))$ into $(q(t), p(t))$ surface time t later, sketched in 1 dimension. While the number of trajectories and the phase space Liouville volume are conserved, the density of trajectories projected on the q coordinate varies; trajectories which started in dq' at time zero end up in the interval dq.

31.1.4 Semiclassical wave function

Now we have all ingredients to write down the semiclassical wave function at time t. Consider first the case when our initial wave function can be written in terms of single-valued functions $A(q', 0)$ and $R(q', 0)$. For sufficiently short times, $R(q, t)$ will remain a single-valued function of q, and every $d^D q$ configuration space volume element keeps its orientation. The evolved wave function is in the semiclassical approximation then given by

$$\begin{aligned}\psi_{sc}(q,t) &= A(q,t)e^{iR(q,t)/\hbar} = \sqrt{\det\frac{\partial q'}{\partial q}}\,A(q',0)e^{i(R(q',0)+R(q,q',t))/\hbar} \\ &= \sqrt{\det\frac{\partial q'}{\partial q}}\,e^{iR(q,q',t)/\hbar}\,\psi(q',0)\,.\end{aligned}$$

As the time progresses the Lagrangian manifold $\partial_q R(q, t)$ can develop folds, so for longer times the value of the phase $R(q, t)$ is not necessarily unique; in general more than one trajectory will connect points q and q' with different phases $R(q, q', t)$ accumulated along these paths, see figure 31.3.

We thus expect in general a collection of different trajectories from q' to q which we will index by j, with different phase increments $R_j(q, q', t)$. The hypothetical particles of the density flow at a given configuration space point can move with different momenta $p = \partial_q R_j(q, t)$. This is not an ambiguity, since in the full (q, p) phase space each particle follows its own trajectory with a unique momentum.

Whenever the Lagrangian manifold develops a fold, the density of the phase space trajectories in the fold projected on the configuration coordinates diverges. As illustrated in figure 31.3, when the Lagrangian manifold develops a fold at $q = q_1$; the volume element dq_1 in the neighborhood of the folding point is proportional to $\sqrt{dq'}$ instead of dq'. The Jacobian $\partial q'/\partial q$ diverges like $1/\sqrt{q_1 - q(t)}$ when computed along the trajectory going trough the folding point at q_1. After the folding the orientation of the interval dq' has changed when being mapped into dq_2; in addition the function R, as well as its derivative which defines the Lagrangian manifold, becomes multi-valued. Distinct trajectories starting from different initial

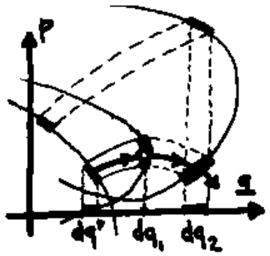

Figure 31.3: Folding of the Lagrangian surface $(q, \partial_q R(q, t))$.

points q' can now reach the same final point q_2. (That is, the point q' may have more than one pre-image.) The projection of a simple fold, or of an envelope of a family of phase space trajectories, is called a *caustic*; this expression comes from the Greek word for "capable of burning", evoking the luminous patterns that one observes swirling across the bottom of a swimming pool.

The folding also changes the orientation of the pieces of the Lagrangian manifold $(q, \partial_q R(q, t))$ with respect to the initial manifold, so the eigenvalues of the Jacobian determinant change sign at each fold crossing. We can keep track of the signs by writing the Jacobian determinant as

$$\det\frac{\partial q'}{\partial q}\bigg|_j = e^{-i\pi m_j(q,q',t)}\left|\det\frac{\partial q'}{\partial q}\right|_j\,,$$

where $m_j(q, q', t)$ counts the number of sign changes of the Jacobian determinant on the way from q' to q along the trajectory indexed with j, see figure 31.3. We shall refer to the integer $m_j(q, q', t)$ as the *topological* of the trajectory. So in general the semiclassical approximation to the wave function is thus a sum over possible trajectories that start at any inital q' and end in q in time t

$$\psi_{sc}(q,t) = \int dq' \sum_j \left|\det\frac{\partial q'}{\partial q}\right|_j^{1/2} e^{iR_j(q,q',t)/\hbar - i\pi m_j(q,q',t)/2}\psi(q'_j,0)\,, \quad (31.22)$$

each contribution weighted by corresponding density, phase increment and the topological index.

That the correct topological index is obtained by simply counting the number of eigenvalue sign changes and taking the square root is not obvious - the careful argument requires that quantum wave functions evaluated across the folds remain single valued.

31.2 Semiclassical propagator

We saw in chapter 29 that the evolution of an initial wave function $\psi(q, 0)$ is completely determined by the propagator (29.12). As $K(q, q', t)$ itself satisfies the Schrödinger equation (29.14), we can treat it as a wave function parameterized by the configuration point q'. In order to obtain a semiclassical approximation to the propagator we follow now the ideas developed in the last section. There is, however, one small complication: the initial condition (29.15) demands that the propagator at $t = 0$ is a δ-function at $q = q'$, that is, the amplitude is infinite at q' and the phase is not well defined. Our hypothetical cloud of particles is thus initially localized at $q = q'$ with *any* initial velocity. This is in contrast to the situation in the previous section where we assumed that the particles at a given point q have well defined velocity (or a discrete set of velocities) given by $\dot{q} = \partial_p H(q,p)$. We will now derive at a semiclassical expression for $K(q,q',t)$ by considering the propagator for short times first, and extrapolating from there to arbitrary times t.

31.2
586

31.2.1 Short time propagator

For infinitesimally short times δt away from the singular point $t = 0$ we assume that it is again possible to write the propagator in terms of a well defined phase and amplitude, that is

$$K(q,q',\delta t) = A(q,q',\delta t) e^{\frac{i}{\hbar} R(q,q',\delta t)} .$$

As all particles start at $q = q'$, $R(q,q',\delta t)$ will be of the form (31.12), that is

$$R(q,q',\delta t) = p\dot{q}\delta t - H(q,p)\delta t , \qquad (31.23)$$

with $\dot{q} \approx (q-q')/\delta t$. For Hamiltonians of the form (29.2) we have $\dot{q} = p/m$, which leads to

$$R(q,q',\delta t) = \frac{m(q-q')^2}{2\delta t} - V(q)\delta t .$$

Here V can be evaluated any place along the trajectory from q to q', for example at the midway point $V((q+q')/2)$. Inserting this into our ansatz for the propagator we obtain

$$K_{sc}(q,q',\delta t) \approx A(q,q',\delta t) e^{\frac{i}{\hbar}\left(\frac{m}{2\delta t}(q-q')^2 - V(q)\delta t\right)} . \qquad (31.24)$$

For infinitesimal times we can neglect the term $V(q)\delta t$, so $K_{sc}(q,q',\delta t)$ is a d-dimensional Gaussian with width $\sigma^2 = i\hbar\delta t/m$. This Gaussian is a finite width approximation to the Dirac delta function

$$\delta(z) = \lim_{\sigma\to 0} \frac{1}{\sqrt{2\pi\sigma^2}} e^{-z^2/2\sigma^2} \qquad (31.25)$$

if $A = (m/2\pi i\hbar\delta t)^{D/2}$, with $A(q,q',\delta t)$ fixed by the Dirac delta function normalization condition. The correctly normalized propagator for infinitesimal times δt is therefore

$$K_{sc}(q,q',\delta t) \approx \left(\frac{m}{2\pi i\hbar\delta t}\right)^{D/2} e^{\frac{i}{\hbar}\left(\frac{m(q-q')^2}{2\delta t} - V(q)\delta t\right)} . \qquad (31.26)$$

The short time dynamics of the Lagrangian manifold $(q, \partial_q R)$ which corresponds to the quantum propagator can now be deduced from (31.23); one obtains

$$\frac{\partial R}{\partial q} = p \approx \frac{m}{\delta t}(q-q') ,$$

i.e., is the particles start for short times on a Lagrangian manifold which is a plane in phase space, see figure 31.4. Note, that for $\delta t \to 0$, this plane is given by the condition $q = q'$, that is, particles start on a plane parallel to the momentum axis. As we have already noted, all particles start at $q = q'$ but with different velocities for $t = 0$. The inital surface $(q', p' = \partial_q R(q', 0))$ is mapped into the surface $(q(t), p(t))$ some time t later. The slope of the Lagrangian plane for a short finite time is given as

$$\frac{\partial p_i}{\partial q_j} = -\frac{\partial^2 R}{\partial q_j \partial q'_i} = -\frac{\partial p'_i}{\partial q_j} = \frac{m}{\delta t}\delta_{ij} .$$

The prefactor $(m/\delta t)^{D/2}$ in (31.26) can therefore be interpreted as the determinant of the Jacobian of the transformation from final position coordinates q to initial momentum coordinates p', that is

$$K_{sc}(q,q',\delta t) = \frac{1}{(2\pi i\hbar)^{D/2}} \left(\det \frac{\partial p'}{\partial q}\right)^{1/2} e^{iR(q,q',\delta t)/\hbar}, \qquad (31.27)$$

where

$$\left.\frac{\partial p'_i}{\partial q_j}\right|_{t,q'} = \frac{\partial^2 R(q,q',\delta t)}{\partial q_j \partial q'_i} \qquad (31.28)$$

The subscript $\cdots|_{t,q'}$ indicates that the partial derivatives are to be evaluated with t, q' fixed.

The propagator in (31.27) has been obtained for short times. It is, however, already more or less in its final form. We only have to evolve our short time approximation of the propagator according to (31.22)

$$K_{sc}(q'',q',t'+\delta t) = \sum_j \left|\det \frac{\partial q}{\partial q''}\right|_j^{1/2} e^{iR_j(q'',q,t')/\hbar - i\pi m_j(q'',q,t')/2} K(q,q'_j,\delta t) ,$$

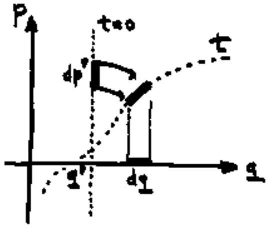

Figure 31.4: Evolution of the semiclassical propagator. The configuration which corresponds to the initial conditions of the propagator is a Lagrangian manifold $q = q'$, that is, a plane parallel to the p axis. The hypothetical particles are thus initially all placed at q' but take on all possible momenta p'. The Jacobian matrix C (31.29) relates an initial volume element in momentum space dp' to a final configuration space volume dq.

and we included here already the possibility that the phase becomes multi-valued, that is, that there is more than one path from q' to q''. The topological index $m_j = m_j(q'', q', t)$ is the number of singularities in the Jacobian along the trajectory j from q' to q''. We can write $K_{sc}(q'', q', t'+\delta t)$ in closed form using the fact that $R(q'', q, t') + R(q, q', \delta t) = R(q'', q', t' + \delta t)$ and the multiplicativity of Jacobian determinants, that is

$$\det \left.\frac{\partial q}{\partial q''}\right|_t \det \left.\frac{\partial p'}{\partial q}\right|_{q',\delta t} = \det \left.\frac{\partial p'}{\partial q''}\right|_{q',t'+\delta t} . \tag{31.29}$$

The final form of the semiclassical or *Van Vleck propagator*, is thus

$$K_{sc}(q, q', t) = \sum_j \frac{1}{(2\pi i\hbar)^{D/2}} \left|\det \frac{\partial p'}{\partial q}\right|^{1/2} e^{iR_j(q,q',t)/\hbar - im_j\pi/2} . \tag{31.30}$$

This Van Vleck propagator is the essential ingredient of the semiclassical quantization to follow.

The apparent simplicity of the semiclassical propagator is deceptive. The wave function is not evolved simply by multiplying by a complex number of magnitude $\sqrt{\det \partial p'/\partial q}$ and phase $R(q, q', t)$; the more difficult task in general is to find the trajectories connecting q' and q in a given time t.

In addition, we have to treat the approximate propagator (31.30) with some care. Unlike the full quantum propagator, which satisfies the group property (29.13) exactly, the semiclassical propagator performs this only approximately, that is

$$K_{sc}(q, q', t_1 + t_2) \approx \int dq''\, K_{sc}(q, q'', t_2) K_{sc}(q'', q', t_1) . \tag{31.31}$$

The connection can be made explicit by the stationary phase approximation, sect. 30.2. Approximating the integral in (31.31) by integrating only over regions near points q'' at which the phase is stationary, leads to the stationary phase condition

$$\frac{\partial R(q, q'', t_2)}{\partial q''_i} + \frac{\partial R(q'', q', t_1)}{\partial q''_i} = 0. \tag{31.32}$$

Classical trajectories contribute whenever the final momentum for a path from q' to q'' and the initial momentum for a path from q'' to q coincide. Unlike the classical evolution of sect. 15.2, the semiclassical evolution is not an evolution by linear operator multiplication, but evolution supplemented by a stationary phase condition $p_{out} = p_{in}$ that matches up the classical momenta at each evolution step.

31.2.2 Free particle propagator

To develop some intuition about the above formalism, consider the case of a free particle. For a free particle the potential energy vanishes, the kinetic energy is $\frac{m}{2}\dot{q}^2$, and the Hamilton's principal function (31.12) is

$$R(q, q', t) = \frac{m(q - q')^2}{2t} . \tag{31.33}$$

The weight $\det \frac{\partial p'}{\partial q}$ from (31.28) can be evaluated explicitly, and the Van Vleck propagator is

$$K_{sc}(q, q', t) = \left(\frac{m}{2\pi i\hbar t}\right)^{D/2} e^{im(q-q')^2/2\hbar t} , \tag{31.34}$$

identical to the short time propagator (31.26), with $V(q) = 0$. This case is rather exceptional: for a free particle the semiclassical propagator turns out to be the exact quantum propagator $K(q, q', t)$, as can be checked by substitution in the Schrödinger equation (31.2). The Feynman path integral formalism uses this fact to construct an exact quantum propagator ☞ remark 31.3 by integrating the free particle propagator (with $V(q)$ treated as constant for short times) along all possible (not necessarily classical) paths from q' to q.

31.12 page 587
31.13 page 588
31.14 page 588

31.3 Semiclassical Green's function

So far we have derived semiclassical formulas for the time evolution of wave functions, that is, we obtained approximate solutions to the time dependent Schrödinger equation (29.1). Even though we assumed in the calculation a time independent Hamiltonian of the special form (29.2), the derivation would lead to the same final result (31.30) were one to consider more complicated or explicitly time dependent Hamiltonians. The propagator is thus important when we are interested in finite time quantum mechanical effects. For time independent Hamiltonians, the time dependence of the propagator as well as of wave functions is, however, essentially given in terms of the energy eigen-spectrum of the system, as in (29.10). It is therefore advantageous to switch from a time representation to an energy representation, that is from the propagator (29.12) to the energy dependent

Green's function (29.16). A semiclassical approximation of the Green's function $G_{sc}(q,q',E)$ is given by the Laplace transform (29.16) of the Van Vleck propagator $K_{sc}(q,q',t)$:

$$G_{sc}(q,q',E) = \frac{1}{i\hbar}\int_0^\infty dt\, e^{iEt/\hbar} K_{sc}(q,q',t)\,. \tag{31.35}$$

The expression as it stands is not very useful; in order to evaluate the integral, at least to the leading order in $\hbar$, we need to turn to the method of stationary phase again.

31.3.1 Stationary phase in higher dimensions

30.1 page 563

Generalizing the method of sect. 30.2 to d dimensions, consider stationary phase points fulfilling

$$\left.\frac{d}{dx_i}\Phi(x)\right|_{x=x_0} = 0 \quad \forall i = 1,\dots d\,.$$

An expansion of the phase up to second order involves now the symmetric matrix of second derivatives of $\Phi(x)$, that is

$$D_{ij}(x_0) = \left.\frac{\partial^2}{\partial x_i \partial x_j}\Phi(x)\right|_{x=x_0}\,.$$

After choosing a suitable coordinate system which diagonalizes D, we can approximate the d-dimensional integral by d one-dimensional Fresnel integrals; the stationary phase estimate of (30.13) is then

$$I \approx \sum_{x_0} (2\pi i/s)^{d/2}\, |\det D(x_0)|^{-1/2} A(x_0)\, e^{is\Phi(x_0) - \frac{i\pi}{2}m(x_0)}\,, \tag{31.36}$$

where the sum runs over all stationary phase points x_0 of $\Phi(x)$ and $m(x_0)$ counts the number of negative eigenvalues of $D(x_0)$.

31.3 page 586
31.4 page 586
30.3 page 563

The stationary phase approximation is all that is needed for the semiclassical approximation, with the proviso that D in (31.36) has no zero eigenvalues.

31.3.2 Long trajectories

When evaluating the integral (31.35) approximately we have to distinguish between two types of contributions: those coming from stationary points of

the phase and those coming from infinitesimally short times. The first type of contributions can be obtained by the stationary phase approximation and will be treated in this section. The latter originate from the singular behavior of the propagator for $t \to 0$ where the assumption that the amplitude changes slowly compared to the phase is not valid. The short time contributions therefore have to be treated separately, which we will do in sect. 31.3.3.

The stationary phase points t^* of the integrand in (31.35) are given by the condition

$$\frac{\partial}{\partial t} R(q,q',t^*) + E = 0\,. \tag{31.37}$$

We recognize this condition as the solution of (31.18), the time $t^* = t^*(q,q',E)$ in which a particle of energy E starting out in q' reaches q. Taking into account the second derivative of the phase evaluated at the stationary phase point,

$$R(q,q',t) + Et = R(q,q',t^*) + Et^* + \frac{1}{2}(t-t^*)^2 \frac{\partial^2}{\partial t^2} R(q,q',t^*) + \cdots$$

the stationary phase approximation of the integral corresponding to a classical trajectory j in the Van Vleck propagator sum (31.30) yields

$$G_j(q,q',E) = \frac{1}{i\hbar(2i\pi\hbar)^{(D-1)/2}} \left|\det C_j \left(\frac{\partial^2 R_j}{\partial t^2}\right)^{-1}\right|^{1/2} e^{\frac{i}{\hbar}S_j - \frac{i\pi}{2}m_j}\,, \tag{31.38}$$

where $m_j = m_j(q,q',E)$ now includes a possible additional phase arising from the time stationary phase integration (30.16), and $C_j = C_j(q,q',t^*)$, $R_j = R_j(q,q',t^*)$ are evaluated at the transit time t^*. We re-express the phase in terms of the energy dependent action (31.16)

$$S(q,q',E) = R(q,q',t^*) + Et^*\,, \qquad \text{with} \quad t^* = t^*(q,q',E)\,, \tag{31.39}$$

the Legendre transform of Hamilton's principal function. Note that the partial derivative of the action (31.39) with respect to q_i

$$\frac{\partial S(q,q',E)}{\partial q_i} = \frac{\partial R(q,q',t^*)}{\partial q_i} + \left(\frac{\partial R(q,q',t)}{\partial t^*} + E\right)\frac{\partial t}{\partial q_i}.$$

is equal to

$$\frac{\partial S(q,q',E)}{\partial q_i} = \frac{\partial R(q,q',t^*)}{\partial q_i}, \tag{31.40}$$

due to the stationary phase condition (31.37), so the definition of momentum as a partial derivative with respect to q remains unaltered by the Legendre transform from time to energy domain.

31.15
page 588

Next we will simplify the amplitude term in (31.38) and rewrite it as an explicit function of the energy. Consider the $[(D+1)\times(D+1)]$ matrix

$$D(q,q',E) = \begin{pmatrix} \frac{\partial^2 S}{\partial q'\partial q} & \frac{\partial^2 S}{\partial q'\partial E} \\ \frac{\partial^2 S}{\partial q\partial E} & \frac{\partial^2 S}{\partial E^2} \end{pmatrix} = \begin{pmatrix} -\frac{\partial p'}{\partial q} & -\frac{\partial p'}{\partial E} \\ \frac{\partial t}{\partial q} & \frac{\partial t}{\partial E} \end{pmatrix}, \tag{31.41}$$

where $S = S(q,q',E)$ and we used (31.14–31.17) here to obtain the left hand side of (31.41). The minus signs follow from observing from the definition of (31.15) that $S(q,q',E) = -S(q',q,E)$. Note that D is nothing but the Jacobian matrix of the coordinate transformation $(q,E) \to (p',t)$ for fixed q'. We can therefore use the multiplication rules of determinants of Jacobians, which are just ratios of volume elements, to obtain

$$\begin{aligned} \det D &= (-1)^{D+1}\left(\det\frac{\partial(p',t)}{\partial(q,E)}\right)_{q'} = (-1)^{D+1}\left(\det\frac{\partial(p',t)}{\partial(q,t)}\frac{\partial(q,t)}{\partial(q,E)}\right)_{q'} \\ &= (-1)^{D+1}\left(\det\frac{\partial p'}{\partial q}\right)_{t,q'}\left(\det\frac{\partial t}{\partial E}\right)_{q',q} = \det C\left(\frac{\partial^2 R}{\partial t^2}\right)^{-1}. \end{aligned}$$

We use here the notation $(\det .)_{q',t}$ for a Jacobian determinant with partial derivatives evaluated at t,q' fixed, and likewise for other subscripts. Using the relation (31.19) which relates the term $\frac{\partial t}{\partial E}$ to $\partial_t^2 R$ we can write the determinant of D as a product of the Van Vleck determinant (31.28) and the amplitude factor arising from the stationary phase approximation. The amplitude in (31.38) can thus be interpreted as the determinant of a Jacobian of a coordinate transformation which includes time and energy as independent coordinates. This causes the increase in the dimensionality of the matrix D relative to the Van Vleck determinant (31.28).

We can now write down the semiclassical approximation of the contribution of the jth trajectory to the Green's function (31.38) in explicitly energy dependent form:

$$G_j(q,q',E) = \frac{1}{i\hbar(2i\pi\hbar)^{(D-1)/2}}\,|\det D_j|^{1/2}\, e^{\frac{i}{\hbar}S_j - \frac{i\pi}{2}m_j}\,. \tag{31.42}$$

However, this is still not the most convenient form of the Green's function.

The trajectory contributing to $G_j(q,q',E)$ is constrained to a given energy E, and will therefore be on a phase space manifold of constant energy, that is $H(q,p) = E$. Writing this condition as a partial differential equation for $S(q,q',E)$, that is

$$H(q,\frac{\partial S}{\partial q}) = E\,,$$

one obtains

$$\begin{aligned} \frac{\partial}{\partial q'_i}H(q,p) &= 0 = \frac{\partial H}{\partial p_j}\frac{\partial p_j}{\partial q'_i} = \dot q_j \frac{\partial^2 S}{\partial q_j \partial q'_i} \\ \frac{\partial}{\partial q_i}H(q',p') &= 0 = \frac{\partial^2 S}{\partial q_i \partial q'_j}\dot q'_j\,, \end{aligned} \tag{31.43}$$

that is the sub-matrix $\partial^2 S/\partial q_i \partial q'_j$ has (left- and right-) eigenvectors corresponding to an eigenvalue 0. Rotate the local coordinate system at the either end of the trajectory

$$(q_1,q_2,q_3,\cdots,q_d) \to (q_\parallel, q_{\perp 1}, q_{\perp 2},\cdots,q_{\perp(D-1)})$$

so that one axis points along the trajectory and all others are perpendicular to it

$$(\dot q_1,\dot q_2,\dot q_3,\cdots,\dot q_d) \to (\dot q,0,0,\cdots,0)\,.$$

With such local coordinate systems at both ends, with the longitudinal coordinate axis $q_\parallel$ pointing along the velocity vector of magnitude $\dot q$, the stability matrix of $S(q,q',E)$ has a column and a row of zeros as (31.43) takes form

$$\dot q \frac{\partial^2 S}{\partial q_\parallel \partial q'_i} = \frac{\partial^2 S}{\partial q_i \partial q'_\parallel}\dot q' = 0\,.$$

The initial and final velocities are non-vanishing except for points $|\dot q| = 0$. These are the turning points (where all energy is potential), and we assume that neither q nor q' is a turning point (in our application - periodic orbits - we can always chose $q = q'$ not a turning point). In the local coordinate system with one axis along the trajectory and all other perpendicular to it the determinant of (31.41) is of the form

$$\det D(q,q',E) = (-1)^{D+1}\begin{pmatrix} & 0 & 0 & \frac{\partial^2 S}{\partial E\partial q'_\parallel} \\ \det & 0 & \frac{\partial^2 S}{\partial q_\perp \partial q'_\perp} & * \\ & \frac{\partial^2 S}{\partial q_\parallel \partial E} & * & * \end{pmatrix}. \tag{31.44}$$

The corner entries can be evaluated using (31.17)

$$\frac{\partial^2 S}{\partial q_\parallel \partial E} = \frac{\partial}{\partial q_\parallel}t = \frac{1}{\dot q}\,, \qquad \frac{\partial^2 S}{\partial E \partial q'_\parallel} = \frac{1}{\dot q'}\,.$$

As the $q_\parallel$ axis points along the velocity direction, velocities $\dot q$, $\dot q'$ are by construction almost always positive non-vanishing numbers. In this way the determinant of the $[(D+1)\times(D+1)]$ dimensional matrix $D(q,q',E)$ can be reduced to the determinant of a $[(D-1)\times(D-1)]$ dimensional *transverse* matrix $D_\perp(q,q',E)$

$$\begin{aligned} \det D(q,q',E) &= \frac{1}{\dot{q}\dot{q}'}\det D_\perp(q,q',E) \\ D_\perp(q,q',E)_{ik} &= -\frac{\partial^2 S(q,q',E)}{\partial q_{\perp i}\partial q'_{\perp k}}\,. \end{aligned} \qquad (31.45)$$

31.17 page 588

Putting everything together we obtain the jth trajectory contribution to the semiclassical Green's function

$$G_j(q,q',E) = \frac{1}{i\hbar(2\pi i\hbar)^{(D-1)/2}}\frac{1}{|\dot{q}\dot{q}'|^{1/2}}\left|\det D_\perp^j\right|^{1/2} e^{\frac{i}{\hbar}S_j-\frac{i\pi}{2}m_j}, \quad (31.46)$$

where the topological index $m_j = m_j(q,q',E)$ now counts the number of changes of sign of $\det D_\perp^j$ along the trajectory j which connects q' to q at energy E.

The endpoint velocities $\dot{q}$, $\dot{q}'$ also depend on (q,q',E) and the trajectory j.

31.3.3 Short trajectories

The stationary phase method cannot be used when t^* is small, both because we cannot extend the integration in (30.16) to $-\infty$, and because the amplitude of $K(q,q',t)$ is divergent. In this case we have to evaluate the integral involving the short time form of the exact quantum mechanical propagator (31.26)

$$G_0(q,q',E) = \frac{1}{i\hbar}\int_0^\infty dt\left(\frac{m}{2\pi i\hbar t}\right)^{D/2} e^{\frac{i}{\hbar}\left(\frac{m(q-q')^2}{2t}-V(q)t+Et\right)}\,. \qquad (31.47)$$

By introducing a dimensionless variable $\tau = t\sqrt{2m(E-V(q))}/m|q-q'|$, the integral can be rewritten as

$$G_0(q,q',E) = \frac{m}{i\hbar^2(2\pi i)^{D/2}}\left(\frac{\sqrt{2m(E-V)}}{\hbar|q-q'|}\right)^{\frac{D}{2}-1}\int_0^\infty \frac{d\tau}{\tau^{D/2}}e^{\frac{i}{2\hbar}S_0(q,q',E)(\tau+1/\tau)},$$

where $S_0(q,q',E) = \sqrt{2m(E-V)}|q-q'|$ is the short distance form of the action. Using the integral representation of the Hankel function of first kind

$$H_\nu^+(z) = -\frac{i}{\pi}e^{-i\nu\pi/2}\int_0^\infty e^{\frac{1}{2}iz(\tau+1/\tau)}\tau^{-\nu-1}d\tau$$

we can write the short distance form of the Green's function as

$$G_0(q,q',E) \approx -\frac{im}{2\hbar^2}\left(\frac{\sqrt{2m(E-V)}}{2\pi\hbar|q-q'|}\right)^{\frac{D-2}{2}} H^+_{\frac{D-2}{2}}(S_0(q,q',E)/\hbar)\,. \quad (31.48)$$

Hankel functions are stabdard, and their the short wavelength asymptotics is described in standard reference books. The short distance Green's function approximation is valid when $S_0(q,q',E)\leq\hbar$.

Commentary

Remark 31.1 Limit $\hbar\to 0$. The semiclassical limit "$\hbar\to 0$" discussed in sect. 31 is a shorthand notation for the limit in which typical quantities like the actions R or S in semiclassical expressions for the propagator or the Green's function become large compared to $\hbar$. In the world that we live in the quantity $\hbar$ is a fixed physical constant whose value [31.8] is 1.054571596(82) 10^{-34} Js.

Remark 31.2 Madelung's fluid dynamics. Already Schrödinger [31.3] noted that

$$\rho = \rho(q,t) := A^2 = \psi^*\psi$$

plays the role of a density, and that the gradient of R may be interpreted as a local semiclassical momentum, as the momentum density is

$$\psi(q,t)^*(-i\hbar\frac{\partial}{\partial q})\psi(q,t) \;=\; -i\hbar A\frac{\partial A}{\partial q}+\rho\frac{\partial R}{\partial q}\,.$$

A very different interpretation of (31.3–31.4) has been given by Madelung [31.2], and then built upon by Bohm [31.6] and others [31.3, 31.7]. Keeping the $\hbar$ dependent term in (31.3), the ordinary differential equations driving the flow (31.10) have to be altered; if the Hamiltonian can be written as kinetic plus potential term $V(q)$ as in (29.2), the $\hbar^2$ term modifies the p equation of motion as

$$\dot{p}_i = -\frac{\partial}{\partial q_i}\left(V(q)+Q(q,t)\right)\,, \qquad (31.49)$$

where, for the example at hand,

$$Q(q,t) = -\frac{\hbar^2}{2m}\frac{1}{\sqrt{\rho}}\frac{\partial^2}{\partial q^2}\sqrt{\rho} \qquad (31.50)$$

interpreted by Bohm [31.6] as the "quantum potential". Madelung observed that Hamilton's equation for the momentum (31.49) can be rewritten as

$$\frac{\partial v_i}{\partial t}+\left(v\cdot\frac{\partial}{\partial q}\right)v_i = -\frac{1}{m}\frac{\partial V}{\partial q_i}-\frac{1}{m\rho}\frac{\partial}{\partial q_j}\sigma_{ij}\,, \qquad (31.51)$$

where $\sigma_{ij} = \frac{\hbar^2 \rho}{4m} \frac{\partial^2 \ln \rho}{\partial q_i \partial q_j}$ is the "pressure" stress tensor, $v_i = p_i/m$, and $\rho = A^2$ as defined [31.3] in sect. 31.1.3. We recall that the Eulerian $\frac{\partial}{\partial t} + \frac{\partial q_i}{\partial t} \frac{\partial}{\partial q_i}$ is the ordinary derivative of Lagrangian mechanics, that is $\frac{d}{dt}$. For comparison, the Euler equation for classical hydrodynamics is

$$\frac{\partial v_i}{\partial t} + \left(v \cdot \frac{\partial}{\partial q} \right) v_i = -\frac{1}{m} \frac{\partial V}{\partial q_i} - \frac{1}{m\rho} \frac{\partial}{\partial q_j} (p\delta_{ij}) ,$$

where $p\delta_{ij}$ is the pressure tensor.

The classical dynamics corresponding to quantum evolution is thus that of an "hypothetical fluid" experiencing $\hbar$ and ρ dependent stresses. The "hydrodynamic" interpretation of quantum mechanics has, however, not been very fruitful in practice.

Remark 31.3 Path integrals. The semiclassical propagator (31.30) can also be derived from Feynman's path integral formalism. Dirac was the first to discover that in the short-time limit the quantum propagator (31.34) is exact. Feynman noted in 1946 that one can construct the exact propagator of the quantum Schrödinger equation by formally summing over all possible (and emphatically not classical) paths from q' to q .

Gutzwiller started from the path integral to rederive Van Vleck's semiclassical expression for the propagator; Van Vleck's original derivation is very much in the spirit of what has presented in this chapter. He did, however, not consider the possibility of the formation of caustics or folds of Lagrangian manifolds and thus did not include the topological phases in his semiclassical expression for the propagator. Some 40 years later Gutzwiller [32.4] added the topological indices when deriving the semiclassical propagator from Feynman's path integral by stationary phase conditions.

Résumé

The aim of the semiclassical or short-wavelength methods is to approximate a solution of the Schrödinger equation with a semiclassical wave function

$$\psi_{sc}(q,t) = \sum_j A_j(q,t) e^{iR_j(q,t)/\hbar} ,$$

accurate to the leading order in $\hbar$. Here the sum is over all classical trajectories that connect the initial point q' to the final point q in time t. "Semi–" refers to $\hbar$, the quantum unit of phase in the exponent. The quantum mechanics enters only through this atomic scale, in units of which the variation of the phase across the classical potential is assumed to be large. "–classical" refers to the rest - both the amplitudes $A_j(q,t)$ and the phases $R_j(q,t)$ - which are determined by the classical Hamilton-Jacobi equations.

In the semiclassical approximation the quantum time evolution operator is given by the *semiclassical propagator*

$$K_{sc}(q,q',t) = \frac{1}{(2\pi i\hbar)^{D/2}} \sum_j \left| \det \frac{\partial p'}{\partial q} \right|_j^{1/2} e^{\frac{i}{\hbar}R_j - \frac{i\pi}{2}m_j} ,$$

where the topological index $m_j(q,q',t)$ counts the number of the direction reversal along the jth classical trajectory that connects $q' \to q$ in time t. Until very recently it was not possible to resolve quantum evolution on quantum time scales (such as one revolution of electron around a nucleus) - physical measurements are almost always done at time scales asymptotically large compared to the intrinsic quantum time scale. Formally this information is extracted by means of a Laplace transform of the propagator which yields the energy dependent *semiclassical Green's function*

$$\begin{aligned} G_{sc}(q,q',E) &= G_0(q,q',E) + \sum_j G_j(q,q',E) \\ G_j(q,q',E) &= \frac{1}{i\hbar(2\pi i\hbar)^{\frac{(D-1)}{2}}} \left| \frac{1}{\dot{q}\dot{q}'} \det \frac{\partial p'_\perp}{\partial q_\perp} \right|_j^{1/2} e^{\frac{i}{\hbar}S_j - \frac{i\pi}{2}m_j} \qquad (31.52) \end{aligned}$$

where $G_0(q,q',E)$ is the contribution of short trajectories with $S_0(q,q',E) \leq \hbar$, while the sum is over the contributions of long trajectories (31.46) going from q' to q with fixed energy E, with $S_j(q,q',E) \gg \hbar$.

References

[31.1] A. Einstein, "On the Quantum Theorem of Sommerfeld and Epstein," p. 443, English translation of "Zum Quantensatz von Sommerfeld und Epstein", *Verh. Deutsch. Phys. Ges.* **19**, 82 (1917), in *The Collected Papers of Albert Einstein*, Volume **6**: *The Berlin Years: Writings, 1914-1917*, A. Engel, transl. and E. Schucking, (Princeton University Press, Princeton, New Jersey 1997).

[31.2] E. Madelung, *Zeitschr. fr Physik* **40**, 332 (1926).

[31.3] E. Schrödinger, *Annalen der Physik* **79**, 361, 489; **80**, 437, **81**, 109 (1926).

[31.4] J. H. van Vleck, *Quantum Principles and the Line Spectra*, Bull. Natl. Res. Council **10**, 1 (1926).

[31.5] J. H. van Vleck, *Proc. Natl. Acad. Sci.* **14**, 178 (1928).

[31.6] D. Bohm, *Phys. Rev.* **85**, 166 (1952).

[31.7] P.R. Holland, *The quantum theory of motion - An account of the de Broglie-Bohm casual interpretation of quantum mechanics* (Cambridge Univ. Press, Cambridge 1993).

[31.8] `physics.nist.gov/cgi-bin/cuu`

Exercises

Exercise 31.1 **Who ordered $\sqrt{\pi}$?** *Derive the Gaussian integral*

$$\frac{1}{\sqrt{2\pi}}\int_{-\infty}^{\infty} dx\, e^{-\frac{x^2}{2a}} = \sqrt{a}\,, \qquad a > 0\,.$$

assuming only that you know to integrate the exponential function e^{-x}. Hint, hint: x^2 is a radius-squared of something. π is related to the area or circumference of something.

Exercise 31.2 **Dirac delta function, Gaussian representation.** *Consider the Gaussian distribution function*

$$\delta_\sigma(z) = \frac{1}{\sqrt{2\pi\sigma^2}} e^{-z^2/2\sigma^2}\,.$$

Show that in $\sigma \to 0$ limit this is the Dirac delta function

$$\int_{\mathcal{M}} dx\,\delta(x) = 1 \text{ if } 0 \in \mathcal{M}\,, \text{ zero otherwise}\,.$$

Exercise 31.3 **D-dimensional Gaussian integrals.** *Show that the Gaussian integral in D-dimensions is given by*

$$\frac{1}{(2\pi)^{d/2}}\int d^d\phi\, e^{-\frac{1}{2}\phi^T\cdot M^{-1}\cdot\phi+\phi\cdot J} = |\det M|^{\frac{1}{2}}\, e^{\frac{1}{2}J^T\cdot M\cdot J}\,, \tag{31.53}$$

where M is a real positive definite $[d\times d]$ matrix, that is a matrix with strictly positive eigenvalues. x, J are D-dimensional vectors, and x^T is the transpose of x.

Exercise 31.4 **Stationary phase approximation in higher dimensions.** *All semiclassical approximations are based on saddlepoint evaluations of integrals of type*

$$I = \int d^D x A(x) e^{i\Phi(x)/\hbar} \tag{31.54}$$

for small values of $\hbar$. Obtain the stationary phase estimate

$$I \approx \sum_n A(x_n) e^{i\Phi(x_n)/\hbar} \frac{(2\pi i\hbar)^{D/2}}{\sqrt{\det \mathbf{D}^2\Phi(x_n)}},$$

where $\mathbf{D}^2\Phi(x_n)$ denotes the second derivative matrix.

Exercise 31.5 **Schrödinger equation in the Madelung form.** *Verify the decomposition of Schrödinger equation into real and imaginary parts, eqs. (31.3) and (31.4).*

Exercise 31.6 **Transport equations.** *Write the wave-function in the asymptotic form*

$$\psi(q,t) = e^{\frac{i}{\hbar}R(x,t)+\frac{i}{\hbar}\varepsilon t}\sum_{n\geq 0}(i\hbar)^n A_n(x,t)\,.$$

Derive the transport equations for the A_n by substituting this into the Schrödinger equation and then collecting terms by orders of $\hbar$. Notice that equation for $\dot{A}_n$ only requires knowledge of A_{n-1} and R.

Exercise 31.7 **Easy examples of the Hamilton's principal function.** *Calculate $R(q,q',t)$ for*

a) a D-dimensional free particle

b) a 3-dimensional particle in constant magnetic field

c) a 1-dimensional harmonic oscillator.

(Continuation: exercise 31.15.)

Exercise 31.8 **1-dimensional harmonic oscillator.** *Take a 1-dimensional harmonic oscillator $U(q) = \frac{1}{2}kq^2$. Take a WKB wave function of form $A(q,t) = a(t)$ and $R(q,t) = r(t) + b(t)q + c(t)q^2$, where $r(t), a(t), b(t)$ and $c(t)$ are time dependent coefficients. Derive ordinary differential equations by using (31.3) and (31.4) and solve them. (Continuation: exercise 31.11.)*

Exercise 31.9 **1-dimensional linear potential.** *Take a 1-dimensional linear potential $U(q) = -Fq$. Take a WKB wave function of form $A(q,t) = a(t)$ and $R(q,t) = r(t) + b(t)q + c(t)q^2$, where $r(t), a(t), b(t)$ and $c(t)$ are time dependent coefficients. Derive and solve the ordinary differential equations from (31.3) and (31.4).*

Exercise 31.10 **D-dimensional quadratic potentials.** *Generalize the above method to general D-dimensional quadratic potentials.*

Exercise 31.11 **Time evolution of R.** *(Continuation of exercise 31.8). Calculate the time evolution of $R(q,0) = a + bq + cq^2$ for a 1-dimensional harmonic oscillator using (31.12) and (31.14).*

Exercise 31.12 **D-dimensional free particle propagator.** *Verify the results in sect. 31.2.2; show explicitly that (31.34), the semiclassical Van Vleck propagator in D dimensions, solves the Schrödinger's equation.*

Exercise 31.13 **Propagator, charged particle in constant magnetic field.** *Calculate the semiclassical propagator for a charged particle in constant magnetic field in 3 dimensions. Verify that the semiclassical expression coincides with the exact solution.*

Exercise 31.14 **1-dimensional harmonic oscillator propagator.** *Calculate the semiclassical propagator for a 1-dimensional harmonic oscillator and verify that it is identical to the exact quantum propagator.*

Exercise 31.15 **Free particle action.** *Calculate the energy dependent action for a free particle, a charged particle in a constant magnetic field and for the harmonic oscillator.*

Exercise 31.16 **Zero length orbits.** *Derive the classical trace (16.1) rigorously and either add the $t \to 0_+$ zero length contribution to the trace formula, or show that it vanishes. Send us a reprint of* Phys. Rev. Lett. *with the correct derivation.*

Exercise 31.17 **Free particle semiclassical Green's functions.** *Calculate the semiclassical Green's functions for the systems of exercise 31.15.*

Chapter 32

Semiclassical quantization

(G. Vattay, G. Tanner and P. Cvitanović)

We derive here the Gutzwiller trace formula and the semiclassical zeta function, the central results of the semiclassical quantization of classically chaotic systems. In chapter 33 we will rederive these formulas for the case of scattering in open systems. Quintessential wave mechanics effects such as creeping, diffraction and tunneling will be taken up in chapter 36.

32.1 Trace formula

Our next task is to evaluate the Green's function trace (29.17) in the semiclassical approximation. The trace

$$\mathrm{tr}\, G_{sc}(E) = \int d^D q\, G_{sc}(q,q,E) = \mathrm{tr}\, G_0(E) + \sum_j \int d^D q\, G_j(q,q,E)$$

receives contributions from "long" classical trajectories labeled by j which start and end in q after finite time, and the "zero length" trajectories whose lengths approach zero as $q' \to q$.

First, we work out the contributions coming from the finite time *returning* classical orbits, i.e., trajectories that originate and end at a given configuration point q. As we are identifying q with q', taking of a trace involves (still another!) stationary phase condition in the $q' \to q$ limit,

$$\left.\frac{\partial S_j(q,q',E)}{\partial q_i}\right|_{q'=q} + \left.\frac{\partial S_j(q,q',E)}{\partial q'_i}\right|_{q'=q} = 0\,,$$

meaning that the initial and final momenta (31.40) of contributing trajectories should coincide

$$p_i(q,q,E) - p'_i(q,q,E) = 0\,, \qquad q \in j\text{th periodic orbit}\,, \tag{32.1}$$

Figure 32.1: A returning trajectory in the configuration space. The orbit is periodic in the full phase space only if the initial and the final momenta of a returning trajectory coincide as well.

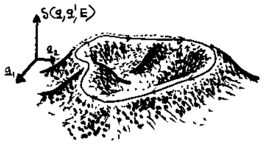

Figure 32.2: A romanticized sketch of $S_p(E) = S(q,q,E) = \oint p(q,E)dq$ landscape orbit. Unstable periodic orbits traverse isolated ridges and saddles of the mountainous landscape of the action $S(q_\parallel, q_\perp, E)$. Along a periodic orbit $S_p(E)$ is constant; in the transverse directions it generically changes quadratically.

so the trace receives contributions only from those long classical trajectories which are *periodic* in the full phase space.

For a periodic orbit the natural coordinate system is the intrinsic one, with $q_\parallel$ axis pointing in the $\dot q$ direction along the orbit, and $q_\perp$, the rest of the coordinates transverse to $\dot q$. The jth periodic orbit contribution to the trace of the semiclassical Green's function in the intrinsic coordinates is

$$\mathrm{tr}\, G_j(E) = \frac{1}{i\hbar(2\pi\hbar)^{(d-1)/2}} \oint_j \frac{dq_\parallel}{\dot q} \int_j d^{d-1}q_\perp |\det D_\perp^j|^{1/2} e^{\frac{i}{\hbar}S_j - \frac{i\pi}{2}m_j},$$

where the integration in $q_\parallel$ goes from 0 to L_j, the geometric length of small tube around the orbit in the configuration space. As always, in the stationary phase approximation we worry only about the fast variations in the phase $S_j(q_\parallel, q_\perp, E)$, and assume that the density varies smoothly and is well approximated by its value $D_\perp^j(q_\parallel, 0, E)$ on the classical trajectory, $q_\perp = 0$. The topological index $m_j(q_\parallel, q_\perp, E)$ is an integer which does not depend on the initial point $q_\parallel$ and not change in the infinitesimal neighborhood of an isolated periodic orbit, so we set $m_j(E) = m_j(q_\parallel, q_\perp, E)$.

The transverse integration is again carried out by the stationary phase method, with the phase stationary on the periodic orbit, $q_\perp = 0$. The result of the transverse integration can depend only on the parallel coordinate

$$\mathrm{tr}\, G_j(E) = \frac{1}{i\hbar} \oint \frac{dq_\parallel}{\dot q} \left| \frac{\det D_{\perp j}(q_\parallel, 0, E)}{\det D'_{\perp j}(q_\parallel, 0, E)} \right|^{1/2} e^{\frac{i}{\hbar}S_j - \frac{i\pi}{2}m_j},$$

where the new determinant in the denominator, $\det D'_{\perp j} =$

$$\det \left(\frac{\partial^2 S(q,q',E)}{\partial q_{\perp i}\partial q_{\perp j}} + \frac{\partial^2 S(q,q',E)}{\partial q'_{\perp i}\partial q_{\perp j}} + \frac{\partial^2 S(q,q',E)}{\partial q_{\perp i}\partial q'_{\perp j}} + \frac{\partial^2 S(q,q',E)}{\partial q'_{\perp i}\partial q'_{\perp j}} \right),$$

is the determinant of the second derivative matrix coming from the stationary phase integral in transverse directions. Mercifully, this integral also removes most of the $2\pi\hbar$ prefactors in (??).

The ratio $\det D_{\perp j}/\det D'_{\perp j}$ is here to enforce the periodic boundary condition for the semiclassical Green's function evaluated on a periodic orbit. It can be given a meaning in terms of the monodromy matrix of the periodic orbit by following observations

$$\begin{aligned}
\det D_\perp &= \left\| \frac{\partial p'_\perp}{\partial q_\perp} \right\| = \left\| \frac{\partial(q'_\perp, p'_\perp)}{\partial(q_\perp, q'_\perp)} \right\| \\
\det D'_\perp &= \left\| \frac{\partial p_\perp}{\partial q_\perp} - \frac{\partial p'_\perp}{\partial q_\perp} + \frac{\partial p_\perp}{\partial q'_\perp} - \frac{\partial p'_\perp}{\partial q'_\perp} \right\| = \left\| \frac{\partial(p_\perp - p'_\perp, q_\perp - q'_\perp),}{\partial(q_\perp, q'_\perp)} \right\| .
\end{aligned}$$

Defining the $2(D-1)$-dimensional transverse vector $x_\perp = (q_\perp, p_\perp)$ in the full phase space we can express the ratio

$$\begin{aligned}
\frac{\det D'_\perp}{\det D_\perp} &= \left\| \frac{\partial(p_\perp - p'_\perp, q_\perp - q'_\perp)}{\partial(q'_\perp, p'_\perp)} \right\| = \left\| \frac{\partial(x_\perp - x'_\perp)}{\partial x'_\perp} \right\| \\
&= \det\,(M - \mathbf{1}) \,, \qquad (32.2)
\end{aligned}$$

in terms of the monodromy matrix M for a surface of section transverse to the orbit within the constant energy $E = H(q,p)$ shell.

The classical periodic orbit action $S_j(E) = \oint p(q_\parallel, E)dq_\parallel$ is an integral around a loop defined by the periodic orbit, and does not depend on the starting point $q_\parallel$ along the orbit, see figure 32.2. The eigenvalues of the monodromy matrix are also independent of where M_j is evaluated along the orbit, so $\det(1 - M_j)$ can also be taken out of the the $q_\parallel$ integral

$$\mathrm{tr}\, G_j(E) = \frac{1}{i\hbar} \sum_j \frac{1}{|\det(1 - M_j)|^{1/2}} e^{r(\frac{i}{\hbar}S_j - \frac{i\pi}{2}m_j)} \oint \frac{dq_\parallel}{\dot q_\parallel} .$$

Here we have assumed that M_j has no marginal eigenvalues. The determinant of the monodromy matrix, the action $S_p(E) = \oint p(q_\parallel, E)dq_\parallel$ and the topological index are all classical invariants of the periodic orbit. The integral in the parallel direction we now do exactly.

First, we take into account the fact that any repeat of a periodic orbit is also a periodic orbit. The action and the topological index are additive along the trajectory, so for rth repeat they simply get multiplied by r. The monodromy matrix of the rth repeat of a prime cycle p is (by the chain rule for derivatives) M_p^r, where M_p is the prime cycle monodromy matrix. Let us denote the time period of the prime cycle p, the single, shortest traversal of a periodic orbit by T_p. The remaining integral can be carried out by change of variables $dt = dq_\parallel/\dot q(t)$

$$\int_0^{L_p} \frac{dq_\parallel}{\dot q(t)} = \int_0^{T_p} dt = T_p \,.$$

Note that the spatial integral corresponds to a *single* traversal. If you do not see why this is so, rethink the derivation of the classical trace formula (16.23) - that derivation takes only three pages of text. Regrettably, in the quantum case we do not know of an honest derivation that takes less than 30 pages. The final result, the *Gutzwiller trace formula*

$$\operatorname{tr} G_{sc}(E) = \operatorname{tr} G_0(E) + \frac{1}{i\hbar}\sum_p T_p \sum_{r=1}^{\infty} \frac{1}{|\det(1-M_p^r)|^{1/2}} e^{r(\frac{i}{\hbar}S_p - \frac{i\pi}{2}m_p)}, \quad (32.3)$$

an expression for the trace of the semiclassical Green's function in terms of periodic orbits, is beautiful in its simplicity and elegance.

The topological index $m_p(E)$ counts the number of changes of sign of the matrix of second derivatives evaluated along the prime periodic orbit p. By now we have gone through so many stationary phase approximations that you have surely lost track of what the total $m_p(E)$ actually is. The rule is this: The topological index of a closed curve in a $2D$ phase space is the sum of the number of times the partial derivatives $\frac{\partial p_i}{\partial q_i}$ for each dual pair (q_i, p_i), $i = 1, 2, \ldots, D$ (no sum on i) change their signs as one goes once around the curve.

32.1.1 Average density of states

We still have to evaluate $\operatorname{tr} G_0(E)$, the contribution coming from the infinitesimal trajectories. The real part of $\operatorname{tr} G_0(E)$ is infinite in the $q' \to q$ limit, so it makes no sense to write it down explicitly here. However, the imaginary part is finite, and plays an important role in the density of states formula, which we derive next.

The semiclassical contribution to the density of states (29.17) is given by the imaginary part of the Gutzwiller trace formula (32.3) multiplied with $-1/\pi$. The contribution coming from the zero length trajectories is the imaginary part of (31.48) for $q' \to q$ integrated over the configuration space

$$d_0(E) = -\frac{1}{\pi}\int d^D q \, \mathrm{Im}\, \mathrm{G}_0(\mathrm{q},\mathrm{q},\mathrm{E}),$$

The resulting formula has a pretty interpretation; it estimates the number of quantum states that can be accomodated up to the energy E by counting the available quantum cells in the phase space. This number is given by the *Weyl rule* , as the ratio of the phase space volume bounded by energy E divided by h^D, the volume of a quantum cell,

$$N_{sc}(E) = \frac{1}{h^D}\int d^D p d^D q \, \Theta(E - H(q,p)) \,. \quad (32.4)$$

where $\Theta(x)$ is the Heaviside function (29.22). $N_{sc}(E)$ is an estimate of the spectral staircase (29.21), so its derivative yields the average density of states

$$d_0(E) = \frac{d}{dE}N_{sc}(E) = \frac{1}{h^D}\int d^D p d^D q \, \delta(E - H(q,p)) \,, \quad (32.5)$$

precisely the semiclassical result (32.6). For Hamiltonians of type $p^2/2m + V(q)$, the energy shell volume in (32.5) is a sphere of radius $\sqrt{2m(E-V(q))}$. The surface of a d-dimensional sphere of radius r is $\pi^{d/2} r^{d-1}/\Gamma(d/2)$, so the average density of states is given by

32.3 page 602

$$d_0(E) = \frac{2m}{\hbar^D 2^d \pi^{D2}\Gamma(D/2)}\int_{V(q)<E} d^D q \, [2m(E - V(q))]^{D/2-1} \,, \quad (32.6)$$

and

$$N_{sc}(E) = \frac{1}{h^D}\frac{\pi^{D/2}}{\Gamma(1+D/2)}\int_{V(q)<E} d^D q \, [2m(E - V(q))]^{D/2} \,. \quad (32.7)$$

Physically this means that at a fixed energy the phase space can support $N_{sc}(E)$ distinct eigenfunctions; anything finer than the quantum cell h^D cannot be resolved, so the quantum phase space is effectively finite dimensional. The average density of states is of a particularly simple form in one spatial dimension

32.4 page 602

$$d_0(E) = \frac{T(E)}{2\pi\hbar} \,, \quad (32.8)$$

where $T(E)$ is the period of the periodic orbit of fixed energy E. In two spatial dimensions the average density of states is

$$d_0(E) = \frac{m\mathcal{A}(E)}{2\pi\hbar^2} \,, \quad (32.9)$$

where $\mathcal{A}(E)$ is the classically allowed area of configuration space for which $V(q) < E$.

32.5 page 602

The semiclassical density of states is a sum of the average density of states and the oscillation of the density of states around the average, $d_{sc}(E) = d_0(E) + d_{osc}(E)$, where

$$d_{osc}(E) = \frac{1}{\pi\hbar}\sum_p T_p \sum_{r=1}^{\infty} \frac{\cos(rS_p(E)/\hbar - rm_p\pi/2)}{|\det(1-M_p^r)|^{1/2}} \quad (32.10)$$

follows from the trace formula (32.3).

32.1.2 Regularization of the trace

The real part of the $q' \to q$ zero length Green's function (31.48) is ultraviolet divergent in dimensions $d > 1$, and so is its formal trace (29.17). The short distance behavior of the real part of the Green's function can be extracted from the real part of (31.48) by using the Bessel function expansion for small z

$$Y_\nu(z) \approx \begin{cases} -\frac{1}{\pi}\Gamma(\nu)\left(\frac{z}{2}\right)^{-\nu} & \text{for } \nu \neq 0 \\ \frac{2}{\pi}(\ln(z/2)+\gamma) & \text{for } \nu = 0 \end{cases},$$

where $\gamma = 0.577...$ is the Euler constant. The real part of the Green's function for short distance is dominated by the singular part

$$G_{sing}(|q-q'|, E) = \begin{cases} -\frac{m}{2\hbar^2\pi^{\frac{d}{2}}}\Gamma((d-2)/2)\frac{1}{|q-q'|^{d-2}} & \text{for } d \neq 2 \\ \\ \frac{m}{2\pi\hbar^2}(\ln(2m(E-V)|q-q'|/2\hbar)+\gamma) & \text{for } d = 2 \end{cases}.$$

The *regularized* Green's function

$$G_{reg}(q, q', E) = G(q, q', E) - G_{sing}(|q-q'|, E)$$

is obtained by subtracting the $q' \to q$ ultraviolet divergence. For the regularized Green's function the Gutzwiller trace formula is

$$\operatorname{tr} G_{reg}(E) = -i\pi d_0(E) + \frac{1}{i\hbar}\sum_p T_p \sum_{r=1}^{\infty} \frac{e^{r(\frac{i}{\hbar}S_p(E) - \frac{i\pi}{2}m_p(E))}}{|\det(1-M_p^r)|^{1/2}}. \qquad (32.11)$$

Now you stand where Gutzwiller stood in 1990. You hold the trace formula in your hands. You have no clue how good is the $\hbar \to 0$ approximation, how to take care of the sum over an infinity of periodic orbits, and whether the formula converges at all.

32.2 Semiclassical spectral determinant

The problem with trace formulas is that they diverge where we need them, at the individual energy eigenvalues. What to do? Much of the quantum chaos literature responds to the challenge of wrestling the trace formulas by replacing the delta functions in the density of states (29.18) by Gaussians. But there is no need to do this - we can compute the eigenenergies without any further ado by remembering that the smart way to determine the eigenvalues of linear operators is by determining zeros of their spectral determinants.

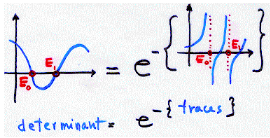

Figure 32.3: A sketch of how spectral determinants convert poles into zeros: The trace shows $1/(E-E_n)$ type singularities at the eigenenergies while the spectral determinant goes smoothly through zeroes.

A sensible way to compute energy levels is to construct the spectral determinant whose zeroes yield the eigenenergies, $\det(\hat{H}-E)_{sc} = 0$. A first guess might be that the spectral determinant is the Hadamard product of form

$$\det(\hat{H}-E) = \prod_n (E-E_n),$$

but this product is not well defined, since for fixed E we multiply larger and larger numbers $(E-E_n)$. This problem is dealt with by *regularization*, discussed below in appendix 32.1.2. Here we offer an impressionistic sketch of regularization.

The logarithmic derivative of $\det(\hat{H}-E)$ is the (formal) trace of the Green's function

$$-\frac{d}{dE}\ln\det(\hat{H}-E) = \sum_n \frac{1}{E-E_n} = \operatorname{tr} G(E).$$

This quantity, not surprisingly, is divergent again. The relation, however, opens a way to derive a convergent version of $\det(\hat{H}-E)_{sc}$, by replacing the trace with the regularized trace

$$-\frac{d}{dE}\ln\det(\hat{H}-E)_{sc} = \operatorname{tr} G_{reg}(E).$$

The regularized trace still has $1/(E-E_n)$ poles at the semiclassical eigenenergies, poles which can be generated only if $\det(\hat{H}-E)_{sc}$ has a zero at $E = E_n$, see figure 32.3. By integrating and exponentiating we obtain

$$\det(\hat{H}-E)_{sc} = \exp\left(-\int^E dE' \operatorname{tr} G_{reg}(E')\right)$$

Now we can use (32.11) and integrate the terms coming from periodic orbits, using the relation (31.17) between the action and the period of a periodic orbit, $dS_p(E) = T_p(E)dE$, and the relation (29.21) between the density of states and the spectral staircase, $dN_{sc}(E) = d_0(E)dE$. We obtain the *semiclassical zeta function*

$$\det(\hat{H}-E)_{sc} = e^{i\pi N_{sc}(E)} \exp\left(-\sum_p \sum_{r=1}^{\infty} \frac{1}{r}\frac{e^{ir(S_p/\hbar - m_p\pi/2)}}{|\det(1-M_p^r)|^{1/2}}\right). \qquad (32.12)$$

chapter 18

We already know from the study of classical evolution operator spectra of chapter 17 that this can be evaluated by means of cycle expansions. The beauty of this formula is that everything on the right side – the cycle action S_p, the topological index m_p and monodromy matrix M_p determinant – is intrinsic, coordinate-choice independent property of the cycle p.

32.3 One-dof systems

It has been a long trek, a stationary phase upon stationary phase. Let us check whether the result makes sense even in the simplest case, for quantum mechanics in one spatial dimension.

In one dimension the average density of states follows from the one-dof form of the oscillating density (32.10) and of the average density (32.8)

$$d(E) = \frac{T_p(E)}{2\pi\hbar} + \sum_r \frac{T_p(E)}{\pi\hbar} \cos(rS_p(E)/\hbar - rm_p(E)\pi/2). \qquad (32.13)$$

The classical particle oscillates in a single potential well with period $T_p(E)$. There is no monodromy matrix to evaluate, as in one dimension there is only the parallel coordinate, and no transverse directions. The r repetition sum in (32.13) can be rewritten by using the Fourier series expansion of a delta spike train

$$\sum_{n=-\infty}^{\infty} \delta(x-n) = \sum_{k=-\infty}^{\infty} e^{i2\pi kx} = 1 + \sum_{k=1}^{\infty} 2\cos(2\pi kx).$$

We obtain

$$d(E) = \frac{T_p(E)}{2\pi\hbar} \sum_n \delta(S_p(E)/2\pi\hbar - m_p(E)/4 - n). \qquad (32.14)$$

This expression can be simplified by using the relation (31.17) between T_p and S_p, and the identity (14.7) $\delta(x-x^*) = |f'(x)|\delta(f(x))$, where x^* is the only zero of the function $f(x^*) = 0$ in the interval under consideration. We obtain

$$d(E) = \sum_n \delta(E - E_n),$$

where the energies E_n are the zeroes of the arguments of delta functions in (32.14)

$$S_p(E_n)/2\pi\hbar = n - m_p(E)/4\,,$$

where $m_p(E) = m_p = 2$ for smoth potential at both turning points, and $m_p(E) = m_p = 4$ for two billiard (infinite potential) walls. These are precisely the *Bohr-Sommerfeld quantized energies* E_n, defined by the condition

$$\oint p(q, E_n)dq = h\left(n - \frac{m_p}{4}\right). \qquad (32.15)$$

In this way the trace formula recovers the well known 1-dof quantization rule. In one dimension, the average of states can be expressed from the quantization condition. At $E = E_n$ the exact number of states is n, while the average number of states is $n - 1/2$ since the staircase function $N(E)$ has a unit jump in this point

$$N_{sc}(E) = n - 1/2 = S_p(E)/2\pi\hbar - m_p(E)/4 - 1/2. \qquad (32.16)$$

The 1-dof spectral determinant follows from (32.12) by dropping the monodromy matrix part and using (32.16)

$$\det(\hat{H} - E)_{sc} = \exp\left(-\frac{i}{2\hbar}S_p + \frac{i\pi}{2}m_p\right) \exp\left(-\sum_r \frac{1}{r} e^{\frac{i}{\hbar}rS_p - \frac{i\pi}{2}rm_p}\right). \qquad (32.17)$$

Summation yields a logarithm by $\sum_r t^r/r = -\ln(1-t)$ and we get

$$\begin{aligned} \det(\hat{H} - E)_{sc} &= e^{-\frac{i}{2\hbar}S_p + \frac{im_p}{4} + \frac{i\pi}{2}}(1 - e^{\frac{i}{\hbar}S_p - i\frac{m_p}{2}}) \\ &= 2\sin\left(S_p(E)/\hbar - m_p(E)/4\right). \end{aligned}$$

So in one dimension, where there is only one periodic orbit for a given energy E, nothing is gained by going from the trace formula to the spectral determinant. The spectral determinant is a real function for real energies, and its zeros are again the Bohr-Sommerfeld quantized eigenenergies (32.15).

32.4 Two-dof systems

For flows in two configuration dimensions the monodromy matrix M_p has two eigenvalues Λ_p and $1/\Lambda_p$, as explained in sect. 6.2. Isolated periodic orbits can be elliptic or hyperbolic. Here we discuss only the hyperbolic case, when the eigenvalues are real and their absolute value is not equal to one. The determinant appearing in the trace formulas can be written in terms of the expanding eigenvalue as

$$|\det(1 - M_p^r)|^{1/2} = |\Lambda_p^r|^{1/2}\left(1 - 1/\Lambda_p^r\right),$$

and its inverse can be expanded as a geometric series

$$\frac{1}{|\det(1-M_p^r)|^{1/2}} = \sum_{k=0}^{\infty} \frac{1}{|\Lambda_p^r|^{1/2}\Lambda_p^{kr}}.$$

With the 2-dof expression for the average density of states (32.9) the spectral determinant becomes

$$\begin{aligned}
\det(\hat{H}-E)_{sc} &= e^{i\frac{mAE}{2\hbar^2}} \exp\left(-\sum_p \sum_{r=1}^{\infty}\sum_{k=0}^{\infty} \frac{e^{ir(S_p/\hbar - m_p\pi/2)}}{r|\Lambda_p^r|^{1/2}\Lambda_p^{kr}}\right) \\
&= e^{i\frac{mAE}{2\hbar^2}} \prod_p \prod_{k=0}^{\infty}\left(1-\frac{e^{\frac{i}{\hbar}S_p - \frac{i\pi}{2}m_p}}{|\Lambda_p|^{1/2}\Lambda_p^k}\right). \qquad (32.18)
\end{aligned}$$

Commentary

Remark 32.1 Zeta functions. For "zeta function" nomenclature, see remark 17.4 on page 332.

Résumé

Spectral determinants and dynamical zeta functions arise both in classical and quantum mechanics because in both the dynamical evolution can be described by the action of linear evolution operators on infinite-dimensional vector spaces. In quantum mechanics the periodic orbit theory arose from studies of semi-conductors, and the unstable periodic orbits have been measured in experiments on the very paradigm of Bohr's atom, the hydrogen atom, this time in strong external fields.

In practice, most "quantum chaos" calculations take the stationary phase approximation to quantum mechanics (the Gutzwiller trace formula, possibly improved by including tunneling periodic trajectories, diffraction corrections, etc.) as the point of departure. Once the stationary phase approximation is made, what follows is *classical* in the sense that all quantities used in periodic orbit calculations - actions, stabilities, geometrical phases - are classical quantities. The problem is then to understand and control the convergence of classical periodic orbit formulas.

While various periodic orbit formulas are formally equivalent, practice shows that some are preferable to others. Three classes of periodic orbit formulas are frequently used:

Trace formulas. The trace of the semiclassical Green's function

$$\mathrm{tr}\, G_{sc}(E) = \int dq\, G_{sc}(q,q,E)$$

is given by a sum over the periodic orbits (32.11). While easiest to derive, in calculations the trace formulas are inconvenient for anything other than the leading eigenvalue estimates, as they tend to be divergent in the region of physical interest. In classical dynamics trace formulas hide under a variety of appelations such as the f–α or multifractal formalism; in quantum mechanics they are known as the Gutzwiller trace formulas.

Zeros of *Ruelle or dynamical zeta functions*

$$1/\zeta(s) = \prod_p (1-t_p), \quad t_p = \frac{1}{|\Lambda_p|^{1/2}} e^{\frac{i}{\hbar}S_p - i\pi m_p/2}$$

yield, in combination with cycle expansions, the semiclassical estimates of *quantum* resonances. For hyperbolic systems the dynamical zeta functions have good convergence and are a useful tool for determination of classical and quantum mechanical averages.

Spectral determinants, Selberg-type zeta functions, Fredholm determinants, functional determinants are the natural objects for spectral calculations, with convergence better than for dynamical zeta functions, but with less transparent cycle expansions. The 2-dof semiclassical spectral determinant (32.18)

$$\det(\hat{H}-E)_{sc} = e^{i\pi N_{sc}(E)} \prod_p \prod_{k=0}^{\infty}\left(1-\frac{e^{iS_p/\hbar - i\pi m_p/2}}{|\Lambda_p|^{1/2}\Lambda_p^k}\right)$$

is a typical example. Most periodic orbit calculations are based on cycle expansions of such determinants.

As we have assumed repeatedly during the derivation of the trace formula that the periodic orbits are isolated, and do not form families (as is the case for integrable systems or in KAM tori of systems with mixed phase space), the formulas discussed so far are valid only for hyperbolic and elliptic periodic orbits.

For deterministic dynamical flows and number theory, spectral determinants and zeta functions are exact. The quantum-mechanical ones, derived by the Gutzwiller approach, are at best only the stationary phase approximations to the exact quantum spectral determinants, and for quantum mechanics an important conceptual problem arises already at the level of derivation of the semiclassical formulas; how accurate are they, and can the periodic orbit theory be systematically improved?

References

[32.1] R.G. Littlejohn, *J. Stat. Phys.* **68**, 7 (1992).

[32.2] L.D. Landau and E.M. Lifshitz, *Mechanics* (Pergamon, London, 1959).

[32.3] R.G. Littlejohn, *"Semiclassical structure of trace formulas"*, in G. Casati and B. Chirikov, eds., *Quantum Chaos*, (Cambridge University Press, Cambridge 1994).

[32.4] M.C. Gutzwiller, *J. Math. Phys.* **8**, 1979 (1967); **10**, 1004 (1969); **11**, 1791 (1970); **12**, 343 (1971).

[32.5] M.C. Gutzwiller, *J. Math. Phys.* **12**, 343 (1971)

[32.6] M.C. Gutzwiller, *Physica* **D5**, 183 (1982)

[32.7] M.C. Gutzwiller, *J. Phys. Chem.* **92**, 3154 (1984).

[32.8] A. Voros, *J. Phys.* **A 21**, 685 (1988).

[32.9] A. Voros, *Aspects of semiclassical theory in the presence of classical chaos*, *Prog. Theor. Phys. Suppl.* **116**, 17 (1994).

[32.10] P. Cvitanović and P.E. Rosenqvist, in G.F. Dell'Antonio, S. Fantoni and V.R. Manfredi, eds., *From Classical to Quantum Chaos, Soc. Italiana di Fisica Conf. Proceed.* **41**, pp. 57-64 (Ed. Compositori, Bologna 1993).

[32.11] A. Wirzba, *CHAOS* **2**, 77 (1992).

[32.12] P. Cvitanović, G. Vattay and A. Wirzba, *"Quantum fluids and classical determinants"*, in H. Friedrich and B. Eckhardt., eds., *Classical, Semiclassical and Quantum Dynamics in Atoms – in Memory of Dieter Wintgen*, *Lecture Notes in Physics* **485** (Springer, New York 1997), `chao-dyn/9608012`.

[32.13] E.B. Bogomolny, CHAOS **2**, 5 (1992).

[32.14] E.B. Bogomolny, *Nonlinearity* **5**, 805 (1992).

[32.15] M. Kline, *Mathematical Thought from Ancient to Modern Times* (Oxford Univ. Press, Oxford 1972); on Monge and theory of characteristics - chapter 22.7.

[32.16] E.T. Bell, *Men of Mathematics* (Penguin, London 1937).

[32.17] R.P. Feynman, *Statistical Physics* (Addison Wesley, New York 1990).

[32.18] H. Goldstein, *Classical Mechanics* (Addison-Wesley, Reading, 1980); chapter 9.

[32.19] G. Tanner and D. Wintgen, *CHAOS* **2**, 53 (1992).

[32.20] P. Cvitanović and F. Christiansen, *CHAOS* **2**, 61 (1992).

[32.21] M.V. Berry and J.P. Keating, *J. Phys.* **A 23**, 4839 (1990).

[32.22] H.H. Rugh, *"Generalized Fredholm determinants and Selberg zeta functions for Axiom A dynamical systems"*, *Ergodic Theory Dynamical Systems* **16**, 805 (1996).

[32.23] B. Eckhard and G. Russberg, Phys. Rev. **E 47**, 1578 (1993).

[32.24] D. Ruelle, *Statistical Mechanics, Thermodynamical Formalism* (Addison-Wesley, Reading MA, 1987).

[32.25] P. Szépfalusy, T. Tél, A. Csordás and Z. Kovács, Phys. Rev. **A 36**, 3525 (1987).

[32.26] H.H. Rugh, Nonlinearity **5**, 1237 (1992) and H.H. Rugh, *Ph.D. Thesis* (Niels Bohr Institute, 1993).

[32.27] P. Cvitanović, P.E. Rosenqvist, H.H. Rugh and G. Vattay, *Scattering Theory - special issue*, CHAOS (1993).

[32.28] E.J. Heller, S. Tomsovic and A. Sepúlveda CHAOS **2**, *Periodic Orbit Theory - special issue*, 105, (1992).

[32.29] V.I. Arnold, *Geometrical Methods in the Theory of Ordinary Differential Equations*, (Springer, New York 1983).

[32.30] R. Dashen, B. Hasslacher and A. Neveu , "Nonperturbative methods and extended hadron models in field theory. 1. Semiclassical functional methods.", *Phys. Rev.* **D10**, 4114 (1974).

[32.31] V.I. Arnold, *Geometrical Methods in the Theory of Ordinary Differential Equations* (Springer, New York 1983).

Exercises

Exercise 32.1 **Monodromy matrix from second variations of the action.** *Show that*

$$D_{\perp j}/D'_{\perp j} = (\mathbf{1} - M) \tag{32.19}$$

Exercise 32.2 **Jacobi gymnastics.** *Prove that the ratio of determinants in (S.46) can be expressed as*

$$\frac{\det D'_{\perp j}(q_\parallel, 0, E)}{\det D_{\perp j}(q_\parallel, 0, E)} = \det \begin{pmatrix} I - M_{qq} & -M_{qp} \\ -M_{pq} & I - M_{pp} \end{pmatrix} = \det(1 - M_j), \tag{32.20}$$

where M_j is the monodromy matrix of the periodic orbit.

Exercise 32.3 **Volume of d-dimensional sphere.** *Show that the volume of a d-dimensional sphere of radius r equals $\pi^{d/2} r^d / \Gamma(1 + d/2)$. Show that $\Gamma(1 + d/2) = \Gamma(d/2)d/2$.*

Exercise 32.4 **Average density of states in 1 dimension.** *Show that in one dimension the average density of states is given by (32.8)*

$$\bar{d}(E) = \frac{T(E)}{2\pi\hbar},$$

where $T(E)$ is the time period of the 1-dimensional motion and show that

$$\bar{N}(E) = \frac{S(E)}{2\pi\hbar}, \tag{32.21}$$

where $S(E) = \oint p(q, E)\, dq$ is the action of the orbit.

Exercise 32.5 **Average density of states in 2 dimensions.** *Show that in 2 dimensions the average density of states is given by (32.9)*

$$\bar{d}(E) = \frac{m\mathcal{A}(E)}{2\pi\hbar^2},$$

where $\mathcal{A}(E)$ is the classically allowed area of configuration space for which $U(q) < E$.

Chapter 33

Quantum scattering

Scattering is easier than gathering.
—Irish proverb

(A. Wirzba, P. Cvitanović and N. Whelan)

So far the trace formulas have been derived assuming that the system under consideration is bound. As we shall now see, we are in luck - the semiclassics of bound systems is all we need to understand the semiclassics for open, scattering systems as well. We start by a brief review of the quantum theory of elastic scattering of a point particle from a (repulsive) potential, and then develop the connection to the standard Gutzwiller theory for bound systems. We do this in two steps - first, a heuristic derivation which helps us understand in what sense density of states is "density", and then we sketch a general derivation of the central result of the spectral theory of quantum scattering, the Krein-Friedel-Lloyd formula. The end result is that we establish a connection between the scattering resonances (both positions and widths) of an open quantum system and the poles of the trace of the Green function, which we learned to analyze in earlier chapters.

33.1 Density of states

For a scattering problem the density of states (29.18) appear ill defined since formulas such as (32.6) involve integration over infinite spatial extent. What we will now show is that a quantity that makes sense physically is the difference of two densities - the first with the scatterer present and the second with the scatterer absent.

In nonrelativistic dynamics the relative motion can be separated from the center-of-mass motion. Therefore the elastic scattering of two particles can be treated as the scattering of one particle from a static potential $V(q)$. We will study the scattering of a point-particle of (reduced) mass m by a short-range potential $V(q)$, excluding *inter alia* the Coulomb potential.

(The Coulomb potential decays slowly as a function of q so that various asymptotic approximations which apply to general potentials fail for it.) Although we can choose the spatial coordinate frame freely, it is advisable to place its origin somewhere near the geometrical center of the potential. The scattering problem is solved, if a scattering solution to the time-independent Schrödinger equation (29.5)

$$\left(-\frac{\hbar^2}{2m}\frac{\partial^2}{\partial q^2}+V(q)\right)\phi_{\vec{k}}(q)=E\phi_{\vec{k}}(q) \tag{33.1}$$

can be constructed. Here E is the energy, $\vec{p}=\hbar\vec{k}$ the initial momentum of the particle, and $\vec{k}$ the corresponding wave vector.

When the argument $r=|q|$ of the wave function is large compared to the typical size a of the scattering region, the Schrödinger equation effectively becomes a free particle equation because of the short-range nature of the potential. In the asymptotic domain $r\gg a$, the solution $\phi_{\vec{k}}(q)$ of (33.1) can be written as superposition of ingoing and outgoing solutions of the free particle Schrödinger equation for fixed angular momentum:

$$\phi(q)=A\phi^{(-)}(q)+B\phi^{(+)}(q)\,,\qquad (+\text{ boundary conditions})\,,$$

where in 1-dimensional problems $\phi^{(-)}(q)$, $\phi^{(+)}(q)$ are the "left", "right" moving plane waves, and in higher-dimensional scattering problems the "incoming", "outgoing" radial waves, with the constant matrices A, B fixed by the boundary conditions. What are the boundary conditions? The scatterer can modify only the outgoing waves (see figure 33.1), since the incoming ones, by definition, have yet to encounter the scattering region. This defines the quantum mechanical scattering matrix, or the S *matrix*

$$\phi_m(r)=\phi_m^{(-)}(r)+S_{mm'}\phi_{m'}^{(+)}(r)\,. \tag{33.2}$$

All scattering effects are incorporated in the deviation of $\mathbf{S}$ from the unit matrix, the transition matrix $\mathbf{T}$

$$\mathbf{S}=\mathbf{1}-i\mathbf{T}\,. \tag{33.3}$$

For concreteness, we have specialized to two dimensions, although the final formula is true for arbitrary dimensions. The indices m and m' are the angular momenta quantum numbers for the incoming and outgoing state of the scattering wave function, labeling the S-matrix elements $S_{mm'}$. More generally, given a set of quantum numbers β, γ, the S matrix is a collection $S_{\beta\gamma}$ of transition amplitudes $\beta\to\gamma$ normalized such that $|S_{\beta\gamma}|^2$ is the probability of the $\beta\to\gamma$ transition. The total probability that the ingoing state β ends up in some outgoing state must add up to unity

$$\sum_\gamma |S_{\beta\gamma}|^2=1\,, \tag{33.4}$$

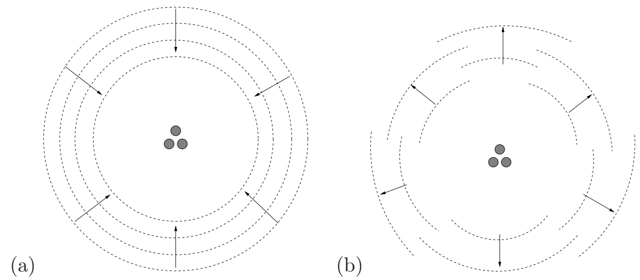

Figure 33.1: (a) *Incoming* spherical waves running into an obstacle. (b) Superposition of *outgoing* spherical waves scattered from an obstacle.

so the S matrix is unitary: $\mathbf{S}^\dagger\mathbf{S}=\mathbf{S}\mathbf{S}^\dagger=\mathbf{1}$.

We have already encountered a solution to the 2-dimensional problem; free particle propagation Green's function (31.48) is a radial solution, given in terms of the Hankel function

$$G_0(r,0,E)=-\frac{im}{2\hbar^2}H_0^{(+)}(kr)\,,$$

where we have used $S_0(r,0,E)/\hbar=kr$ for the action. The mth angular momentum eigenfunction is proportional to $\phi_m^{(\pm)}(q)\propto H_m^{(\pm)}(kr)$, and given a potential $V(q)$ we can in principle compute the infinity of matrix elements $S_{mm'}$. We will not need much information about $H_m^{(t)}(kr)$, other than that for large r its asymptotic form is

$$H^\pm\propto e^{\pm ikr}$$

In general, the potential $V(q)$ is not radially symmetric and (33.1) has to be solved numerically, by explicit integration, or by diagonalizing a large matrix in a specific basis. To simplify things a bit, we assume for the time being that a radially symmetric scatterer is centered at the origin; the final formula will be true for arbitrary asymmetric potentials. Then the solutions of the Schrödinger equation (29.5) are separable, $\phi_m(q)=\phi(r)e^{im\theta}$, $r=|q|$, the scattering matrix cannot mix different angular momentum eigenstates, and S is diagonal in the radial basis (33.2) with matrix elements given by

$$S_m(k)=e^{2i\delta_m(k)}. \tag{33.5}$$

The matrix is unitary so in a diagonal basis all entries are pure phases. This means that an incoming state of the form $H_m^{(-)}(kr)e^{im\theta}$ gets scattered into an outgoing state of the form $S_m(k)H_m^{(+)}(kr)e^{im\theta}$, where $H_m^{(\mp)}(z)$ are incoming and outgoing Hankel functions respectively. We now embed the

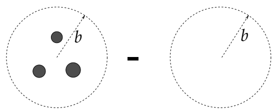

Figure 33.2: The "difference" of two bounded reference systems, one with and one without the scattering system.

scatterer in a infinite cylindrical well of radius R, and will later take $R \to \infty$. Angular momentum is still conserved so that each eigenstate of this (now bound) problem corresponds to some value of m. For large $r \gg a$ each eigenstate is of the asymptotically free form

$$\begin{aligned}\phi_m(r) &\approx e^{im\theta}\left(S_m(k)H_m^{(+)}(kr) + H_m^{(-)}(kr)\right) \\ &\approx \cdots \cos(kr + \delta_m(k) - \chi_m)\,,\end{aligned} \tag{33.6}$$

where $\cdots$ is a common prefactor, and $\chi_m = m\pi/2 + \pi/4$ is an annoying phase factor from the asymptotic expansion of the Hankel functions that will play no role in what follows.

The state (33.6) must satisfy the external boundary condition that it vanish at $r = R$. This implies the quantization condition

$$k_n R + \delta_m(k_n) - \chi_m = \pi\,(n + 12)\ .$$

We now ask for the difference in the eigenvalues of two consecutive states of fixed m. Since R is large, the density of states is high, and the phase $\delta_m(k)$ does not change much over such a small interval. Therefore, to leading order we can include the effect of the change of the phase on state $n+1$ by Taylor expanding. is

$$k_{n+1}R + \delta_m(k_n) + (k_{n+1} - k_n)\delta'_m(k_n) - \chi_m \approx \pi + \pi(n + 12)\,.$$

Taking the difference of the two equations we obtain $\Delta k \approx \pi(R + \delta'_m(k))^{-1}$. This is the eigenvalue spacing which we now interpret as the inverse of the density of states within m angular momentum sbuspace

$$d_m(k) \approx \frac{1}{\pi}\left(R + \delta'_m(k)\right)\,.$$

The R term is essentially the $1-d$ Weyl term (32.8), appropriate to $1-d$ radial quantization. For large R, the dominant behavior is given by the size of the circular enclosure with a correction in terms of the derivative of the scattering phase shift, approximation accurate to order $1/R$. However, not all is well: the area under consideration tends to infinity. We regularize this by subtracting from the result from the free particle density of states $d_0(k)$, for the same size container, but this time without any scatterer, figure 33.2. We also sum over all m values so that

$$\begin{aligned}d(k) - d_0(k) = \frac{1}{\pi}\sum_m \delta'_m(k) &= \frac{1}{2\pi i}\sum_m \frac{d}{dk}\log S_m \\ &= \frac{1}{2\pi i}\mathrm{Tr}\left(S^\dagger \frac{dS}{dk}\right)\,.\end{aligned} \tag{33.7}$$

The first line follows from the definition of the phase shifts (33.5) while the second line follows from the unitarity of S so that $S^{-1} = S^\dagger$. We can now take the limit $R \to \infty$ since the R dependence has been cancelled away.

This is essentially what we want to prove since for the left hand side we already have the semiclassical theory for the trace of the difference of Green's functions,

$$d(k) - d_0(k) = -\frac{1}{2\pi k}\mathrm{Im}\left(\mathrm{tr}\left(G(k) - G_0(k)\right)\right)\,. \tag{33.8}$$

There are a number of generalizations. This can be done in any number of dimensions. It is also more common to do this as a function of energy and not wave number k. However, as the asymptotic dynamics is free wave dynamics labeled by the wavenumber k, we have adapted k as the natural variable in the above discussion.

Finally, we state without proof that the relation (33.7) applies even when there is no circular symmetry. The proof is more difficult since one cannot appeal to the phase shifts δ_m but must work directly with a non-diagonal S matrix.

33.2 Quantum mechanical scattering matrix

The results of the previous section indicate that there is a connection between the scattering matrix and the trace of the quantum Green's function (more formally between the difference of the Green's function with and without the scattering center.) We now show how this connection can be derived in a more rigorous manner. We will also work in terms of the energy E rather than the wavenumber k, since this is the more usual exposition. Suppose particles interact via forces of sufficiently short range, so that in the remote past they were in a free particle state labeled β, and in the distant future they will likewise be free, in a state labeled γ. In the Heisenberg picture the S-matrix is defined as $\mathbf{S} = \Omega_-\Omega_+^\dagger$ in terms of the Møller operators

$$\Omega_\pm = \lim_{t\to\pm\infty} e^{iHt/\hbar}e^{-iH_0t/\hbar}\,, \tag{33.9}$$

where H is the full Hamiltonian, whereas H_0 is the free Hamiltonian. In the interaction picture the S-matrix is given by

$$\mathbf{S} \;=\; \Omega_+^\dagger\Omega_- = \lim_{t\to\infty} e^{iH_0t/\hbar}e^{-2iHt/\hbar}e^{iH_0t/\hbar}$$

$$= T\exp\left(-i\int_{-\infty}^{+\infty}dtH'(t)\right), \tag{33.10}$$

where $H' = V = H - H_0$ is the interaction Hamiltonian and T is the time-ordering operator. In stationary scattering theory the S matrix has the following spectral representation

$$\begin{aligned} S &= \int_0^\infty dE\, S(E)\delta(H_0 - E) \\ S(E) &= Q_+(E)Q_-^{-1}(E), \qquad Q_\pm(E) = \mathbf{1} + (H_0 - E \pm i\epsilon)^{-1}V \end{aligned} \tag{33.11}$$

such that

$$\mathrm{Tr}\left[S^\dagger(E)\frac{d}{dE}S(E)\right] = \mathrm{Tr}\left[\frac{1}{H_0 - E - i\epsilon} - \frac{1}{H - E - i\epsilon} - (\epsilon \leftrightarrow -\epsilon)\right]. \tag{33.12}$$

☞ appendix J

The manipulations leading to (33.12) are justified if the operators $Q_\pm(E)$ can be linked to trace-class operators.

We can now use this result to derive the Krein-Lloyd formula which is the central result of this chapter. The Krein-Lloyd formula provides the connection between the trace of the Green's function and the poles of the scattering matrix, implicit in all of the trace formulas for open quantum systems which will be presented in the subsequent chapters.

33.3 Krein-Friedel-Lloyd formula

The link between quantum mechanics and semiclassics for scattering problems is provided by the semiclassical limit of the Krein-Friedel-Lloyd sum for the spectral density which we now derive. This derivation builds on the results of the last section and extends the discussion of the opening section.

In chapter 31 we linked the spectral density (see (29.18)) of a bounded system

$$d(E) \equiv \sum_n \delta(E_n - E) \tag{33.13}$$

via the identity

$$\begin{aligned} \delta(E_n - E) &= -\lim_{\epsilon\to 0}\frac{1}{\pi}\mathrm{Im}\frac{1}{E - E_n + i\epsilon} \\ &= -\lim_{\epsilon\to 0}\frac{1}{\pi}\mathrm{Im}\langle E_n|\frac{1}{E - H + i\epsilon}|E_n\rangle \\ &= \frac{1}{2\pi i}\lim_{\epsilon\to 0}\left\langle E_n\left|\frac{1}{E - H - i\epsilon} - \frac{1}{E - H + i\epsilon}\right|E_n\right\rangle \end{aligned} \tag{33.14}$$

to the trace of the Green's function (32.1.1). Furthermore, in the semiclassical approximation, the trace of the Green's function is given by the Gutzwiller trace formula (32.11) in terms of a smooth Weyl term and an oscillating contribution of periodic orbits.

Therefore, the task of constructing the semiclassics of a scattering system is completed, if we can find a connection between the spectral density $d(E)$ and the scattering matrix S. We will see that (33.12) provides the clue. Note that the right hand side of (33.12) has nearly the structure of (33.14) when the latter is inserted into (33.13). The principal difference between these two types of equations is that the S matrix refers to *outgoing* scattering wave functions which are not normalizable and which have a *continuous* spectrum, whereas the spectral density $d(E)$ refers to a bound system with normalizable wave functions with a discrete spectrum. Furthermore, the bound system is characterized by a *hermitian* operator, the Hamiltonian H, whereas the scattering system is characterized by a *unitary* operator, the S-matrix. How can we reconcile these completely different classes of wave functions, operators and spectra? The trick is to put our scattering system into a finite box as in the opening section. We choose a spherical conatiner with radius R and with its center at the center of our finite scattering system. Our scattering potential $V(\vec{r})$ will be unaltered within the box, whereas at the box walls we will choose an infinitely high potential, with the Dirichlet boundary conditions at the outside of the box:

$$\phi(\vec{r})|_{r=R} = 0\,. \tag{33.15}$$

In this way, for any finite value of the radius R of the box, we have mapped our scattering system into a bound system with a spectral density $d(E;R)$ over discrete eigenenergies $E_n(R)$. It is therefore important that our scattering potential was chosen to be short-ranged to start with. (Which explains why the Coulomb potential requires special care.) The hope is that in the limit $R\to\infty$ we will recover the scattering system. But some care is required in implementing this. The smooth Weyl term $\bar{d}(E;R)$ belonging to our box with the enclosed potential V diverges for a spherical two-dimensional box of radius R quadratically, as $\pi R^2/(4\pi)$ or as R^3 in the three-dimensional case. This problem can easily be cured if the spectral density of an empty reference box of the *same* size (radius R) is subtracted (see figure 33.2). Then all the divergences linked to the increasing radius R in the limit $R\to\infty$ drop out of the difference. Furthermore, in the limit $R\to\infty$ the energy-eigenfunctions of the box are only normalizable as a delta distribution, similarly to a plane wave. So we seem to recover a continous spectrum. Still the problem remains that the wave functions do not discriminate between incoming and outgoing waves, whereas this symmetry, namely the hermiticity, is broken in the scattering problem. The last problem can be tackled if we replace the spectral density over discrete delta distributions by a smoothed spectral density with a small finite imaginary part η in the energy E:

$$d(E+i\eta;R) \equiv \frac{1}{i\,2\pi}\sum_n\left\{\frac{1}{E - E_n(R) - i\eta} - \frac{1}{E - E_n(R) + i\eta}\right\}. \tag{33.16}$$

Note that $d(E+i\eta;R) \neq d(E-i\eta;R) = -d(E+i\eta;R)$. By the introduction of the positive *finite* imaginary part η the time-dependent behavior of the wave function has effectively been altered from an oscillating one to a decaying one and the hermiticity of the Hamiltonian is removed. Finally the limit $\eta \to 0$ can be carried out, respecting the order of the limiting procedures. First, the limit $R \to \infty$ has to be performed for a *finite* value of η, only then the limit $\eta \to 0$ is allowed. In practice, one can try to work with a finite value of R, but then it will turn out (see below) that the scattering system is only recovered if $R\sqrt{\eta} \gg 1$.

Let us summarize the relation between the smoothed spectral densities $d(E+i\eta;R)$ of the boxed potential and $d^{(0)}(E+i\eta;R)$ of the empty reference system and the S matrix of the corresponding scattering system:

$$\begin{aligned}\lim_{\eta\to+0}\lim_{R\to\infty}\left(d(E+i\eta;R)-d^{(0)}(E+i\eta;R)\right) &= \frac{1}{2\pi i}\mathrm{Tr}\left[S^{\dagger}(E)\frac{d}{dE}S(E)\right]\\ =\frac{1}{2\pi i}\mathrm{Tr}\frac{d}{dE}\ln S(E) &= \frac{1}{2\pi i}\frac{d}{dE}\ln\det S(E) .\end{aligned} \tag{33.17}$$

This is the *Krein-Friedel-Lloyd formula*. It replaces the scattering problem by the difference of two bounded reference billiards of the same radius R which finally will be taken to infinity. The first billiard contains the scattering region or potentials, whereas the other does not (see figure 33.2). Here $d(E+i\eta;R)$ and $d^{(0)}(E+i\eta;R)$ are the *smoothed* spectral densities in the presence or in the absence of the scatterers, respectively. In the semiclassical approximation, they are replaced by a Weyl term (32.10) and an oscillating sum over periodic orbits. As in (32.2), the trace formula (33.17) can be integrated to give a relation between the smoothed staircase functions and the determinant of the S-matrix:

$$\lim_{\eta\to+0}\lim_{R\to\infty}\left(N(E+i\eta;R)-N^{(0)}(E+i\eta;R)\right) = \frac{1}{2\pi i}\ln\det S(E) . \tag{33.18}$$

Furthermore, in both versions of the Krein-Friedel-Lloyd formulas the energy argument $E+i\eta$ can be replaced by the wavenumber argument $k+i\eta'$. These expressions only make sense for wavenumbers on or above the real k-axis. In particular, if k is chosen to be real, η' must be greater than zero. Otherwise, the exact left hand sides (33.18) and (33.17) would give discontinuous staircase or even delta function sums, respectively, whereas the right hand sides are continuous to start with, since they can be expressed by continuous phase shifts. Thus the order of the two limits in (33.18) and (33.17) is essential.

The necessity of the $+i\eta$ prescription can also be understood by purely phenomenological considerations in the semiclassical approximation: Without the $i\eta$ term there is no reason why one should be able to neglect spurious periodic orbits which are there solely because of the introduction of the confining boundary. The subtraction of the second (empty) reference system removes those spurious periodic orbits which never encounter the scattering

region – in addition to the removal of the divergent Weyl term contributions in the limit $R \to \infty$. The periodic orbits that encounter both the scattering region and the external wall would still survive the first limit $R \to \infty$, if they were not exponentially suppressed by the $+i\eta$ term because of their

$$e^{iL(R)\sqrt{2m(E+i\eta)}} = e^{iL(R)k}\,e^{-L(R)\eta'}$$

behavior. As the length $L(R)$ of a spurious periodic orbit grows linearly with the radius R. The bound $R\eta' \gg 1$ is an essential precondition on the suppression of the unwanted spurious contributions of the container if the Krein-Friedel-Lloyd formulas (33.17) and (33.18) are evaluated at a finite value of R.

33.1 page 616

Finally, the semiclassical approximation can also help us in the interpretation of the Weyl term contributions for scattering problems. In scattering problems the Weyl term appears with a negative sign. The reason is the subtraction of the empty container from the container with the potential. If the potential is a dispersing billiard system (or a finite collection of dispersing billiards), we expect an excluded volume (or the sum of excluded volumes) relative to the empty container. In other words, the Weyl term contribution of the empty container is larger than of the filled one and therefore a negative net contribution is left over. Second, if the scattering potential is a collection of a finite number of non-overlapping scattering regions, the Krein-Friedel-Lloyd formulas show that the corresponding Weyl contributions are completely independent of the position of the single scatterers, as long as these do not overlap.

33.4 Wigner time delay

The term $\frac{d}{dE}\ln\det S$ in the density formula (33.17) is dimensionally time. This suggests another, physically important interpretation of such formulas for scattering systems, the Wigner delay, defined as

$$\begin{aligned} d(k) &= \frac{d}{dk}\mathrm{Argdet}\,(\mathbf{S}(k))\\ &= -i\frac{d}{dk}\log\det(\mathbf{S}(k)\\ &= -i\,\mathrm{tr}\left(\mathbf{S}^{\dagger}(k)\frac{d\mathbf{S}}{dk}(k)\right)\end{aligned} \tag{33.19}$$

and can be shown to equal the total delay of a wave packet in a scattering system. We now review this fact.

A related quantity is the total scattering *phase shift* $\Theta(k)$ defined as

$$\det\mathbf{S}(k) = e^{+i\,\Theta(k)} ,$$

so that $d(k) = \frac{d}{dk}\Theta(k)$.

The time delay may be both positive and negative, reflecting attractive respectively repulsive features of the scattering system. To elucidate the connection between the scattering determinant and the time delay we study a plane wave:

The phase of a wave packet will have the form:

$$\phi = \vec{k}\cdot\vec{x} - \omega\, t \;+ \Theta\,.$$

Here the term in the parenthesis refers to the phase shift that will occur if scattering is present. The center of the wave packet will be determined by the principle of stationary phase:

$$0 = d\phi = d\vec{k}\cdot\vec{x} - d\omega\, t \;+ d\Theta\,.$$

Hence the packet is located at

$$\vec{x} = \frac{\partial\omega}{\partial\vec{k}}\,t \;- \frac{\partial\Theta}{\partial\vec{k}}\,.$$

The first term is just the group velocity times the given time t. Thus the the packet is retarded by a length given by the derivative of the phase shift with respect to the wave vector $\vec{k}$. The arrival of the wave packet at the position $\vec{x}$ will therefore be delayed. This *time delay* can similarly be found as

$$\tau(\omega) = \frac{\partial\Theta(\omega)}{\partial\omega}.$$

To show this we introduce the *slowness* of the phase $\vec{s} = \vec{k}/\omega$ for which $\vec{s}\cdot\vec{v}_g = 1$, where $\vec{v}_g$ is the group velocity to get

$$d\vec{k}\cdot\vec{x} = \vec{s}\cdot\vec{x}\,d\omega = \frac{x}{v_g}\,d\omega\,,$$

since we may assume $\vec{x}$ is parallel to the group velocity (consistent with the above). Hence the arrival time becomes

$$t = \frac{x}{v_g} \;+ \frac{\partial\Theta(\omega)}{\partial\omega}\,.$$

If the scattering matrix is not diagonal, one interprets

$$\Delta t_{ij} = \mathrm{Re}\left(-\mathrm{i}\,\mathrm{S}_{\mathrm{ij}}^{-1}\frac{\partial \mathrm{S}_{\mathrm{ij}}}{\partial\omega}\right) = \mathrm{Re}\left(\frac{\partial\Theta_{\mathrm{ij}}}{\partial\omega}\right)$$

as the delay in the jth scattering channel after an injection in the ith. The probability for appearing in channel j goes as $|S_{ij}|^2$ and therefore the average delay for the incoming states in channel i is

$$\begin{aligned}\langle\Delta t_i\rangle &= \sum_j |S_{ij}|^2\Delta t_{ij} = \mathrm{Re}\,(-\mathrm{i}\sum_{\mathrm{j}} \mathrm{S}_{\mathrm{ij}}^*\frac{\partial \mathrm{S}_{\mathrm{ij}}}{\partial\omega}) = \mathrm{Re}\,(-\mathrm{i}\,\mathbf{S}^\dagger\cdot\frac{\partial\mathbf{S}}{\partial\omega})_{\mathrm{ii}}\\ &= -i\left(\mathbf{S}^\dagger\cdot\frac{\partial\mathbf{S}}{\partial\omega}\right)_{ii}\,,\end{aligned}$$

where we have used the derivative, $\partial/\partial\omega$, of the unitarity relation $\mathbf{S}\cdot\mathbf{S}^\dagger = \mathbf{1}$ valid for real frequencies. This discussion can in particular be made for wave packets related to partial waves and superpositions of these like an incoming plane wave corresponding to free motion. The total Wigner delay therefore corresponds to the sum over all channel delays (33.19).

Commentary

Remark 33.1 Krein-Friedel-Lloyd formula. The third volume of Thirring [33.1], sections 3.6.14 (Levison Theorem) and 3.6.15 (the proof), or P. Scherer's thesis [33.15] (appendix) discusses the Levison Theorem.

It helps to start with a toy example or simplified example instead of the general theorem, namely for the radially symmetric potential in a symmetric cavity. Have a look at the book of K. Huang, chapter 10 (on the "second virial coefficient"), or Beth and Uhlenbeck [33.5], or Friedel [33.7]. These results for the correction to the density of states are particular cases of the Krein formula [33.3]. The Krein-Friedel-Lloyd formula (33.17) was derived in refs. [33.3, 33.7, 33.8, 33.9], see also refs. [33.11, 33.14, 33.15, 33.17, 33.18]. The original papers are by Krein and Birman [33.3, 33.4] but beware, they are mathematicans.

Also, have a look at pages 15-18 of Wirzba's talk on the Casimir effect [33.16]. Page 16 discusses the Beth-Uhlenbeck formula [33.5], the predecessor of the more general Krein formula for spherical cases.

Remark 33.2 Weyl term for empty container. For a discussion of why the Weyl term contribution of the empty container is larger than of the filled one and therefore a negative net contribution is left over, see ref. [33.15].

Remark 33.3 Wigner time delay. Wigner time delay and the Wigner-Smith time delay matrix, are powerful concepts for a statistical description of scattering. The diagonal elements Q_{aa} of the lifetime matrix $\mathbf{Q} = -i\mathbf{S}^{-1}\partial\mathbf{S}/\partial\omega$, where $\mathbf{S}$ is the $[2N\times 2N]$ scattering matrix, are interpreted in terms of the time spent in the scattering region by a wave packet incident in one channel. As shown by Smith [33.26], they are the sum over all ouput channels (both in reflection and transmission) of $\Delta t_{ab} = \mathrm{Re}\,[(-\mathrm{i}/\mathrm{S}_{\mathrm{ab}})(\partial\mathrm{S}_{\mathrm{ab}}/\partial\omega)]$ weighted by the probability of emerging from that channel. The sum of the Q_{aa} over all $2N$ channels is the Wigner time delay $\tau_W = \sum_a Q_{aa}$, which is the trace of the lifetime matrix and is proportional to the density of states.

References

[33.1] W. Thirring, *Quantum mechanics of atoms and molecules*, *A course in mathematical physics* Vol. **3** (Springer, New York, 1979). (Springer, Wien 1979).

[33.2] A. Messiah, *Quantum Mechanics, Vol.* **I** (North-Holland, Amsterdam, 1961).

[33.3] M.G. Krein, *On the Trace Formula in Perturbation Theory*, Mat. Sborn. (N.S.) **33**, 597 (1953) ; *Perturbation Determinants and Formula for Traces of Unitary and Self-adjoint Operators*, Sov. Math.-Dokl. **3**, 707 (1962).

[33.4] M.Sh. Birman and M.G. Krein, *On the Theory of Wave Operators and Scattering Operators*, Sov. Math.-Dokl. **3**, 740 (1962); M.Sh. Birman and D.R. Yafaev, *St. Petersburg Math. J.* **4**, 833 (1993).

[33.5] E. Beth and G.E. Uhlenbeck, *Physica* **4**, 915 (1937).

[33.6] K. Huang, *Statistical Mechanics* (John Wiley & Sons, New York (1987).

[33.7] J. Friedel, *Phil. Mag.* **43**, 153 (1952); *Nuovo Cim. Ser. 10 Suppl.* **7**, 287 (1958).

[33.8] P. Lloyd, Wave propagation through an assembly of spheres. II. The density of single-particle eigenstates, *Proc. Phys. Soc.* **90**, 207 (1967).

[33.9] P. Lloyd and P.V. Smith, Multiple-scattering theory in condensed materials, *Adv. Phys.* **21**, 69 (1972), and references therein.

[33.10] R. Balian and C. Bloch, *Ann. Phys. (N.Y.)* **63**, 592 (1971)

[33.11] R. Balian and C. Bloch, *Solution of the Schrödinger Equation in Terms of Classical Paths Ann. Phys. (NY)* **85**, 514 (1974).

[33.12] R. Balian and C. Bloch, *Distribution of eigenfrequencies for the wave equation in a finite domain: III. Eigenfrequency density oscillations*, *Ann. Phys. (N.Y.)* **69**,76 (1972).

[33.13] J.S. Faulkner, "Scattering theory and cluster calculations", *J. Phys.* **C 10**, 4661 (1977).

[33.14] P. Gaspard and S.A. Rice, Semiclassical quantization of the scattering from a classically chaotic repeller, *J. Chem. Phys.* **90**, 2242 (1989).

[33.15] P. Scherer, *Quantenzustände eines klassisch chaotischen Billards*, Ph.D. thesis, Univ. Köln (Berichte des Forschungszentrums Jülich 2554, ISSN 0366-0885, Jülich, Nov. 1991).

[33.16] A. Wirzba, "A force from nothing into nothing: Casimir interactions" `ChaosBook.org/projects/Wirzba/openfull.ps.gz` (overheads, 2003).

[33.17] P. Gaspard, Scattering Resonances: Classical and Quantum Dynamics, in: *Proceedings of the Int. School of Physics "Enrico Fermi"*, Course CXIX, Varena, 23 July - 2 August 1991, eds G. Casati, I. Guarneri and U. Smilansky (North-Holland, Amsterdam, 1993).

[33.18] A. Norcliffe and I. C. Percival, J. Phys. B **1**, 774 (1968); L. Schulman, Phys. Rev. **176**, 1558 (1968).

[33.19] W. Franz, *Theorie der Beugung Elektromagnetischer Wellen* (Springer, Berlin 1957); "Über die Greenschen Funktionen des Zylinders und der Kugel", *Z. Naturforschung* **9a**, 705 (1954).

[33.20] G.N. Watson, *Proc. Roy. Soc. London Ser.* **A 95**, 83 (1918).

[33.21] M. Abramowitz and I.A. Stegun, *Handbook of Mathematical Functions with Formulas, Graphs and Mathematical Tables*, (Dover, New York, 1964).

[33.22] W. Franz and R. Galle, "Semiasymptotische Reihen für die Beugung einer ebenen Welle am Zylinder", *Z. Naturforschung* **10a**, 374 (1955).

[33.23] A. Wirzba, "Validity of the semiclassical periodic orbit approximation in the 2-and 3-disk problems", *CHAOS* **2**, 77 (1992).

[33.24] M.V. Berry, "Quantizing a Classically Ergodic System: Sinai's Billiard and the KKR Method", *Ann. Phys. (N.Y.)* **131**, 163 (1981).

[33.25] E.P. Wigner, *Phys. Rev.* **98**, 145 (1955).

[33.26] F.T. Smith, *Phys. Rev.* **118**, 349 (1960).

[33.27] A. Wirzba, *Quantum Mechanics and Semiclassics of Hyperbolic n-Disk Scattering*, *Physics Reports* **309**, 1-116 (1999); `chao-dyn/9712015`.

[33.28] V. A. Gopar, P. A. Mello, and M. Buttiker, Phys. Rev. Lett. 77, 3005 (1996).

[33.29] P. W. Brouwer, K. M. Frahm, and C. W. J. Beenakker, Phys. Rev. Lett. 78, 4737 (1997).

[33.30] Following the thesis of Eisenbud, the local delay time Dtab is defined in ref. [33.26] as the appearance of the peak in the outgoing signal in channel b after the injection of a wave packet in channel a. Our definition of the local delay time tab in Eq. (1) coincides with the definition of Dtab in the limit of narrow bandwidth pulses, as shown in Eq. (3).

[33.31] E. Doron and U. Smilansky, Phys. Rev. Lett. 68, 1255 (1992).

[33.32] G. Iannaccone, Phys. Rev. B 51, 4727 (1995).

[33.33] V. Gasparian, T. Christen, and M. Büttiker, Phys. Rev. A 54, 4022 (1996).

[33.34] For a complete and insightful review see Y. V. Fyodorv and H.-J. Sommers, J. Math. Phys. 38, 1918 (1997).

[33.35] R. Landauer and Th. Martin, Rev. Mod. Phys. 66, 217 (1994). j

[33.36] E. H. Hauge and J. A. Støveng, Rev. Mod. Phys. 61, 917 (1989).

Exercises

Exercise 33.1 Spurious orbits under the Krein-Friedel-Lloyd contruction. *Draw examples for the three types of period orbits under the Krein-Friedel-Lloyd construction: (a) the genuine periodic orbits of the scattering region, (b) spurious periodic orbits which can be removed by the subtraction of the reference system, (c) spurious periodic orbits which cannot be removed by this subtraction. What is the role of the double limit* $\eta \to 0$*, container size* $b \to \infty$*?*

Exercise 33.2 The one-disk scattering wave function. *Derive the one-disk scattering wave function.*

(Andreas Wirzba)

Exercise 33.3 Quantum two-disk scattering. *Compute the quasiclassical spectral determinant*

$$Z(\varepsilon) = \prod_{p,j,l} \left(1 - \frac{t_p}{\Lambda_p^{j+2l}}\right)^{j+1}$$

for the two disk problem. Use the geometry

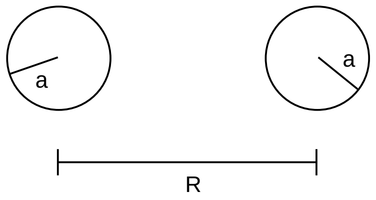

The full quantum mechanical version of this problem can be solved by finding the zeros in k *for the determinant of the matrix*

$$M_{m,n} = \delta_{m,n} + \frac{(-1)^n}{2}\frac{J_m(ka)}{H_n^{(1)}(ka)}\left(H_{m-n}^{(1)}(kR) + (-1)^n H_{m+n}^{(1)}(kR)\right),$$

where J_n *is the* n*th Bessel function and* $H_n^{(1)}$ *is the Hankel function of the first kind. Find the zeros of the determinant closest to the origin by solving* $\det M(k) = 0$*. (Hints: notice the structure* $M = I + A$ *to approximate the determinant; or read* Chaos **2**, *79 (1992))*

Exercise 33.4 Pinball topological index. *Upgrade your pinball simulator so that it computes the topological index for each orbit it finds.*

Chapter 34

Chaotic multiscattering

(A. Wirzba and P. Cvitanović)

We discuss here the semiclassics of scattering in open systems with a finite number of non-overlapping finite scattering regions. Why is this interesting at all? The semiclassics of scattering systems has five advantages compared to the bound-state problems such as the helium quantization discussed in chapter 35.

- For bound-state problem the semiclassical approximation does not respect quantum-mechanical unitarity, and the semi-classical eigenenergies are not real. Here we construct *a manifestly unitary* semiclassical scattering matrix.
- The Weyl-term contributions decouple from the multi-scattering system.
- The close relation to the classical escape processes discussed in chapter 1.
- For scattering systems the derivation of cycle expansions is more direct and controlled than in the bound-state case: the semiclassical cycle expansion is the saddle-point approximation to the cumulant expansion of the determinant of the exact quantum-mechanical multi-scattering matrix.
- The region of convergence of the semiclassical spectral function is larger than is the case for the bound-state case.

We start by a brief review of the elastic scattering of a point particle from finite collection of non-overlapping scattering regions in terms of the standard textbook scattering theory, and then develop the semiclassical scattering trace formulas and spectral determinants for scattering off N disks in a plane.

34.1 Quantum mechanical scattering matrix

We now specialize to the elastic scattering of a point particle from finite collection of N non-overlapping reflecting disks in a 2-dimensional plane. As the point particle moves freely between the static scatterers, the time independent Schrödinger equation outside the scattering regions is the Helmholtz equation:

$$\left(\vec{\nabla}_r^2 + \vec{k}^2\right)\psi(\vec{r}) = 0\,, \qquad \vec{r}\text{ outside the scattering regions.} \tag{34.1}$$

Here $\psi(\vec{r})$ is the wave function of the point particle at spatial position $\vec{r}$ and $E = \hbar^2\vec{k}^2/2m$ is its energy written in terms of its mass m and the wave vector $\vec{k}$ of the incident wave. For reflecting wall billiards the scattering problem is a boundary value problem with Dirichlet boundary conditions:

$$\psi(\vec{r}) = 0\,, \qquad \vec{r}\text{ on the billiard perimeter} \tag{34.2}$$

As usual for scattering problems, we expand the wave function $\psi(\vec{r})$ in the (2-dimensional) angular momentum eigenfunctions basis

$$\psi(\vec{r}) = \sum_{m=-\infty}^{\infty} \psi_m^k(\vec{r}) e^{-im\Phi_k}\,, \tag{34.3}$$

where k and Φ_k are the length and angle of the wave vector, respectively. A plane wave in two dimensions expaned in the angular momentum basis is

$$e^{i\vec{k}\cdot\vec{r}} = e^{ikr\cos(\Phi_r-\Phi_k)} = \sum_{m=-\infty}^{\infty} J_m(kr) e^{im(\Phi_r-\Phi_k)}\,, \tag{34.4}$$

where r and Φ_r denote the distance and angle of the spatial vector $\vec{r}$ as measured in the global 2-dimensional coordinate system.

The mth angular component $J_m(kr)e^{im\Phi_r}$ of a plane wave is split into a superposition of incoming and outgoing 2-dimensional spherical waves by decomposing the ordinary Bessel function $J_m(z)$ into the sum

$$J_m(z) = \frac{1}{2}\left(H_m^{(1)}(z) + H_m^{(2)}(z)\right) \tag{34.5}$$

of the Hankel functions $H_m^{(1)}(z)$ and $H_m^{(2)}(z)$ of the first and second kind. For $|z| \gg 1$ the Hankel functions behave asymptotically as:

$$\begin{aligned} H_m^{(2)}(z) &\sim \sqrt{\frac{2}{\pi z}} e^{-i(z-\frac{\pi}{2}m-\frac{\pi}{4})} \quad \text{incoming,} \\ H_m^{(1)}(z) &\sim \sqrt{\frac{2}{\pi z}} e^{+i(z-\frac{\pi}{2}m-\frac{\pi}{4})} \quad \text{outgoing.} \end{aligned} \tag{34.6}$$

Thus for $r \to \infty$ and k fixed, the mth angular component $J_m(kr)e^{im\Phi_r}$ of the plane wave can be written as superposition of incoming and outgoing 2-dimensional spherical waves:

$$J_m(kr)e^{im\Phi_r} \sim \frac{1}{\sqrt{2\pi kr}}\left[e^{-i(kr-\frac{\pi}{2}m-\frac{\pi}{4})} + e^{i(kr-\frac{\pi}{2}m-\frac{\pi}{4})}\right] e^{im\Phi_r}\,. \tag{34.7}$$

In terms of the asymptotic (angular momentum) components ψ_m^k of the wave function $\psi(\vec{r})$, the scattering matrix (33.3) is defined as

$$\psi_m^k \sim \frac{1}{\sqrt{2\pi kr}} \sum_{m'=-\infty}^{\infty} \left[\delta_{mm'} e^{-i(kr-\frac{\pi}{2}m'-\frac{\pi}{4})} + S_{mm'} e^{i(kr-\frac{\pi}{2}m'-\frac{\pi}{4})}\right] e^{im'\Phi_r} \tag{34.8}$$

The matrix element $S_{mm'}$ describes the scattering of an incoming wave with angular momentum m into an outgoing wave with angular momentum m'. If there are no scatterers, then $\mathbf{S} = \mathbf{1}$ and the asymptotic expression of the plane wave $e^{i\vec{k}\cdot\vec{r}}$ in two dimensions is recovered from $\psi(\vec{r})$.

34.1.1 1-disk scattering matrix

In general, $\mathbf{S}$ is nondiagonal and nonseparable. An exception is the 1-disk scatterer. If the origin of the coordinate system is placed at the center of the disk, by (34.5) the mth angular component of the time-independent scattering wave function is a superposition of incoming and outgoing 2-dimensional spherical waves

33.2
page 616

$$\begin{aligned} \psi_m^k &= \frac{1}{2}\left(H_m^{(2)}(kr) + S_{mm}H_m^{(1)}(kr)\right) e^{im\Phi_r} \\ &= \left(J_m(kr) - \frac{i}{2}T_{mm}H_m^{(1)}(kr)\right) e^{im\Phi_r}\,. \end{aligned}$$

The vanishing (34.2) of the wave function on the disk perimeter

$$0 = J_m(ka) - \frac{i}{2}T_{mm}H_m^{(1)}(ka)$$

yields the 1-disk scattering matrix in analytic form:

$$S_{mm'}^s(k) = \left(1 - \frac{2J_m(ka_s)}{H_m^{(1)}(ka_s)}\right)\delta_{mm'} = -\frac{H_m^{(2)}(ka_s)}{H_m^{(1)}(ka_s)}\delta_{mm'}\,, \tag{34.9}$$

where $a = a_s$ is radius of the disk and the suffix ^{s} indicates that we are dealing with a disk whose label is s. We shall derive a semiclassical approximation to this 1-disk $\mathbf{S}$-matrix in sect. 34.3.

34.1.2 Multi-scattering matrix

Consider next a scattering region consisting of N non-overlapping disks labeled $s \in \{1, 2, \cdots, N\}$, following the notational conventions of sect. 10.5. The strategy is to construct the full **T**-matrix (33.3) from the exact 1-disk scattering matrix (34.9) by a succession of coordinate rotations and translations such that at each step the coordinate system is centered at the origin of a disk. Then the **T**-matrix in $S_{mm'} = \delta_{mm'} - i\,T_{mm'}$ can be split into a product over three kinds of matrices,

$$T_{mm'}(k) = \sum_{s,s'=1}^{N} \sum_{l_s,l_{s'}=-\infty}^{\infty} C_{ml_s}^{\;s}(k)\mathbf{M}^{-1}(k)_{l_s l_{s'}}^{ss'} D_{l_{s'}m'}^{s'}(k)\,.$$

The outgoing spherical wave scattered by the disk s is obtained by shifting the global coordinates origin distance R_s to the center of the disk s, and measuring the angle Φ_s with respect to direction $\mathbf{k}$ of the outgoing spherical wave. As in (34.9), the matrix $\mathbf{C}^s$ takes form

$$C_{ml_s}^{\;s} = \frac{2i}{\pi a_s}\frac{J_{m-l_s}(kR_s)}{H_{l_s}^{(1)}(ka_s)}e^{im\Phi_s}\,. \tag{34.10}$$

If we now describe the ingoing spherical wave in the disk s' coordinate frame by the matrix $\mathbf{D}^{s'}$

$$D_{l_{s'}m'}^{s'} = -\pi a_{s'} J_{m'-l_{s'}}(kR_{s'}) J_{l_{s'}}(ka_{s'}) e^{-im'\Phi_{s'}}\,, \tag{34.11}$$

and apply the Bessel function addition theorem

$$J_m(y+z) = \sum_{\ell=-\infty}^{\infty} J_{m-\ell}(y)J_\ell(z),$$

we recover the **T**-matrix (34.9) for the single disk $s = s'$, $M = 1$ scattering. The Bessel function sum is a statement of the completness of the spherical wave basis; as we shift the origin from the disk s to the disk s' by distance $R_{s'}$, we have to reexpand all basis functions in the new coordinate frame.

The labels m and m' refer to the angular momentum quantum numbers of the ingoing and outgoing waves in the global coordinate system, and $l_s, l_{s'}$ refer to the (angular momentum) basis fixed at the sth and s'th scatterer, respectively. Thus, $\mathbf{C}^s$ and $\mathbf{D}^{s'}$ depend on the origin and orientation of the global coordinate system of the 2-dimensional plane as well as on the internal coordinates of the scatterers. As they can be made separable in the scatterer label s, they describe the single scatterer aspects of what, in general, is a multi-scattering problem.

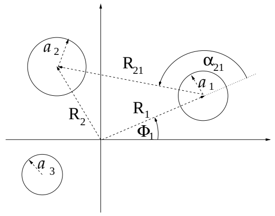

Figure 34.1: Global and local coordinates for a general 3-disk problem.

The matrix **M** is called the *multi-scattering matrix.* If the scattering problem consists only of one scatterer, **M** is simply the unit matrix $M_{l_s l_{s'}}^{ss'} = \delta^{ss'}\delta_{l_s l_{s'}}$. For scattering from more than one scatterer we separate out a "single traversal" matrix **A** which transports the scattered wave from a scattering region $\mathcal{M}_s$ to the scattering region $\mathcal{M}_{s'}$,

$$M_{l_s l_{s'}}^{ss'} = \delta^{ss'}\delta_{l_s l_{s'}} - A_{l_s l_{s'}}^{ss'}\,. \tag{34.12}$$

The matrix $\mathbf{A}^{ss'}$ reads:

$$A_{l_s l_{s'}}^{ss'} = -(1-\delta^{ss'})\,\frac{a_s}{a_{s'}}\,\frac{J_{l_s}(ka_s)}{H_{l_{s'}}^{(1)}(ka_{s'})}\,H_{l_s-l_{s'}}^{(1)}(kR_{ss'})\,e^{i(l_s\alpha_{s's}-l_{s'}(\alpha_{ss'}-\pi))}\,. \tag{34.13}$$

Here, a_s is the radius of the sth disk. R_s and Φ_s are the distance and angle, respectively, of the ray from the origin in the 2-dimensional plane to the center of disk s as measured in the global coordinate system. Furthermore, $R_{ss'} = R_{s's}$ is the separation between the centers of the sth and s'th disk and $\alpha_{s's}$ of the ray from the center of disk s to the center of disk s' as measured in the local (body-fixed) coordinate system of disk s (see figure 34.1).

Expanded as a geometrical series about the unit matrix **1**, the inverse matrix $\mathbf{M}^{-1}$ generates a multi-scattering series in powers of the single-traversal matrix **A**. All genuine multi-scattering dynamics is contained in the matrix **A**; by construction **A** vanishes for a single-scatterer system.

34.2 N-scatterer spectral determinant

In the following we limit ourselves to a study of the spectral properties of the **S**-matrix: resonances, time delays and phase shifts. The resonances are given by the poles of the **S**-matrix in the lower complex wave number (k) plane; more precisely, by the poles of the **S** on the second Riemann sheet of the complex energy plane. As the **S**-matrix is unitary, it is also natural to focus on its total phase shift $\eta(k)$ defined by $\det \mathbf{S} = \exp^{2i\eta(k)}$. The time-delay is proportional to the derivative of the phase shift with respect to the wave number k.

As we are only interested in spectral properties of the scattering problem, it suffices to study $\det \mathbf{S}$. This determinant is basis and coordinate-system independent, whereas the $\mathbf{S}$-matrix itself depends on the global coordinate system and on the choice of basis for the point particle wave function.

As the $\mathbf{S}$-matrix is, in general, an infinite dimensional matrix, it is not clear whether the corresponding determinant exists at all. If $\mathbf{T}$-matrix is trace-class, the determinant does exist. What does this mean?

34.2.1 Trace-class operators

An operator (an infinite-dimensional matrix) is called *trace-class* if and only if, for any choice of orthonormal basis, the sum of the diagonal matrix elements converges absolutely; it is called "Hilbert-Schmidt", if the sum of the absolute squared diagonal matrix elements converges. Once an operator is diagnosed as trace-class, we are allowed to manipulate it as we manipulate finite-dimensional matrices. We review the theory of trace-class operators in appendix J; here we will assume that the $\mathbf{T}$-matrix (33.3) is trace-class, and draw the conlusions.

If $\mathbf{A}$ is trace-class, the determinant $\det(\mathbf{1} - z\mathbf{A})$, as defined by the cumulant expansion, exists and is an entire function of z. Furthermore, the determinant is invariant under any unitary transformation.

The cumulant expansion is the analytical continuation (as Taylor expansion in the book-keeping variable z) of the determinant

$$\det(\mathbf{1} - z\mathbf{A}) = \exp[\mathrm{tr}\,\ln(\mathbf{1} - z\mathbf{A})] = \exp\left(-\sum_{n=1}^{\infty} \frac{z^n}{z^n} \mathrm{tr}\,(\mathbf{A}^n)\right) .$$

That means

$$\det(\mathbf{1} - z\mathbf{A}) := \sum_{m=0}^{\infty} z^m Q_m(\mathbf{A}) , \qquad (34.14)$$

where the cumulants $Q_m(\mathbf{A})$ satisfy the Plemelj-Smithies recursion formula (J.26), a generalization of Newton's formula to determinants of infinite-dimensional matrices,

$$\begin{aligned} Q_0(\mathbf{A}) &= 1 \\ Q_m(\mathbf{A}) &= -\frac{1}{m}\sum_{j=1}^{m} Q_{m-j}(\mathbf{A})\,\mathrm{tr}\,(\mathbf{A}^j) \quad \text{for } m \geq 1 , \end{aligned} \qquad (34.15)$$

in terms of cumulants of order $n < m$ and traces of order $n \leq m$. Because of the trace-class property of $\mathbf{A}$, all cumulants and traces exist separately.

For the general case of $N < \infty$ non-overlapping scatterers, the $\mathbf{T}$-matrix can be shown to be trace-class, so the determinant of the $\mathbf{S}$-matrix is well defined. What does trace-class property mean for the corresponding matrices $\mathbf{C}^s$, $\mathbf{D}^s$ and $\mathbf{A}^{ss'}$? Manipulating the operators as though they were finite matrices, we can perform the following transformations:

$$\begin{aligned} \det \mathbf{S} &= \det\left(\mathbf{1} - i\mathbf{C}\mathbf{M}^{-1}\mathbf{D}\right) \\ &= \mathrm{Det}\left(\mathbf{1} - i\mathbf{M}^{-1}\mathbf{D}\mathbf{C}\right) = \mathrm{Det}\left(\mathbf{M}^{-1}(\mathbf{M} - i\mathbf{D}\mathbf{C})\right) \\ &= \frac{\mathrm{Det}\,(\mathbf{M} - i\mathbf{D}\mathbf{C})}{\mathrm{Det}\,(\mathbf{M})} \,.\,. \end{aligned} \qquad (34.16)$$

In the first line of (34.16) the determinant is taken over small ℓ (the angular momentum with respect to the global system). In the remainder of (34.16) the determinant is evaluated over the multiple indices $L_s = (s, l_s)$. In order to signal this difference we use the following notation: det ... and tr ... refer to the $|\ell\rangle$ space, Det ... and Tr... refer to the multiple index space. The matrices in the multiple index space are expanded in the complete basis $\{|L_s\rangle\} = \{|s, \ell_s\rangle\}$ which refers for fixed index s to the origin of the sth scatterer and not any longer to the origin of the 2-dimensional plane.

Let us explicitly extract the product of the determinants of the subsystems from the determinant of the total system (34.16):

$$\begin{aligned} \det \mathbf{S} &= \frac{\mathrm{Det}\,(\mathbf{M} - i\mathbf{D}\mathbf{C})}{\mathrm{Det}\,(\mathbf{M})} \\ &= \frac{\mathrm{Det}\,(\mathbf{M} - i\mathbf{D}\mathbf{C})}{\mathrm{Det}\,\mathbf{M}} \frac{\prod_{s=1}^{N} \det \mathbf{S}^s}{\prod_{s=1}^{N} \det \mathbf{S}^s} \\ &= \left(\prod_{s=1}^{N} \det \mathbf{S}^s\right) \frac{\mathrm{Det}\,(\mathbf{M} - i\mathbf{D}\mathbf{C})/\prod_{s=1}^{N} \det \mathbf{S}^s}{\mathrm{Det}\,\mathbf{M}} \,. \end{aligned} \qquad (34.17)$$

The final step in the reformulation of the determinant of the $\mathbf{S}$-matrix of the N-scatterer problem follows from the unitarity of the $\mathbf{S}$-matrix. The unitarity of $\mathbf{S}^\dagger(k^*)$ implies for the determinant

$$\det(\mathbf{S}(k^*)^\dagger) = 1/\det \mathbf{S}(k) , \qquad (34.18)$$

where this manipulation is allowed because the $\mathbf{T}$-matrix is trace-class. The unitarity condition should apply for the $\mathbf{S}$-matrix of the total system, $\mathbf{S}$, as for the each of the single subsystems, $\mathbf{S}^s$, $s = 1, \cdots, N$. In terms of the result of (34.17), this implies

$$\frac{\mathrm{Det}\,(\mathbf{M}(k) - i\mathbf{D}(k)\mathbf{C}(k))}{\prod_{s=1}^{N} \det \mathbf{S}^s} = \mathrm{Det}\,(\mathbf{M}(k^*)^\dagger)$$

since all determinants in (34.17) exist separately and since the determinants $\det \mathbf{S}^s$ respect unitarity by themselves. Thus, we finally have

$$\det \mathbf{S}(k) = \left\{ \prod_{s=1}^{N} (\det \mathbf{S}^s(k)) \right\} \frac{\mathrm{Det}\, \mathbf{M}(k^*)^\dagger}{\mathrm{Det}\, \mathbf{M}(k)} \,, \tag{34.19}$$

where all determinants exist separately.

In summary: We assumed a scattering system of a *finite* number of *non-overlapping* scatterers which can be of different shape and size, but are all of finite extent. We assumed the trace-class character of the $\mathbf{T}$-matrix belonging to the total system and of the single-traversal matrix $\mathbf{A}$ and finally unitarity of the $\mathbf{S}$-matrices of the complete and all subsystems.

What can one say about the point-particle scattering from a finite number of scatterers of arbitrary shape and size? As long as each of $N < \infty$ single scatterers has a finite spatial extent, i.e., can be covered by a finite disk, the total system has a finite spatial extent as well. Therefore, it too can be put insided a circular domain of finite radius b, e.g., inside a single disk. If the impact parameter of the point particle measured with respect to the origin of this disk is larger than the disk size (actually larger than $(e/2) \times b$), then the $\mathbf{T}$ matrix elements of the N-scatterer problem become very small. If the wave number k is kept fixed, the modulus of the *diagonal* matrix elements, $|T_{mm}|$ with the angular momentum $m > (e/2)kb$, is bounded by the corresponding quantity of the covering disk.

34.2.2 Quantum cycle expansions

In formula (34.19) the genuine multi-scattering terms are separated from the single-scattering ones. We focus on the multi-scattering terms, i.e., on the ratio of the determinants of the multi-scattering matrix $\mathbf{M} = \mathbf{1} - \mathbf{A}$ in (34.19), since they are the origin of the periodic orbit sums in the semiclassical reduction. The resonances of the multi-scattering system are given by the zeros of $\mathrm{Det}\, \mathbf{M}(k)$ in the lower complex wave number plane.

In order to set up the problem for the semiclassical reduction, we express the determinant of the multi-scattering matrix in terms of the traces of the powers of the matrix $\mathbf{A}$, by means of the cumulant expansion (34.14). Because of the finite number $N \geq 2$ of scatterers $\mathrm{tr}\,(\mathbf{A}^n)$ receives contributions corresponding to all periodic itineraries $s_1 s_2 s_3 \cdots s_{n-1} s_n$ of total symbol length n with an alphabet $s_i \in \{1, 2, \ldots, N\}$. of N symbols,

$$\begin{aligned} &\mathrm{tr}\, \mathbf{A}^{s_1 s_2} \mathbf{A}^{s_2 s_3} \cdots \mathbf{A}^{s_{n-1} s_n} \mathbf{A}^{s_n s_n} \\ &= \sum_{l_{s_1}=-\infty}^{+\infty} \sum_{l_{s_2}=-\infty}^{+\infty} \cdots \sum_{l_{s_n}=-\infty}^{+\infty} A^{s_1 s_2}_{l_{s_1} l_{s_2}} A^{s_2 s_3}_{l_{s_2} l_{s_3}} \cdots A^{s_{n-1} s_n}_{l_{s_{n-1}} l_{s_n}} A^{s_n s_1}_{l_{s_n} l_{s_1}} \,. \end{aligned} \tag{34.20}$$

Remember our notation that the trace $\mathrm{tr}\,(\cdots)$ refers only to the $|l\rangle$ space. By construction $\mathbf{A}$ describes only scatterer-to-scatterer transitions, so the symbolic dynamics has to respect the no-self-reflection pruning rule: for admissible itineraries the successive symbols have to be different. This rule is implemented by the factor $1 - \delta^{ss'}$ in (34.13).

The trace $\mathrm{tr}\, \mathbf{A}^n$ is the sum of all itineraries of length n,

$$\mathrm{tr}\, \mathbf{A}^n = \sum_{\{s_1 s_2 \cdots s_n\}} \mathrm{tr}\, \mathbf{A}^{s_1 s_2} \mathbf{A}^{s_2 s_3} \cdots \mathbf{A}^{s_{n-1} s_n} \mathbf{A}^{s_n s_1} \,. \tag{34.21}$$

We will show for the N-disk problem that these periodic itineraries correspond in the semiclassical limit, $ka_{s_i} \gg 1$, to *geometrical* periodic orbits with the same symbolic dynamics.

For periodic orbits with creeping sections the symbolic alphabet has to be extended, see sect. 34.3.1. Furthermore, depending on the geometry, there might be nontrivial pruning rules based on the so called ghost orbits, see sect. 34.4.1.

34.2.3 Symmetry reductions

The determinants over the multi-scattering matrices run over the multiple index L of the multiple index space. This is the proper form for the symmetry reduction (in the multiple index space), e.g., if the scatterer configuration is characterized by a discrete symmetry group G, we have

$$\mathrm{Det}\, \mathbf{M} = \prod_\alpha \left(\det \mathbf{M}_{\mathrm{D}_\alpha}(k)\right)^{d_\alpha} \,,$$

where the index α runs over all conjugate classes of the symmetry group G and D_α is the αth representation of dimension d_α. The symmetry reduction on the exact quantum mechanical level is the same as for the classical evolution operators spectral determinant factorization (**??**) of sect. **??**.

34.3 Semiclassical 1-disk scattering

We start by focusing on the single-scatterer problem. In order to be concrete, we will consider the semiclassical reduction of the scattering of a single disk in plane.

Instead of calculating the semiclassical approximation to the determinant of the one-disk system scattering matrix (34.9), we do so for

$$\mathbf{d}(k) \equiv \frac{1}{2\pi i} \frac{d}{dk} \ln \det \mathbf{S}^1(ka) \;= \frac{1}{2\pi i} \frac{d}{dk} \mathrm{tr}\, \left(\ln \mathbf{S}^1(ka) \right) \tag{34.22}$$

the so called *time delay*.

$$\begin{aligned}\mathbf{d}(k) &= \frac{1}{2\pi i}\frac{d}{dk}\mathrm{tr}\,\left(\ln\det\mathbf{S}^1(ka)\right) = \frac{1}{2\pi i}\sum_m \left(\frac{H_m^{(1)}(ka)}{H_m^{(2)}(ka)}\frac{d}{dk}\frac{H_m^{(2)}(ka)}{H_m^{(1)}(ka)}\right)\\ &= \frac{a}{2\pi i}\sum_m\left(\frac{H_m^{(2)\prime}(ka)}{H_m^{(2)}(ka)} - \frac{H_m^{(1)\prime}(ka)}{H_m^{(1)}(ka)}\right)\,. \end{aligned} \tag{34.23}$$

Here the prime denotes the derivative with respect to the argument of the Hankel functions. Let us introduce the abbreviation

$$\chi_\nu = \frac{H_\nu^{(2)\prime}(ka)}{H_\nu^{(2)}(ka)} - \frac{H_\nu^{(1)\prime}(ka)}{H_\nu^{(1)}(ka)}\,. \tag{34.24}$$

We apply the Watson contour method to (34.23)

$$\mathbf{d}(k) = \frac{a_j}{2\pi i}\sum_{m=-\infty}^{+\infty}\chi_m = \frac{a_j}{2\pi i}\frac{1}{2i}\oint_C \mathrm{d}\nu\,\frac{e^{-i\nu\pi}}{\sin(\nu\pi)}\chi_\nu\,. \tag{34.25}$$

Here the contour C encircles in a counter-clockwise manner a small semiinfinite strip D which completely covers the real ν-axis but which only has a small finite extent into the positive and negative imaginary ν direction. The contour C is then split up in the path above and below the real ν-axis such that

$$\mathbf{d}(k) = \frac{a}{4\pi i}\left\{\int_{-\infty+i\epsilon}^{+\infty+i\epsilon}\mathrm{d}\nu\,\frac{e^{-i\nu\pi}}{\sin(\nu\pi)}\chi_\nu - \int_{-\infty-i\epsilon}^{+\infty-i\epsilon}\mathrm{d}\nu\,\frac{e^{-i\nu\pi}}{\sin(\nu\pi)}\chi_\nu\right\}\,.$$

Then, we perform the substitution $\nu \to -\nu$ in the second integral so as to get

$$\begin{aligned}\mathbf{d}(k) &= \frac{a}{4\pi}\left\{\int_{-\infty+i\epsilon}^{+\infty+i\epsilon}\mathrm{d}\nu\,\frac{e^{-i\nu\pi}}{\sin(\nu\pi)}\chi_\nu + \mathrm{d}\nu\,\frac{e^{+i\nu\pi}}{\sin(\nu\pi)}\chi_{-\nu}\right\}\\ &= \frac{a}{2\pi i}\left\{2\int_{-\infty+i\epsilon}^{+\infty+i\epsilon}\mathrm{d}\nu\,\frac{e^{2i\nu\pi}}{1-e^{2i\nu\pi}}\,\chi_\nu + \int_{-\infty}^{+\infty}\mathrm{d}\nu\,\chi_\nu\right\}\,, \end{aligned}\tag{34.26}$$

where we used the fact that $\chi_{-\nu} = \chi_\nu$. The contour in the last integral can be deformed to pass over the real ν-axis since its integrand has no Watson denominator.

We will now approximate the last expression semiclassically, i.e., under the assumption $ka \gg 1$. As the two contributions in the last line of (34.26) differ by the presence or absence of the Watson denominator, they will have to be handled semiclassically in different ways: the first will be closed in the upper complex plane and evaluated at the poles of χ_ν, the second integral will be evaluated on the real ν-axis under the Debye approximation for Hankel functions.

We will now work out the first term. The poles of χ_ν in the upper complex plane are given by the zeros of $H_\nu^{(1)}(ka)$ which will be denoted by $\nu_\ell(ka)$ and by the zeros of $H_\nu^{(2)}(ka)$ which we will denote by $-\bar\nu_\ell(ka)$, $\ell = 1, 2, 3, \cdots$. In the Airy approximation to the Hankel functions they are given by

$$\nu_\ell(ka) = ka + i\alpha_\ell(ka)\,, \tag{34.27}$$

$$-\bar\nu_\ell(ka) = -ka + i(\alpha_\ell(k^*a))^* = -\left(\nu_\ell(k^*a)\right)^*\,, \tag{34.28}$$

with

$$\begin{aligned} i\alpha_\ell(ka) &= e^{i\frac{\pi}{3}}\left(\frac{ka}{6}\right)^{1/3} q_\ell - e^{-i\frac{\pi}{3}}\left(\frac{6}{ka}\right)^{1/3}\frac{q_\ell^2}{180} - \frac{1}{70ka}\left(1-\frac{q_\ell^3}{30}\right)\\ &+ e^{i\frac{\pi}{3}}\left(\frac{6}{ka}\right)^{\frac{5}{3}}\frac{1}{3150}\left(\frac{29q_\ell}{6^2} - \frac{281q_\ell^4}{180\cdot 6^3}\right) + \cdots\,. \end{aligned}\tag{34.29}$$

Here q_ℓ labels the zeros of the Airy integral

$$A(q) \equiv \int_0^\infty \mathrm{d}\tau\,\cos(q\tau - \tau^3) = 3^{-1/3}\pi\mathrm{Ai}(-3^{-1/3}q)\,,$$

with $\mathrm{Ai}(z)$ being the standard Airy function; approximately, $q_\ell \approx 6^{1/3}[3\pi(\ell - 1/4)]^{2/3}/2$. In order to keep the notation simple, we will abbreviate $\nu_\ell \equiv \nu_\ell(ka)$ and $\bar\nu_\ell \equiv \bar\nu_\ell(ka)$. Thus the first term of (34.26) becomes finally

$$\frac{a}{2\pi i}\left\{2\int_{-\infty+i\epsilon}^{+\infty+i\epsilon}\mathrm{d}\nu\,\frac{e^{2i\nu\pi}}{1-e^{2i\nu\pi}}\,\chi_\nu\right\} = 2a\sum_{\ell=1}^{\infty}\left(\frac{e^{2i\nu_\ell\pi}}{1-e^{2i\nu_\ell\pi}} + \frac{e^{-2i\bar\nu_\ell\pi}}{1-e^{-2i\bar\nu_\ell\pi}}\right)\,.$$

In the second term of (34.26) we will insert the Debye approximations for the Hankel functions:

$$\begin{aligned} H_\nu^{(1/2)}(x) &\sim \sqrt{\frac{2}{\pi\sqrt{x^2-\nu^2}}}\exp\left(\pm i\sqrt{x^2-\nu^2} \mp i\nu\arccos\frac{\nu}{x} \mp i\frac{\pi}{4}\right) \quad \text{for } |x| > \nu \\ H_\nu^{(1/2)}(x) &\sim \mp i\sqrt{\frac{2}{\pi\sqrt{\nu^2-x^2}}}\exp\left(-\sqrt{\nu^2-x^2} + \nu\mathrm{ArcCosh}\frac{\nu}{x}\right) \quad \text{for } |x| < \nu\,. \end{aligned}\tag{34.30}$$

Note that for $\nu > ka$ the contributions in χ_ν cancel. Thus the second integral of (34.26) becomes

$$\begin{aligned}\frac{a}{2\pi i}\int_{-\infty}^{+\infty} \mathrm{d}\nu\, \chi_\nu &= \frac{a}{2\pi i}\int_{-ka}^{+ka} \mathrm{d}\nu\, \frac{(-2i)}{a}\frac{d}{dk}\left(\sqrt{k^2a^2-\nu^2} - \nu\arccos\frac{\nu}{ka}\right) + \cdots \\ &= -\frac{1}{k\pi}\int_{-ka}^{ka} \mathrm{d}\nu\sqrt{k^2a^2-\nu^2} + \cdots = -\frac{a^2}{2}k + \cdots\,, \qquad (34.31)\end{aligned}$$

where $\cdots$ takes care of the polynomial corrections in the Debye approximation and the boundary correction terms in the ν integration.

In summary, the semiclassical approximation to $\mathbf{d}(k)$ reads

$$\mathbf{d}(k) = 2a\sum_{\ell=1}^{\infty}\left(\frac{e^{2i\nu_\ell\pi}}{1-e^{2i\nu_\ell\pi}} + \frac{e^{-2i\bar{\nu}_\ell\pi}}{1-e^{-2i\bar{\nu}_\ell\pi}}\right) - \frac{a^2}{2}k + \cdots\,.$$

Using the definition of the time delay (34.22), we get the following expression for $\det \mathbf{S}^1(ka)$:

$$\begin{aligned}&\ln\det\mathbf{S}^1(ka) - \lim_{k_0\to 0}\ln\det\mathbf{S}^1(k_0a) \qquad (34.32)\\ &= 2\pi i a\int_0^k \mathrm{d}\tilde{k}\left(-\frac{a\tilde{k}}{2} + 2\sum_{\ell=1}^{\infty}\left(\frac{e^{i2\pi\nu_\ell(\tilde{k}a)}}{1-e^{i2\pi\nu_\ell(\tilde{k}a)}} + \frac{e^{-i2\pi\bar{\nu}_\ell(\tilde{k}a)}}{1-e^{-i2\pi\bar{\nu}_\ell(\tilde{k}a)}}\right)\right) + \cdots \\ &\sim -2\pi i N(k) + 2\sum_{\ell=1}^{\infty}\int_0^k \mathrm{d}\tilde{k}\,\frac{d}{d\tilde{k}}\left\{-\ln\left(1-e^{i2\pi\nu_\ell(\tilde{k}a)}\right) + \ln\left(1-e^{-i2\pi\bar{\nu}_\ell(\tilde{k}a)}\right)\right\} + \cdots,\end{aligned}$$

where in the last expression it has been used that semiclassically $\frac{d}{dk}\nu_\ell(ka) \sim \frac{d}{dk}\bar{\nu}_\ell(ka) \sim a$ and that the Weyl term for a single disk of radius a goes like $N(k) = \pi a^2k^2/(4\pi) + \cdots$ (the next terms come from the boundary terms in the ν-integration in (34.31)). Note that for the lower limit, $k_0 \to 0$, we have two simplifications: First,

$$\begin{aligned}\lim_{k_0\to 0} S^1_{mm'}(k_0a) = \lim_{k_0\to 0}\frac{-H^{(2)}_m(k_0a)}{H^{(1)}_m(k_0a)}\delta_{mm'} &= 1\times\delta_{mm'} \qquad \forall m,m' \\ \to \quad \lim_{k_0\to 0}\det\mathbf{S}^1(k_0a) &= 1\,.\end{aligned}$$

Secondly, for $k_0 \to 0$, the two terms in the curly bracket of (34.32) cancel.

34.3.1 1-disk spectrum interpreted; pure creeping

To summarize: the semiclassical approximation to the determinant $\mathbf{S}^1(ka)$ is given by

$$\det\mathbf{S}^1(ka) \sim e^{-i2\pi N(k)}\frac{\prod_{\ell=1}^{\infty}\left(1-e^{-2i\pi\bar{\nu}_\ell(ka)}\right)^2}{\prod_{\ell=1}^{\infty}\left(1-e^{2i\pi\nu_\ell(ka)}\right)^2}\,, \qquad (34.33)$$

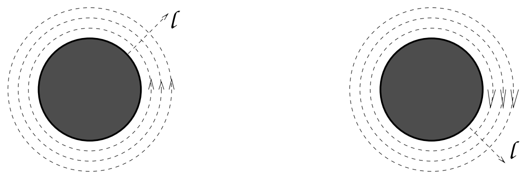

Figure 34.2: Right- and left-handed diffractive creeping paths of increasing mode number ℓ for a single disk.

with

$$\begin{aligned}\nu_\ell(ka) &= ka + i\alpha_\ell(ka) &&= ka + e^{+i\pi/3}(ka/6)^{1/3}q_\ell + \cdots \\ \bar{\nu}_\ell(ka) &= ka - i(\alpha_\ell(k^*a))^* &&= ka + e^{-i\pi/3}(ka/6)^{1/3}q_\ell + \cdots \\ &= (\nu_\ell(k^*a))^*\end{aligned}$$

and $N(ka) = (\pi a^2k^2)/4\pi + \cdots$ the leading term in the Weyl approximation for the staircase function of the wavenumber eigenvalues in the disk interior. From the point of view of the scattering particle, the interior domains of the disks are excluded relatively to the free evolution without scattering obstacles. Therefore the negative sign in front of the Weyl term. For the same reason, the subleading boundary term has here a Neumann structure, although the disks have Dirichlet boundary conditions.

Let us abbreviate the r.h.s. of (34.33) for a disk s as

$$\det\mathbf{S}^s(ka_s) \sim \left(e^{-i\pi N(ka_s)}\right)^2\frac{\widetilde{Z}^s_\ell(k^*a_s)^*}{\widetilde{Z}^s_\ell(ka_s)}\frac{\widetilde{Z}^s_r(k^*a_s)^*}{\widetilde{Z}^s_r(ka_s)}\,, \qquad (34.34)$$

where $\widetilde{Z}^s_\ell(ka_s)$ and $\widetilde{Z}^s_r(ka_s)$ are the *diffractional* zeta functions (here and in the following we will label semiclassical zeta functions *with* diffractive corrections by a tilde) for creeping orbits around the sth disk in the left-handed sense and the right-handed sense, respectively (see figure 34.2). The two orientations of the creeping orbits are the reason for the exponents 2 in (34.33). Equation (34.33) describes the semiclassical approximation to the incoherent part (= the curly bracket on the r.h.s.) of the exact expression (34.19) for the case that the scatterers are disks.

In the following we will discuss the semiclassical resonances in the 1-disk scattering problem with Dirichlet boundary conditions, i.e. the so-called shape resonances. The quantum mechanical resonances are the poles of the S-matrix in the complex k-plane. As the 1-disk scattering problem is separable, the S-matrix is already diagonalized in the angular momentum eigenbasis and takes the simple form (34.9). The exact quantummechanical poles of the scattering matrix are therefore given by the the zeros, k^{res}_{nm}, of the Hankel functions $H^{(1)}_m(ka)$ in the lower complex k plane which can be labeled by two indices, m and n, where m denotes the angular quantum number of the Hankel function and n is a radial quantum number. As the Hankel functions have to vanish at specific k values, one cannot use the usual Debye approximation as semiclassical approximation for the Hankel function, since this approximation only works in case the Hankel function is dominated by only one saddle. However, for the vanishing of the Hankel function, one has to have the interplay of two saddles, thus an Airy approximation is needed as in the case of the creeping poles discussed above. The Airy approximation of the Hankel function $H_\nu^{(1)}(ka)$ of complex-valued index ν reads

$$H_\nu^{(1)}(ka) \sim \frac{2}{\pi} e^{-i\frac{\pi}{3}} \left(\frac{6}{ka}\right)^{1/3} A(q^{(1)}) \,,$$

with

$$q^{(1)} = e^{-i\frac{\pi}{3}} \left(\frac{6}{ka}\right)^{1/3} (\nu - ka) + \mathcal{O}\left((ka)^{-1}\right).$$

Hence the zeros ν_ℓ of the Hankel function in the complex ν plane follow from the zeros q_ℓ of the Airy integral $A(q)$ (see (34.3). Thus if we set $\nu_\ell = m$ (with m integer), we have the following semiclassical condition on $k^{\rm res}$

$$\begin{aligned} m &\sim k^{\rm res} a + i\alpha_\ell(k^{\rm res}a) \\ &= e^{i\frac{\pi}{3}} \left(\frac{k^{\rm res}a}{6}\right)^{1/3} q_\ell - e^{-i\frac{\pi}{3}} \left(\frac{6}{k^{\rm res}a}\right)^{1/3} \frac{q_\ell^2}{180} - \frac{1}{70k^{\rm res}a} \Big(\\ &+ e^{i\frac{\pi}{3}} \left(\frac{6}{k^{\rm res}a}\right)^{\frac{5}{3}} \frac{1}{3150} \left(\frac{29q_\ell}{6^2} - \frac{281q_\ell^4}{180\cdot 6^3}\right) + \cdots , \end{aligned}$$

with $l = 1, 2, 3, \cdots$.

For a given index l this is equivalent to

$$0 \sim 1 - e^{(ik^{\rm res} - \alpha_\ell)2\pi a} \,,$$

the de-Broglie condition on the wave function that encircles the disk. Thus the semiclassical resonances of the 1-disk problem are given by the zeros of the following product

$$\prod_{l=1}^{\infty} \left(1 - e^{(ik - \alpha_\ell)2\pi a}\right),$$

which is of course nothing else than $\widetilde{Z}_{\text{1-disk}}(k)$, the semiclassical diffraction zeta function of the 1-disk scattering problem, see (34.34). Note that this

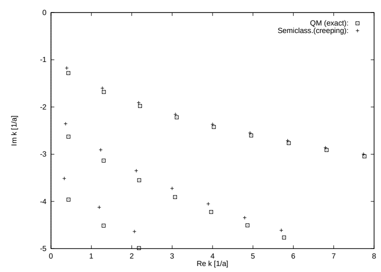

Figure 34.3: The shape resonances of the 1-disk system in the complex k plane in units of the disk radius a. The boxes label the exact quantum mechanical resonances (given by the zeros of $H_m^{(1)}(ka)$ for $m = 0, 1, 2$), the crosses label the diffractional semiclassical resonances (given by the zeros of the creeping formula in the Airy approximation (34.35) up to the order $\mathcal{O}([ka]^{1/3})$).

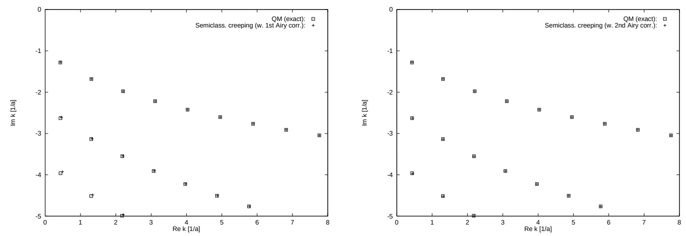

Figure 34.4: Same as in figure 34.3. However, the subleading terms in the Airy approximation (34.35) are taken into account up to the order $\mathcal{O}([ka]^{-1/3})$ (upper panel) and up to order $\mathcal{O}([ka]^{-1})$ (lower panel).

expression includes just the pure creeping contribution and no genuine geometrical parts. Because of

$$H_{-m}^{(1)}(ka) = (-1)^m H_m^{(1)}(ka) \,,$$

the zeros are doubly degenerate if $m \neq 0$, corresponding to right- and left handed creeping turns. The case $m = 0$ is unphysical, since all zeros of the Hankel function $H_0^{(1)}(ka)$ have negative real value.

From figure 34.3 one notes that the creeping terms in the Airy order $\mathcal{O}([ka]^{1/3})$, which are used in the Keller construction, systematically underestimate the magnitude of the imaginary parts of the exact data. However, the creeping data become better for increasing $\mathrm{Re}\, k$ and decreasing $|\mathrm{Im}\, k|$, as they should as semiclassical approximations.

In the upper panel of figure 34.4 one sees the change, when the next order in the Airy approximation (34.35) is taken into account. The approximation is nearly perfect, especially for the leading row of resonances. The second

Airy approximation using (34.35) up to order $\mathcal{O}([ka]^{-1})$ is perfect up to the drawing scale of figure 34.4 (lower panel).

34.4 From quantum cycle to semiclassical cycle

The procedure for the semiclassical approximation of a general periodic itinerary (34.20) of length n is somewhat laborious, and we will only sketch the procedure here. It follows, in fact, rather closely the methods developed for the semiclassical reduction of the determinant of the 1-disk system.

The quantum cycle

$$\mathrm{tr}\,\mathbf{A}^{s_1 s_2}\cdots\mathbf{A}^{s_m s_1} = \sum_{l_{s_1}=-\infty}^{\infty}\cdots\sum_{l_{s_m}=-\infty}^{\infty} A^{s_1 s_2}_{l_{s_1} l_{s_2}}\cdots A^{s_m s_1}_{l_{s_m} l_{s_1}}$$

still has the structure of a "multi-trace" with respect to angular momentum.

Each of the sums $\sum_{l_{s_i}=-\infty}^{\infty}$ – as in the 1-disk case – is replaced by a *Watson contour* resummation in terms of complex angular momentum ν_{s_i}. Then the paths below the real ν_{s_i}-axes are transformed to paths above these axes, and the integrals split into expressions *with* and *without* an explicit Watson $\sin(\nu_{s_i}\pi)$ denominator.

1. In the $\sin(\nu_{s_i}\pi)$ -independent integrals we replace all Hankel and Bessel functions by Debye approximations. Then we evaluate the expression in the saddle point approximation: either left or right *specular reflection* at disk s_i or *ghost tunneling* through disk s_i result.
2. For the $\sin(\nu_{s_i}\pi)$ -dependent integrals, we close the contour in the upper ν_{s_i} plane and evaluate the integral at the residua $H^{(1)}_{\nu_{s_i}}(ka_{s_i})$=0. Then we use the Airy approximation for $J_{\nu_{s_i}}(ka_{s_i})$ and $H^{(1)}_{\nu_{s_i}}(ka_{s_i})$: left and right *creeping paths* around disk s_i result.

In the above we have assumed that no grazing geometrical paths appear. If they do show up, the analysis has to be extended to the case of coninciding saddles between the geometrical paths with $\pi/2$ angle reflection from the disk surface and paths with direct ghost tunneling through the disk.

There are three possibilities of "semiclassical" contact of the point particle with the disk s_i:

1. either geometrical which in turn splits into three alternatives
   (a) *specular reflection* to the right,
   (b) *specular reflection* to the left,

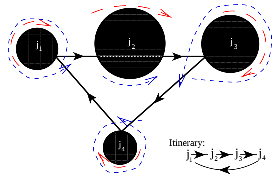

Figure 34.5: A 4-disk problem with three specular reflections, one ghost tunneling, and distinct creeping segments from which all associated creeping paths can be constructed.

   (c) or *'ghost tunneling'* where the latter induce the nontrivial pruning rules (as discussed above)
2. or *right-handed creeping turns*
3. or *left-handed creeping turns*,

see figure 34.5. The specular reflection to the right is linked to left-handed creeping paths with at least one knot. The specular reflection to the left matches a right-handed creeping paths with at least one knot, whereas the shortest left- and right-handed creeping paths in the ghost tunneling case are topologically trivial. In fact, the topology of the creeping paths encodes the choice between the three alternatives for the geometrical contact with the disk. This is the case for the simple reason that creeping sections have to be positive definite in length: the creeping amplitude has to decrease during the creeping process, as tangential rays are constantly emitted. In mathematical terms, it means that the creeping angle has to be positive. Thus, the positivity of the *two* creeping angles for the shortest left *and* right turn uniquely specifies the topology of the creeping sections which in turn specifies which of the three alternatives, either specular reflection to the right or to the left or straight "ghost" tunneling through disk j, is realized for the semiclassical geometrical path. Hence, the existence of a unique saddlepoint is guaranteed.

In order to be concrete, we will restrict ourselves in the following to the scattering from $N<\infty$ non-overlapping *disks* fixed in the 2-dimensional plane. The semiclassical approximation of the periodic itinerary

$$\mathrm{tr}\,\mathbf{A}^{s_1 s_2}\mathbf{A}^{s_2 s_3}\cdots\mathbf{A}^{s_{n-1} s_n}\mathbf{A}^{s_n s_1}$$

becomes a standard periodic orbit labeled by the symbol sequence $s_1 s_2\cdots s_n$. Depending on the geometry, the individual legs $s_{i-1}\to s_i\to s_{i+1}$ result either from a standard specular reflection at disk s_i or from a ghost path passing straight through disk s_i. If furthermore creeping contributions are taken into account, the symbolic dynamics has to be generalized from single-letter symbols $\{s_i\}$ to triple-letter symbols $\{s_i, \sigma_i\times\ell_i\}$ with $\ell_i\geq 1$ integer valued and $\sigma_i=0,\pm 1$ [1] By definition, the value $\sigma_i=0$ represents the non-creeping case, such that $\{s_i, 0\times\ell_i\}=\{s_i,0\}=\{s_i\}$ reduces to the old single-letter symbol. The magnitude of a nonzero ℓ_i corresponds to creeping

[1] Actually, these are double-letter symbols as σ_i and l_i are only counted as a product.

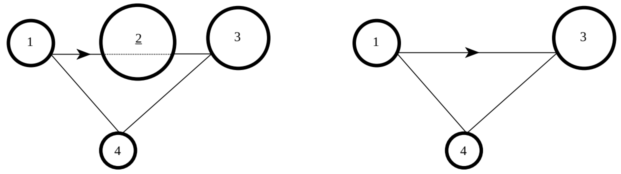

Figure 34.6: (a) The ghost itinerary $(1, \underline{2}, 3, 4)$. (b) The parent itinerary $(1, 3, 4)$.

sections of mode number $|\ell_i|$, whereas the sign $\sigma_i = \pm 1$ signals whether the creeping path turns around the disk s_i in the positive or negative sense. Additional full creeping turns around a disk s_i can be summed up as a geometrical series; therefore they do not lead to the introduction of a further symbol.

34.4.1 Ghost contributions

An itinerary with a semiclassical ghost section at, say, disk s_i can be shown to have the same weight as the corresponding itinerary without the s_ith symbol. Thus, semiclassically, they cancel each other in the $\mathrm{tr}\ln(\mathbf{1} - \mathbf{A})$ expansion, where they are multiplied by the permutation factor n/r with the integer r counting the repeats. For example, let $(1, \underline{2}, 3, 4)$ be a non-repeated periodic itinerary with a ghost section at disk 2 steming from the 4th-order trace $\mathrm{tr}\, A^4$. By convention, an underlined disk index signals a ghost passage (as in figure 34.6a), with corresponding semiclassical ghost traversal matrices also underlined, $\underline{\mathbf{A}}^{i,\underline{i+1}}\underline{\mathbf{A}}^{\underline{i+1},i+2}$. Then its semiclassical, geometrical contribution to $\mathrm{tr}\ln(\mathbf{1} - \mathbf{A})$ cancels exactly against the one of its "parent" itinerary $(1, 3, 4)$ (see figure 34.6b) resulting from the 3rd-order trace:

$$
\begin{aligned}
&-\frac{1}{4}\left(4\,\underline{\mathbf{A}}^{1,\underline{2}}\underline{\mathbf{A}}^{\underline{2},3}\mathbf{A}^{3,4}\mathbf{A}^{4,1}\right) - \frac{1}{3}\left(3\,\mathbf{A}^{1,3}\mathbf{A}^{3,4}\mathbf{A}^{4,1}\right) \\
&= \ (+1-1)\,\mathbf{A}^{1,3}\mathbf{A}^{3,4}\mathbf{A}^{4,1} = 0\,.
\end{aligned}
$$

The prefactors $-1/3$ and $-1/4$ are due to the expansion of the logarithm, the factors 3 and 4 inside the brackets result from the cyclic permutation of the periodic itineraries, and the cancellation stems from the rule

$$
\cdots\,\underline{\mathbf{A}}^{i,\underline{i+1}}\underline{\mathbf{A}}^{\underline{i+1},i+2}\cdots = \cdots\left(-\mathbf{A}^{i,i+2}\right)\cdots\,. \tag{34.36}
$$

The reader might study more complicated examples and convince herself that the rule (34.36).is sufficient to cancel any primary or repeated periodic orbit with one or more ghost sections completely out of the expansion of $\mathrm{tr}\ln(\mathbf{1} - \mathbf{A})$ and therefore also out of the cumulant expansion in the semiclassical limit: Any periodic orbit of length m with $n(<m)$ ghost sections is cancelled by the sum of all 'parent' periodic orbits of length

$m - i$ (with $1 \le i \le n$ and i ghost sections removed) weighted by their cyclic permutation factor and by the prefactor resulting from the *trace-log* expansion. This is the way in which the nontrivial pruning for the N-disk billiards can be derived from the exact quantum mechanical expressions in the semiclassical limit. Note that there must exist at least one index i in any given *periodic* itinerary which corresponds to a non-ghost section, since otherwise the itinerary in the semiclassical limit could only be straight and therefore nonperiodic. Furthermore, the series in the ghost cancelation has to stop at the 2nd-order trace, $\mathrm{tr}\,\mathbf{A}^2$, as $\mathrm{tr}\,\mathbf{A}$ itself vanishes identically in the full domain which is considered here.

34.5 Heisenberg uncertainty

Where is the boundary $ka \approx 2^{m-1}\bar{L}/a$ coming from?

This boundary follows from a combination of the uncertainty principle with ray optics and the non-vanishing value for the topological entropy of the 3-disk repeller. When the wave number k is fixed, quantum mechanics can only resolve the classical repelling set up to the critical topological order n.The quantum wave packet which explores the repelling set has to disentangle 2^n different sections of size $d \sim a/2^n$ on the "visible" part of the disk surface (which is of order a) between any two successive disk collisions. Successive collisions are separated spatially by the mean flight length $\bar{L}$, and the flux spreads with a factor $\bar{L}/a$. In other words, the uncertainty principle bounds the maximal sensible truncation in the cycle expansion order by the highest quantum resolution attainable for a given wavenumber k.

Commentary

Remark 34.1 Sources. This chapter is based in its entirety on ref. [J.1]; the reader is referred to the full exposition for the proofs and discussion of details omitted here. sect. 34.3 is based on appendix E of ref. [J.1]. We follow Franz [33.19] in applying the Watson contour method [33.20] to (34.23). The Airy and Debye approximations to the Hankel functions are given in ref. [33.21], the Airy expansion of the 1-disk zeros can be found in ref. [33.22].For details see refs. [33.19, 33.22, 33.23, J.1]. That the interior domains of the disks are excluded relatively to the free evolution without scattering obstacles was noted in refs. [33.24, 33.15].

The procedure for the semiclassical approximation of a general periodic itinerary (34.20) of length n can be found in ref. [J.1] for the case of the N-disk systems. The reader interested in the details of the semiclassical reduction is advised to consult this reference.

The ghost orbits were introduced in refs. [33.12, 33.24].

Remark 34.2 Krein-Friedel-Lloyd formula. In the literature (see, e.g., refs. [33.14, 33.15] based on ref. [33.11] or ref. [33.1]) the transition from the quantum mechanics to the semiclassics of scattering problems has been performed via the semiclassical limit of the left hand sides of the Krein-Friedel-Lloyd sum for the (integrated) spectral density [J.5, J.6, 33.8, 33.9]. See also ref. [33.13] for a modern discussion of the Krein-Friedel-Lloyd formula and refs. [33.1, 33.17] for the connection of (33.17) to the the Wigner time delay.

The order of the two limits in (33.18) and (33.17) is essential, see e.g. Balian and Bloch [33.11] who stress that smoothed level densities should be inserted into the Friedel sums.

The necessity of the $+i\epsilon$ in the semiclassical calculation can be understood by purely phenomenological considerations: Without the $i\epsilon$ term there is no reason why one should be able to neglect spurious periodic orbits which solely are there because of the introduction of the confining boundary. The subtraction of the second (empty) reference system helps just in the removal of those spurious periodic orbits which never encounter the scattering region. The ones that do would still survive the first limit $b \to \infty$, if they were not damped out by the $+i\epsilon$ term.

33.1
page 616

Remark 34.3 $\mathbf{T}$, $\mathbf{C}^s$, $\mathbf{D}^s$ and $\mathbf{A}^{ss'}$ matrices are trace-class In refs. [J.1] it has explicitly been shown that the $\mathbf{T}$-matrix as well as the $\mathbf{C}^s$, $\mathbf{D}^s$ and $\mathbf{A}^{ss'}$-matrices of the scattering problem from $N < \infty$ non-overlapping finite disks are all trace-class. The corresponding properties for the single-disk systems is particulary easy to prove.

Chapter 35

Helium atom

"But," Bohr protested, "nobody will believe me unless I can explain every atom and every molecule." Rutherford was quick to reply, "Bohr, you explain hydrogen and you explain helium and everybody will believe the rest."
—John Archibald Wheeler (1986)

(G. Tanner)

So far much has been said about 1-dimensional maps, game of pinball and other curious but rather idealized dynamical systems. If you have become impatient and started wondering what good are the methods learned so far in solving real physical problems, we have good news for you. We will show in this chapter that the concepts of symbolic dynamics, unstable periodic orbits, and cycle expansions are essential tools to understand and calculate classical and quantum mechanical properties of nothing less than the helium, a dreaded three-body Coulomb problem.

This sounds almost like one step too much at a time; we all know how rich and complicated the dynamics of the three-body problem is – can we really jump from three static disks directly to three charged particles moving under the influence of their mutually attracting or repelling forces? It turns out, we can, but we have to do it with care. The full problem is indeed not accessible in all its detail, but we are able to analyze a somewhat simpler subsystem – collinear helium. This system plays an important role in the classical dynamics of the full three-body problem and its quantum spectrum.

The main work in reducing the quantum mechanics of helium to a semiclassical treatment of collinear helium lies in understanding why we are allowed to do so. We will not worry about this too much in the beginning; after all, 80 years and many failed attempts separate Heisenberg, Bohr and others in the 1920ties from the insights we have today on the role chaos plays for helium and its quantum spectrum. We have introduced collinear helium and learned how to integrate its trajectories in sect. 7.3.

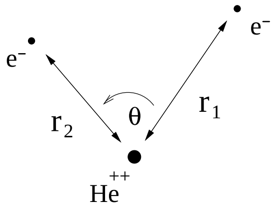

Figure 35.1: Coordinates for the helium three body problem in the plane.

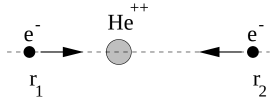

Figure 35.2: Collinear helium, with the two electrons on opposite sides of the nucleus.

Here we will find periodic orbits and determine the relevant eigenvalues of the fundamental matrix in sect. 35.1. We will explain in sect. 35.5 why a quantization of the collinear dynamics in helium will enable us to find parts of the full helium spectrum; we then set up the semiclassical spectral determinant and evaluate its cycle expansion. A full quantum justification of this treatment of helium is briefly discussed in sect. 35.5.1.

35.1 Classical dynamics of collinear helium

Recapitulating briefly what we learned in sect. 7.3: the collinear helium system consists of two electrons of mass m_e and charge $-e$ moving on a line with respect to a fixed positively charged nucleus of charge $+2e$, as in figure 35.2.

The Hamiltonian can be brought to a non–dimensionalized form

$$H = \frac{p_1^2}{2} + \frac{p_2^2}{2} - \frac{2}{r_1} - \frac{2}{r_2} + \frac{1}{r_1 + r_2} = -1\,. \tag{35.1}$$

The case of negative energies chosen here is the most interesting one for us. It exhibits chaos, unstable periodic orbits and is responsible for the bound states and resonances of the quantum problem treated in sect. 35.5.

There is another classical quantity important for a semiclassical treatment of quantum mechanics, and which will also feature prominently in the discussion in the next section; this is the classical action (31.15) which scales with energy as

$$S(E) = \oint d\mathbf{q}(E)\cdot\mathbf{p}(E) = \frac{e^2 m_e^{1/2}}{(-E)^{1/2}}\, S, \tag{35.2}$$

with S being the action obtained from (35.1) for $E=-1$, and coordinates $\mathbf{q} = (r_1, r_2)$, $\mathbf{p} = (p_1, p_2)$. For the Hamiltonian (35.1), the period of a cycle and its action are related by (31.17), $T_p = \frac{1}{2} S_p$.

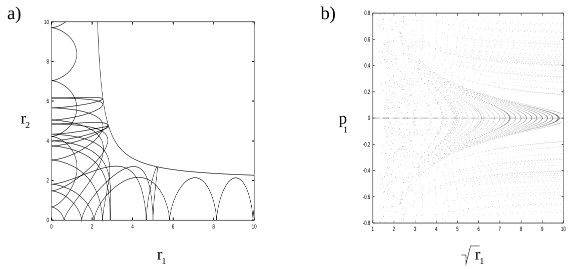

Figure 35.3: (a) A typical trajectory in the $r_1 - r_2$ plane; the trajectory enters here along the r_1 axis and escapes to infinity along the r_2 axis; (b) Poincaré map (r_2=0) for collinear helium. Strong chaos prevails for small r_1 near the nucleus.

After a Kustaanheimo–Stiefel transformation

$$r_1 = Q_1^2\,, \qquad r_2 = Q_2^2\,, \qquad p_1 = \frac{P_1}{2Q_1}\,, \qquad p_2 = \frac{P_2}{2Q_2}\,, \tag{35.3}$$

and reparametrization of time by $d\tau = dt/r_1 r_2$, the equations of motion take form (7.19)

35.1 page 658

$$\dot{P}_1 = 2Q_1\left[2 - \frac{P_2^2}{8} - Q_2^2\left(1 + \frac{Q_2^2}{R_{12}^4}\right)\right]; \qquad \dot{Q}_1 = \frac{1}{4}P_1 Q_2^2 \tag{35.4}$$

$$\dot{P}_2 = 2Q_2\left[2 - \frac{P_1^2}{8} - Q_1^2\left(1 + \frac{Q_1^2}{R_{12}^4}\right)\right]; \qquad \dot{Q}_2 = \frac{1}{4}P_2 Q_1^2.$$

Individual electron–nucleus collisions at $r_1 = Q_1^2 = 0$ or $r_2 = Q_2^2 = 0$ no longer pose a problem to a numerical integration routine. The equations (7.19) are singular only at the triple collision $R_{12} = 0$, i.e., when both electrons hit the nucleus at the same time.

The new coordinates and the Hamiltonian (7.18) are very useful when calculating trajectories for collinear helium; they are, however, less intuitive as a visualization of the three-body dynamics. We will therefore refer to the old coordinates r_1, r_2 when discussing the dynamics and the periodic orbits.

35.2 Chaos, symbolic dynamics and periodic orbits

Let us have a closer look at the dynamics in collinear helium. The electrons are attracted by the nucleus. During an electron–nucleus collision momentum is transferred between the inner and outer electron. The inner electron has a maximal screening effect on the charge of the nucleus, diminishing the attractive force on the outer electron. This electron – electron interaction

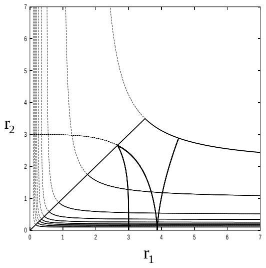

Figure 35.4: The cycle 011 in the fundamental domain $r_1 \geq r_2$ (full line) and in the full domain (dashed line).

is negligible if the outer electron is far from the nucleus at a collision and the overall dynamics is regular like in the 1-dimensional Kepler problem.

Things change drastically if both electrons approach the nucleus nearly simultaneously. The momentum transfer between the electrons depends now sensitively on how the particles approach the origin. Intuitively, these nearly missed triple collisions render the dynamics chaotic. A typical trajectory is plotted in figure 35.3 (a) where we used r_1 and r_2 as the relevant axis. The dynamics can also be visualized in a Poincaré surface of section, see figure 35.3 (b). We plot here the coordinate and momentum of the outer electron whenever the inner particle hits the nucleus, i.e., r_1 or $r_2 = 0$. As the unstructured gray region of the Poincaré section for small r_1 illustrates, the dynamics is chaotic whenever the outer electron is close to the origin during a collision. Conversely, regular motions dominate whenever the outer electron is far from the nucleus. As one of the electrons escapes for almost any starting condition, the system is unbounded: one electron (say electron 1) can escape, with an arbitrary amount of kinetic energy taken by the fugative. The remaining electron is trapped in a Kepler ellipse with total energy in the range $[-1, -\infty]$. There is no energy barrier which would separate the bound from the unbound regions of the phase space. From general kinematic arguments one deduces that the outer electron will not return when $p_1 > 0$, $r_2 \leq 2$ at $p_2 = 0$, the turning point of the inner electron. Only if the two electrons approach the nucleus almost symmetrically along the line $r_1 = r_2$, and pass close to the triple collision can the momentum transfer between the electrons be large enough to kick one of the particles out completely. In other words, the electron escape originates from the near triple collisions.

The collinear helium dynamics has some important properties which we now list.

35.2.1 Reflection symmetry

The Hamiltonian (7.10) is invariant with respect to electron–electron exchange; this symmetry corresponds to the mirror symmetry of the potential along the line $r_1 = r_2$, figure 35.4. As a consequence, we can restrict ourselves to the dynamics in the *fundamental domain* $r_1 \geq r_2$ and treat a crossing

of the diagonal $r_1 = r_2$ as a hard wall reflection. The dynamics in the full domain can then be reconstructed by unfolding the trajectory through back-reflections. As explained in chapter **??**, the dynamics in the fundamental domain is the key to the factorization of spectral determinants, to be implemented here in (35.15). Note also the similarity between the fundamental domain of the collinear potential figure 35.4, and the fundamental domain figure **??** (b) in the 3–disk system, a simpler problem with the same binary symbolic dynamics.

in depth:
sect. ??, p. ??

35.2.2 Symbolic dynamics

We have already made the claim that the triple collisions render the collinear helium fully chaotic. We have no proof of the assertion, but the analysis of the symbolic dynamics lends further credence to the claim.

The potential in (35.1) forms a ridge along the line $r_1 = r_2$. One can show that a trajectory passing the ridge must go through at least one two-body collision $r_1 = 0$ or $r_2 = 0$ before coming back to the diagonal $r_1 = r_2$. This suggests a *binary* symbolic dynamics corresponding to the dynamics in the fundamental domain $r_1 \geq r_2$; the symbolic dynamics is linked to the Poincaré map $r_2 = 0$ and the symbols 0 and 1 are defined as

0: if the trajectory is not reflected from the line $r_1 = r_2$ between two collisions with the nucleus $r_2 = 0$;

1: if a trajectory is reflected from the line $r_1 = r_2$ between two collisions with the nucleus $r_2 = 0$.

Empirically, the symbolic dynamics is complete for a Poincaré map in the fundamental domain, i.e., there exists a one-to-one correspondence between binary symbol sequences and collinear trajectories in the fundamental domain, with exception of the $\overline{0}$ cycle.

35.2.3 Periodic orbits

The existence of a binary symbolic dynamics makes it easy to count the number of periodic orbits in the fundamental domain, as in sect. 13.5.2. However, mere existence of these cycles does not suffice to calculate semiclassical spectral determinants. We need to determine their phase space trajectories and calculate their periods, topological indices and stabilities. A restriction of the periodic orbit search to a suitable Poincaré surface of section, e.g. $r_2 = 0$ or $r_1 = r_2$, leaves us in general with a 2-dimensional search. Methods to find periodic orbits in multi-dimensional spaces have been described in chapter 12. They depend sensitively on good starting guesses. A systematic search for all orbits can be achieved only after combining multi-dimensional Newton methods with interpolation algorithms based on the binary symbolic dynamics phase space partitioning. All cycles up to symbol length 16 (some 8000 primitive cycles) have been computed by such methods, with some examples shown in figure 35.5. All numerical evidence indicates that the dynamics of collinear helium is hyperbolic, and that all periodic orbits are unstable.

Note that the fixed point $\overline{0}$ cycle is not in this list. The $\overline{0}$ cycle would correspond to the situation where the outer electron sits at rest infinitely far from the nucleus while the inner electron bounces back and forth into the nucleus. The orbit is the limiting case of an electron escaping to infinity with zero kinetic energy. The orbit is in the regular (i.e., separable) limit of the dynamics and is thus marginally stable. The existence of this orbit is also related to intermittent behavior generating the quasi–regular dynamics for large r_1 that we have already noted in figure 35.3 (b).

Search algorithm for an arbitrary periodic orbit is quite cumbersome to program. There is, however, a class of periodic orbits, orbits with symmetries, which can be easily found by a one-parameter search. The only symmetry left for the dynamics in the fundamental domain is time reversal symmetry; a time reversal symmetric periodic orbit is an orbit whose trajectory in phase space is mapped onto itself when changing $(p_1, p_2) \to (-p_1, -p_2)$, by reversing the direction of the momentum of the orbit. Such an orbit must be a "libration" or self-retracing cycle, an orbit that runs back and forth along the same path in the (r_1, r_2) plane. The cycles $\overline{1}$, $\overline{01}$ and $\overline{001}$ in figure 35.5 are examples of self-retracing cycles. Luckily, the shortest cycles that we desire most ardently have this symmetry.

Why is this observation helpful? A self-retracing cycle must start perpendicular to the boundary of the fundamental domain, that is, on either of the axis $r_2 = 0$ or $r_1 = r_2$, or on the potential boundary $-\frac{2}{r_1} - \frac{2}{r_2} + \frac{1'}{r_1+r_2} = -1$. By shooting off trajectories perpendicular to the boundaries and monitoring the orbits returning to the boundary with the right symbol length we will find time reversal symmetric cycles by varying the starting point on the boundary as the only parameter. But how can we tell whether a given cycle is self-retracing or not? All the relevant information is contained in the itineraries; a cycle is self-retracing if its itinerary is invariant under time reversal symmetry (i.e., read backwards) and a suitable number of cyclic permutations. All binary strings up to length 5 fulfill this condition. The symbolic dynamics contains even more information; we can tell at which boundary the total reflection occurs. One finds that an orbit starts out perpendicular

- to the diagonal $r_1 = r_2$ if the itinerary is time reversal invariant and has an odd number of 1's; an example is the cycle $\overline{001}$ in figure 35.5;
- to the axis $r_2 = 0$ if the itinerary is time reversal invariant and has an even number of symbols; an example is the cycle $\overline{0011}$ in figure 35.5;

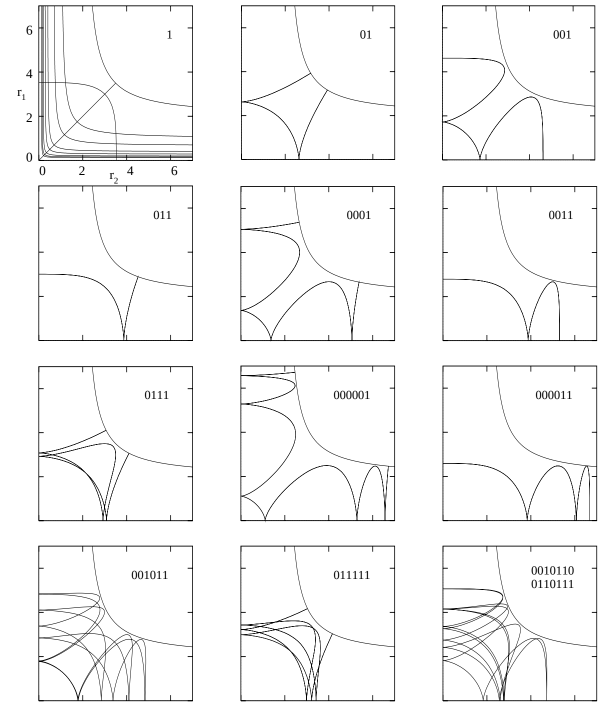

Figure 35.5: Some of the shortest cycles in collinear helium. The classical collinear electron motion is bounded by the potential barrier $-1 = -2/r_1 - 2/r_2 + 1/(r_1 + r_2)$ and the condition $r_i \geq 0$. The orbits are shown in the full r_1–r_2 domain, the itineraries refers to the dynamics in the $r_1 \geq r_2$ fundamental domain. The last figure, the 14-cycle 00101100110111, is an example of a typical cycle with no symmetry.

- to the potential boundary if the itinerary is time reversal invariant and has an odd number of symbols; an example is the cycle $\overline{011}$ in figure 35.5.

All cycles up to symbol length 5 are time reversal invariant, the first two non-time reversal symmetric cycles are cycles $\overline{001011}$ and $\overline{001101}$ in figure 35.5. Their determination would require a two-parameter search. The two cycles are mapped onto each other by time reversal symmetry, i.e., they have the same trace in the r_1–r_2 plane, but they trace out distinct cycles in the full phase space.

We are ready to integrate trajectories for classical collinear helium with the help of the equations of motions (7.19) and to find all cycles up to length 5. There is only one thing not yet in place; we need the governing equations for the matrix elements of the fundamental matrix along a trajectory in order to calculate stability indices. We will provide the main equations in the next section, with the details of the derivation relegated to the appendix B.4.

35.5
page 658

35.3 Local coordinates, fundamental matrix

In this section, we will derive the equations of motion for the fundamental matrix along a collinear helium trajectory. The fundamental matrix is 4-dimensional; the two trivial eigenvectors corresponding to the conservation of energy and displacements along a trajectory can, however, be projected out by suitable orthogonal coordinates transformations, see appendix B. We will give the transformation to local coordinates explicitly, here for the regularized coordinates (7.17), and state the resulting equations of motion for the reduced $[2 \times 2]$ fundamental matrix.

The vector locally parallel to the trajectory is pointing in the direction of the phase space velocity (6.7)

$$v_m = \dot{x}_m(t) = \omega_{mn} \frac{\partial H}{\partial x_n} = (H_{P_1}, H_{P_2}, -H_{Q_1}, -H_{Q_2})^T ,$$

with $H_{Q_i} = \frac{\partial H}{\partial Q_i}$, and $H_{P_i} = \frac{\partial H}{\partial P_i}$, $i = 1{,}2$. The vector perpendicular to a trajectory $x(t) = (Q_1(t), Q_2(t), P_1(t), P_2(t))$ and to the energy manifold is given by the gradient of the Hamiltonian (7.18)

$$\gamma = \nabla H = (H_{Q_1}, H_{Q_2}, H_{P_1}, H_{P_2})^T .$$

By symmetry $v_m \gamma_m = \omega_{mn} \frac{\partial H}{\partial x_n} \frac{\partial H}{\partial x_m} = 0$, so the two vectors are orthogonal.

Next, we consider the orthogonal matrix

$$\mathbf{O} \;=\; (\gamma_1, \gamma_2, \gamma/R, v) \tag{35.5}$$

$$= \begin{pmatrix} -H_{P_2}/R & H_{Q_2} & H_{Q_1}/R & H_{P_1} \\ H_{P_1}/R & -H_{Q_1} & H_{Q_2}/R & H_{P_2} \\ -H_{Q_2}/R & -H_{P_2} & H_{P_1}/R & -H_{Q_1} \\ H_{Q_1}/R & H_{P_1} & H_{P_2}/R & -H_{Q_2} \end{pmatrix}$$

with $R = |\nabla H|^2 = (H_{Q_1}^2 + H_{Q_2}^2 + H_{P_1}^2 + H_{P_2}^2)$, which provides a transformation to local phase space coordinates centered on the trajectory $x(t)$ along the two vectors (γ, v). The vectors $\gamma_{1,2}$ are phase space vectors perpendicular to the trajectory and to the energy manifold in the 4-dimensional phase space of collinear helium. The fundamental matrix (4.6) rotated to the local coordinate system by $\mathbf{O}$ then has the form

35.6
page 659

$$\mathbf{m} = \begin{pmatrix} m_{11} & m_{12} & * & 0 \\ m_{21} & m_{22} & * & 0 \\ 0 & 0 & 1 & 0 \\ * & * & * & 1 \end{pmatrix} , \quad M = \mathbf{O^T m O}$$

The linearized motion perpendicular to the trajectory on the energy manifold is described by the $[2 \times 2]$ matrix $\mathbf{m}$; the 'trivial' directions correspond to unit eigenvalues on the diagonal in the 3rd and 4th column and row.

The equations of motion for the reduced fundamental matrix $\mathbf{m}$ are given by

$$\dot{\mathbf{m}} = \mathbf{l}(t)\mathbf{m}(t), \tag{35.6}$$

with $\mathbf{m}(0) = \mathbf{1}$. The matrix $\mathbf{l}$ depends on the trajectory in phase space and has the form

$$\mathbf{l} = \begin{pmatrix} l_{11} & l_{12} & * & 0 \\ l_{21} & l_{22} & * & 0 \\ 0 & 0 & 0 & 0 \\ * & * & * & 0 \end{pmatrix} ,$$

where the relevant matrix elements l_{ij} are given by

$$\begin{aligned} l_{11} &= \frac{1}{R}[2H_{Q_1Q_2}(H_{Q_2}H_{P_1} + H_{Q_1}H_{P_2}) \\ &\quad + (H_{Q_1}H_{P_1} - H_{Q_2}H_{P_2})(H_{Q_1Q_1} - H_{Q_2Q_2} - H_{P_1P_1} + H_{P_2P_2})] \\ l_{12} &= -2H_{Q_1Q_2}(H_{Q_1}H_{Q_2} - H_{P_1}H_{P_2}) \\ &\quad + (H_{Q_1}^2 + H_{P_2}^2)(H_{Q_2Q_2} + H_{P_1P_1}) + (H_{Q_2}^2 + H_{P_1}^2)(H_{Q_1Q_1} + H_{P_2P_2}) \\ l_{21} &= \frac{1}{R^2}[2(H_{Q_1P_2} + H_{Q_2P_1})(H_{Q_2}H_{P_1} + H_{Q_1}H_{P_8}) \\ &\quad - (H_{P_1}^2 + H_{P_2}^2)(H_{Q_1Q_1} + H_{Q_2Q_2}) - (H_{Q_1}^2 + H_{Q_2}^2)(H_{P_1P_1} + H_{P_2P_2})] \\ l_{22} &= -l_{11} . \end{aligned} \tag{35.7}$$

Here $H_{Q_iQ_j}$, $H_{P_iP_j}$, i, $j = 1, 2$ are the second partial derivatives of H with respect to the coordinates Q_i, P_i, evaluated at the phase space coordinate of the classical trajectory.

p	$S_p/2\pi$	$\ln\|\Lambda_p\|$	σ_p	m_p
1	1.82900	0.6012	0.5393	2
01	3.61825	1.8622	1.0918	4
001	5.32615	3.4287	1.6402	6
011	5.39451	1.8603	1.6117	6
0001	6.96677	4.4378	2.1710	8
0011	7.04134	2.3417	2.1327	8
0111	7.25849	3.1124	2.1705	8
00001	8.56618	5.1100	2.6919	10
00011	8.64306	2.7207	2.6478	10
00101	8.93700	5.1562	2.7291	10
00111	8.94619	4.5932	2.7173	10
01011	9.02689	4.1765	2.7140	10
01111	9.07179	3.3424	2.6989	10
000001	10.13872	5.6047	3.2073	12
000011	10.21673	3.0323	3.1594	12
000101	10.57067	6.1393	3.2591	12
000111	10.57628	5.6766	3.2495	12
001011	10.70698	5.3251	3.2519	12
001101	10.70698	5.3251	3.2519	12
001111	10.74303	4.3317	3.2332	12
010111	10.87855	5.0002	3.2626	12
011111	10.91015	4.2408	3.2467	12

Table 35.1: Action S_p (in units of 2π), Lyapunov exponent $|\Lambda_p|/T_p$ for the motion in the collinear plane, winding number σ_p for the motion perpendicular to the collinear plane, and the topological index m_p for all fundamental domain cycles up to topological length 6.

35.4 Getting ready

Now everything is in place: the regularized equations of motion can be implemented in a Runge–Kutta or any other integration scheme to calculate trajectories. We have a symbolic dynamics and know how many cycles there are and how to find them (at least up to symbol length 5). We know how to compute the fundamental matrix whose eigenvalues enter the semiclassical spectral determinant (32.12). By (31.17) the action S_p is proportional to the period of the orbit, $S_p = 2T_p$.

There is, however, still a slight complication. Collinear helium is an invariant 4-dimensional subspace of the full helium phase space. If we restrict the dynamics to angular momentum equal zero, we are left with 6 phase space coordinates. That is not a problem when computing periodic orbits, they are oblivious to the other dimensions. However, the fundamental matrix does pick up extra contributions. When we calculate the fundamental matrix for the full problem, we must also allow for displacements out of the collinear plane, so the full fundamental matrix for dynamics for $L = 0$ angular momentum is 6 dimensional. Fortunately, the linearized dynamics in and off the collinear helium subspace decouple, and the fundamental matrix can be written in terms of two distinct $[2 \times 2]$ matrices, with trivial eigendirections providing the remaining two dimensions. The submatrix related to displacements off the linear configuration characterizes the linearized dynamics in the additional degree of freedom, the Θ-coordinate in figure 35.1. It turns out that the linearized dynamics in the Θ coordinate is stable, corresponding to a bending type motion of the two electrons. We will need the stability exponents for all degrees of freedom in evaluating the semiclassical spectral determinant in sect. 35.5.

The numerical values of the actions, stability exponents, stability angles, and topological indices for the shortest cycles are listed in table 35.3. These numbers, needed for the semiclassical quantization implemented in the next section, an also be helpful in checking your own calculations.

35.5 Semiclassical quantization of collinear helium

Before we get down to a serious calculation of the helium quantum energy levels let us have a brief look at the overall structure of the spectrum. This will give us a preliminary feel for which parts of the helium spectrum are accessible with the help of our collinear model – and which are not. In order to keep the discussion as simple as possible and to concentrate on the semiclassical aspects of our calculations we offer here only a rough overview. For a guide to more detailed accounts see remark 35.4.

35.5.1 Structure of helium spectrum

We start by recalling Bohr's formula for the spectrum of hydrogen like one-electron atoms. The eigenenergies form a Rydberg series

$$E_N = -\frac{e^4 m_e}{\hbar^2}\frac{Z^2}{2N^2}\,, \tag{35.8}$$

where Ze is the charge of the nucleus and m_e is the mass of the electron. Through the rest of this chapter we adopt the atomic units $e = m_e = \hbar = 1$.

The simplest model for the helium spectrum is obtained by treating the two electrons as independent particles moving in the potential of the nucleus neglecting the electron–electron interaction. Both electrons are then bound in hydrogen like states; the inner electron will see a charge $Z = 2$, screening at the same time the nucleus, the outer electron will move in a Coulomb potential with effective charge $Z-1 = 1$. In this way obtain a first estimate for the total energy

$$E_{N,n} = -\frac{2}{N^2} - \frac{1}{2n^2} \qquad \text{with} \quad n > N. \tag{35.9}$$

This double Rydberg formula contains already most of the information we need to understand the basic structure of the spectrum. The (correct) ionizations thresholds $E_N = -\frac{2}{N^2}$ are obtained in the limit $n \to \infty$, yielding the ground and excited states of the helium ion He^+. We will therefore refer to N as the principal quantum number. We also see that all states $E_{N,n}$ with $N \geq 2$ lie above the first ionization threshold for $N = 1$. As soon as we switch on electron-electron interaction these states are no longer bound states; they turn into resonant states which decay into a bound state of the helium ion and a free outer electron. This might not come as a big surprise if we have the classical analysis of the previous section in mind: we already found that one of the classical electrons will almost always escape after some finite time. More remarkable is the fact that the first, $N = 1$ series consists of true bound states for all n, an effect which can only be understood by quantum arguments.

The hydrogen-like quantum energies (35.8) are highly degenerate; states with different angular momentum but the same principal quantum number N share the same energy. We recall from basic quantum mechanics of hydrogen atom that the possible angular momenta for a given N span $l = 0, 1 \ldots N-1$. How does that affect the helium case? Total angular momentum L for the helium three-body problem is conserved. The collinear helium is a subspace of the classical phase space for $L = 0$; we thus expect that we can only quantize helium states corresponding to the total angular momentum zero, a subspectrum of the full helium spectrum. Going back to our crude estimate (35.9) we may now attribute angular momenta to the two independent electrons, l_1 and l_2 say. In order to obtain total angular momentum $L = 0$ we need $l_1 = l_2 = l$ and $l_{z1} = -l_{z2}$, that is, there

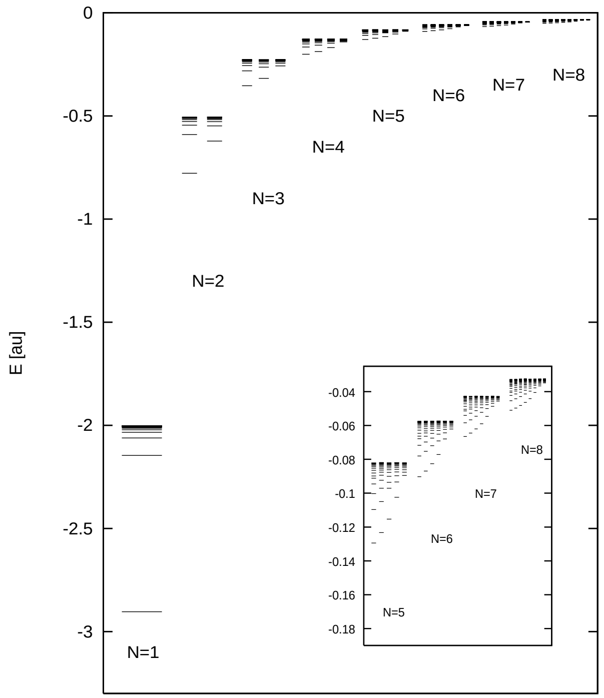

Figure 35.6: The exact quantum helium spectrum for $L = 0$. The energy levels denoted by bars have been obtained from full 3-dimensional quantum calculations [35.3].

are N different states corresponding to $L = 0$ for fixed quantum numbers N, n. That means that we expect N different Rydberg series converging to each ionization threshold $E_N = -2/N^2$. This is indeed the case and the N different series can be identified also in the exact helium quantum spectrum, see figure 35.6. The degeneracies between the different N Rydberg series corresponding to the same principal quantum number N, are removed by the electron-electron interaction. We thus already have a rather good idea of the coarse structure of the spectrum.

In the next step, we may even speculate which parts of the $L = 0$ spectrum can be reproduced by the semiclassical quantization of collinear helium. In the collinear helium, both classical electrons move back and forth along a common axis through the nucleus, so each has zero angular momentum. We therefore expect that collinear helium describes the Rydberg series with $l = l_1 = l_2 = 0$. These series are the energetically lowest states for fixed (N, n), corresponding to the Rydberg series on the outermost left side of the spectrum in figure 35.6. We will see in the next section that this is indeed the case and that the collinear model holds down to the $N = 1$ bound state series, including even the ground state of helium! We will also find a semiclassical quantum number corresponding to the angular momentum l and show that the collinear model describes states for moderate angular momentum l as long as $l \ll N$. .

remark 35.4

35.5.2 Semiclassical spectral determinant for collinear helium

Nothing but lassitude can stop us now from calculating our first semiclassical eigenvalues. The only thing left to do is to set up the spectral determinant in terms of the periodic orbits of collinear helium and to write out the first few terms of its cycle expansion with the help of the binary symbolic dynamics. The semiclassical spectral determinant (32.12) has been written as product over all cycles of the classical systems. The energy dependence in collinear helium enters the classical dynamics only through simple scaling transformations described in sect. 7.3.1 which makes it possible to write the semiclassical spectral determinant in the form

$$\det(\hat{H}-E)_{sc} = \exp\left(-\sum_p \sum_{r=1}^{\infty} \frac{1}{r} \frac{e^{ir(sS_p - m_p\frac{\pi}{2})}}{(-\det(1-M_{p\perp}^r))^{1/2}|\det(1-M_{p\parallel}^r)|^{1/2}}\right), \quad (35.10)$$

with the energy dependence absorbed into the variable

$$s = \frac{e^2}{\hbar}\sqrt{\frac{m_e}{-E}},$$

obtained by using the scaling relation (35.2) for the action. As explained in sect. 35.3, the fact that the $[4 \times 4]$ fundamental matrix decouples into two $[2 \times 2]$ submatrices corresponding to the dynamics *in* the collinear space and *perpendicular* to it makes it possible to write the denominator in terms of a product of two determinants. Stable and unstable degrees of freedom enter the trace formula in different ways, reflected by the absence of the modulus sign and the minus sign in front of $\det(1 - M_\perp)$. The topological index m_p corresponds to the unstable dynamics in the collinear plane. Note that the factor $e^{i\pi\bar{N}(E)}$ present in (32.12) is absent in (35.10). Collinear helium is an open system, i.e., the eigenenergies are resonances corresponding to the complex zeros of the semiclassical spectral determinant and the mean energy staircase $\bar{N}(E)$ not defined. In order to obtain a spectral determinant as an infinite product of the form (32.18) we may proceed as in (17.9) by expanding the determinants in (35.10) in terms of the eigenvalues of the corresponding fundamental matrices. The matrix representing displacements perpendicular to the collinear space has eigenvalues of the form $\exp(\pm 2\pi i\sigma)$, reflecting stable linearized dynamics. σ is the full winding number along the orbit in the stable degree of freedom, multiplicative under multiple repetitions of this orbit .The eigenvalues corresponding to the unstable dynamics along the

collinear axis are paired as $\{\Lambda, 1/\Lambda\}$ with $|\Lambda| > 1$ and real. As in (17.9) and (32.18) we may thus write

$$\begin{aligned}
&\left[-\det(1-M_\perp^r)|\det(1-M_\parallel^r)|\right]^{-1/2} \quad (35.11)\\
&= \left[-(1-\Lambda^r)(1-\Lambda^{-r})|(1-e^{2\pi ir\sigma})(1-e^{-2\pi ir\sigma})\right]^{-1/2}\\
&= \sum_{k,\ell=0}^{\infty} \frac{1}{|\Lambda^r|^{1/2}\Lambda^{rk}} e^{-ir(\ell+1/2)\sigma}.
\end{aligned}$$

The $\pm$ sign corresponds to the hyperbolic/inverse hyperbolic periodic orbits with positive/negative eigenvalues Λ. Using the relation (35.12) we see that the sum over r in (35.10) is the expansion of the logarithm, so the semiclassical spectral determinant can be rewritten as a product over dynamical zeta functions, as in (17.9):

$$\det(\hat{H}-E)_{sc} = \prod_{k=0}^{\infty}\prod_{m=0}^{\infty} \zeta_{k,m}^{-1} = \prod_{k=0}^{\infty}\prod_{m=0}^{\infty}\prod_p (1-t_p^{(k,m)}), \quad (35.12)$$

where the cycle weights are given by

$$t_p^{(k,m)} = \frac{1}{|\Lambda|^{1/2}\Lambda^k} e^{i\left(sS_p - m_p\frac{\pi}{2} - 4\pi(\ell+1/2)\sigma_p\right)}, \quad (35.13)$$

and m_p is the topological index for the motion in the collinear plane which equals twice the topological length of the cycle. The two independent directions perpendicular to the collinear axis lead to a twofold degeneracy in this degree of freedom which accounts for an additional factor 2 in front of the winding number σ. The values for the actions, winding numbers and stability indices of the shortest cycles in collinear helium are listed in table 35.3.

The integer indices ℓ and k play very different roles in the semiclassical spectral determinant (35.12). A linearized approximation of the flow along a cycle corresponds to a harmonic approximation of the potential in the vicinity of the trajectory. Stable motion corresponds to a harmonic oscillator potential, unstable motion to an inverted harmonic oscillator. The index ℓ which contributes as a phase to the cycle weights in the dynamical zeta functions can therefore be interpreted as a harmonic oscillator quantum number; it corresponds to vibrational modes in the Θ coordinate and can in our simplified picture developed in sect. 35.5.1 be related to the quantum number $l = l_1 = l_2$ representing the single particle angular momenta. Every distinct ℓ value corresponds to a full spectrum which we obtain from the zeros of the semiclassical spectral determinant $1/\zeta_\ell$ keeping ℓ fixed. The harmonic oscillator approximation will eventually break down with increasing off-line excitations and thus increasing ℓ. The index k corresponds to 'excitations' along the unstable direction and can be identified with local resonances of the inverted harmonic oscillator centered on the given orbit. The cycle contributions $t_p^{(k,m)}$ decrease exponentially with increasing k. Higher k terms in an expansion of the determinant give corrections which become important only for large negative imaginary s values. As we are interested only in the leading zeros of (35.12), i.e., the zeros closest to the real energy axis, it is sufficient to take only the $k = 0$ terms into account.

Next, let us have a look at the discrete symmetries discussed in sect. 35.2. Collinear helium has a C_2 symmetry as it is invariant under reflection across the $r_1 = r_2$ line corresponding to the electron-electron exchange symmetry. As explained in sects. **??** and **??**, we may use this symmetry to factorize the semiclassical spectral determinant. The spectrum corresponding to the states symmetric or antisymmetric with respect to reflection can be obtained by writing the dynamical zeta functions in the symmetry factorized form

$$1/\zeta^{(\ell)} = \prod_a (1 - t_a)^2 \prod_{\tilde{s}} (1 - t_{\tilde{s}}^2) \,. \tag{35.14}$$

Here, the first product is taken over all asymmetric prime cycles, i.e., cycles that are not self-dual under the C_2 symmetry. Such cycles come in pairs, as two equivalent orbits are mapped into each other by the symmetry transformation. The second product runs over all self-dual cycles; these orbits cross the axis $r_1 = r_2$ twice at a right angle. The self-dual cycles close in the fundamental domain $r_1 \leq r_2$ already at half the period compared to the orbit in the full domain, and the cycle weights $t_{\tilde{s}}$ in (35.14) are the weights of fundamental domain cycles. The C_2 symmetry now leads to the factorization of (35.14) $1/\zeta = \zeta_+^{-1}\zeta_-^{-1}$, with

$$\begin{aligned} 1/\zeta_+^{(\ell)} &= \prod_a (1 - t_a) \prod_{\tilde{s}} (1 - t_{\tilde{s}}) \,, \\ 1/\zeta_-^{(\ell)} &= \prod_a (1 - t_a) \prod_{\tilde{s}} (1 + t_{\tilde{s}}) \,, \end{aligned} \tag{35.15}$$

setting $k = 0$ in what follows. The symmetric subspace resonances are given by the zeros of $1/\zeta_+^{(\ell)}$, antisymmetric resonances by the zeros of $1/\zeta_-^{(\ell)}$, with the two dynamical zeta functions defined as products over orbits in the fundamental domain. The symmetry properties of an orbit can be read off directly from its symbol sequence, as explained in sect. 35.2. An orbit with an odd number of 1's in the itinerary is self-dual under the C_2 symmetry and enters the spectral determinant in (35.15) with a negative or a positive sign, depending on the symmetry subspace under consideration.

35.5.3 Cycle expansion results

So far we have established a factorized form of the semiclassical spectral determinant and have thereby picked up two *good quantum numbers*; the

quantum number m has been identified with an excitation of the bending vibrations, the exchange symmetry quantum number ± 1 corresponds to states being symmetric or antisymmetric with respect to the electron-electron exchange. We may now start writing down the binary cycle expansion (18.7) and determine the zeros of spectral determinant. There is, however, still another problem: there is no cycle 0 in the collinear helium. The symbol sequence $\overline{0}$ corresponds to the limit of an outer electron fixed with zero kinetic energy at $r_1 = \infty$, the inner electron bouncing back and forth into the singularity at the origin. This introduces intermittency in our system, a problem discussed in chapter 22. We note that the behavior of cycles going far out in the channel r_1 or $r_2 \to \infty$ is very different from those staying in the near core region. A cycle expansion using the binary alphabet reproduces states where both electrons are localized in the near core regions: these are the lowest states in each Rydberg series. The states converging to the various ionization thresholds $E_N = -2/N^2$ correspond to eigenfunctions where the wave function of the outer electron is stretched far out into the ionization channel $r_1, r_2 \to \infty$. To include those states, we have to deal with the dynamics in the limit of large r_1, r_2. This turns out to be equivalent to switching to a symbolic dynamics with an infinite alphabet. With this observation in mind, we may write the cycle expansion (....) for a binary alphabet without the $\overline{0}$ cycle as remark 35.5

$$\begin{aligned} 1/\zeta^{\ell}(s) = \; 1 \; & - t_1^{(\ell)} - t_{01}^{(\ell)} - [t_{001}^{(\ell)} + t_{011}^{(\ell)} - t_{01}^{(\ell)} t_1^{(\ell)}] \\ & - [t_{0001}^{(\ell)} + t_{0011}^{(\ell)} - t_{001}^{(\ell)} t_1^{(\ell)} + t_{0111}^{(\ell)} - t_{011}^{(\ell)} t_1^{(\ell)}] - \ldots \end{aligned} \tag{35.16}$$

The weights $t_p^{(\ell)}$ are given in (35.12), with contributions of orbits and composite orbits of the same total symbol length collected within square brackets. The cycle expansion depends only on the classical actions, stability indices and winding numbers, given for orbits up to length 6 in table 35.3. To get reacquainted with the cycle expansion formula (35.16), consider a truncation of the series after the first term

$$1/\zeta^{(\ell)}(s) \approx 1 - t_1 \,.$$

The quantization condition $1/\zeta^{(\ell)}(s) = 0$ leads to

$$E_{m,N} = -\frac{(S_1/2\pi)^2}{[m + \frac{1}{2} + 2(N + \frac{1}{2})\sigma_1]^2}, \qquad m, N = 0, 1, 2, \ldots \,, \tag{35.17}$$

with $S_1/2\pi = 1.8290$ for the action and $\sigma_1 = 0.5393$ for the winding number, see table 35.3, the 1 cycle in the fundamental domain. This cycle can be described as the *asymmetric stretch* orbit, see figure 35.5. The additional quantum number N in (35.17) corresponds to the principal quantum number defined in sect. 35.5.1. The states described by the

N	n	$j=1$	$j=4$	$j=8$	$j=12$	$j=16$	$-E_{\rm qm}$
1	1	3.0970	2.9692	2.9001	2.9390	2.9248	2.9037
2	2	0.8044	0.7714	0.7744	0.7730	0.7727	0.7779
2	3	—	0.5698	0.5906	0.5916	0.5902	0.5899
2	4	—	—	—	0.5383	0.5429	0.5449
3	3	0.3622	0.3472	0.3543	0.3535	0.3503	0.3535
3	4	—	—	0.2812	0.2808	0.2808	0.2811
3	5	—	—	0.2550	0.2561	0.2559	0.2560
3	6	—	—	—	0.2416	0.2433	0.2438
4	4	0.2050	0.1962	0.1980	0.2004	0.2012	0.2010
4	5	—	0.1655	0.1650	0.1654	0.1657	0.1657
4	6	—	—	0.1508	0.1505	0.1507	0.1508
4	7	—	—	0.1413	0.1426	0.1426	0.1426

Table 35.2: Collinear helium, real part of the symmetric subspace resonances obtained by a cycle expansion (35.16) up to cycle length j. The exact quantum energies [35.3] are in the last column. The states are labeled by their principal quantum numbers. A dash as an entry indicates a missing zero at that level of approximation.

quantization condition (35.17) are those centered closest to the nucleus and correspond therefore to the lowest states in each Rydberg series (for a fixed m and N values), in figure 35.6. The simple formula (35.17) gives already a rather good estimate for the ground state of helium! Results obtained from (35.17) are tabulated in table 35.2, see the 3rd column under $j=1$ and the comparison with the full quantum calculations.

In order to obtain higher excited quantum states, we need to include more orbits in the cycle expansion (35.16), covering more of the phase space dynamics further away from the center. Taking longer and longer cycles into account, we indeed reveal more and more states in each N-series for fixed m. This is illustrated by the data listed in table 35.2 for symmetric states obtained from truncations of the cycle expansion of $1/\zeta_+$.

35.7
page 659

Results of the same quality are obtained for antisymmetric states by calculating the zeros of $1/\zeta_-^{(\ell)}$. Repeating the calculation with $\ell=1$ or higher in (35.15) reveals states in the Rydberg series which are to the right of the energetically lowest series in figure 35.6.

Commentary

Remark 35.1 Sources. The full 3-dimensional Hamiltonian after elimination of the center of mass coordinates, and an account of the finite nucleus mass effects is given in ref. [35.2]. The general two–body collision regularizing Kustaanheimo–Stiefel transformation [35.5], a generalization of Levi-Civita's [35.13] Pauli matrix two–body collision regularization for motion in a plane, is due to Kustaanheimo [35.12] who realized that the correct higher-dimensional generalization of the "square

root removal" trick (7.15), by introducing a vector Q with property $r=|Q|^2$, is the same as Dirac's trick of getting linear equation for spin 1/2 fermions by means of spinors. Vector spaces equipped with a product and a known satisfy $|Q\cdot Q|=|Q|^2$ define *normed algebras*. They appear in various physical applications - as quaternions, octonions, spinors. The technique was originally developed in celestial mechanics [35.6] to obtain numerically stable solutions for planetary motions. The basic idea was in place as early as 1931, when H. Hopf [35.14] used a KS transformation in order to illustrate a Hopf's invariant. The KS transformation for the collinear helium was introduced in ref. [35.2].

Remark 35.2 Complete binary symbolic dynamics. No stable periodic orbit and no exception to the binary symbolic dynamics of the collinear helium cycles have been found in numerical investigations. A proof that all cycles are unstable, that they are uniquely labeled by the binary symbolic dynamcis, and that this dynamics is complete is, however, still missing. The conjectured Markov partition of the phase space is given by the triple collision manifold, i.e., by those trajectories which start in or end at the singular point $r_1=r_2=0$. See also ref. [35.2].

Remark 35.3 Spin and particle exchange symmetry. In our presentation of collinear helium we have completely ignored all dynamical effects due to the spin of the particles involved, such as the electronic spin-orbit coupling. Electrons are fermions and that determines the symmetry properties of the quantum states. The total wave function, including the spin degrees of freedom, must be antisymmetric under the electron-electron exchange transformation. That means that a quantum state symmetric in the position variables must have an antisymmetric spin wave function, i.e., the spins are antiparallel and the total spin is zero (singletstate). Antisymmetric states have symmetric spin wave function with total spin 1 (tripletstates). The threefold degeneracy of spin 1 states is lifted by the spin-orbit coupling.

Remark 35.4 Helium quantum numbers. The classification of the helium states in terms of single electron quantum numbers, sketched in sect. 35.5.1, prevailed until the 1960's; a growing discrepancy between experimental results and theoretical predictions made it necessary to refine this picture. In particular, the different Rydberg series sharing a given N-quantum number correspond, roughly speaking, to a quantization of the inter electronic angle Θ, see figure 35.1, and can not be described in terms of single electron quantum numbers l_1, l_2. The fact that something is slightly wrong with the single electron picture laid out in sect. 35.5.1 is highlighted when considering the collinear configuration where both electrons are on the *same* side of the nucleus. As both electrons again have angular momentum equal to zero, the corresponding quantum states should also belong to single electron quantum numbers $(l_1, l_2) = (0,0)$. However, the single electron picture breaks down completely in the limit $\Theta=0$ where electron-electron interaction becomes the dominant effect. The quantum states corresponding to this classical configuration are distinctively different from those obtained from the collinear dynamics with electrons on different sides of the nucleus. The Rydberg series related to the classical $\Theta=0$ dynamics are on the outermost rigth side in each N subspectrum in figure 35.6, and contain the energetically highest states for given N, n quantum numbers, see also remark 35.5. A detailed account of the historical development as well as a modern interpretation of the spectrum can be found in ref. [35.1].

Remark 35.5 Beyond the unstable collinear helium subspace. The semiclassical quantization of the chaotic collinear helium subspace is discussed in refs. [35.7, 35.8, 35.9]. Classical and semiclassical considerations beyond what has been discussed in sect. 35.5 follow several other directions, all outside the main of this book.

A classical study of the dynamics of collinear helium where both electrons are on the same side of the nucleus reveals that this configuration is fully stable both in the collinear plane and perpendicular to it. The corresponding quantum states can be obtained with the help of an approximate EBK-quantization which reveals helium resonances with extremely long lifetimes (quasi - bound states in the continuum). These states form the energetically highest Rydberg series for a given principal quantum number N, see figure 35.6. Details can be found in refs. [35.10, 35.11].

In order to obtain the Rydberg series structure of the spectrum, i.e., the succession of states converging to various ionization thresholds, we need to take into account the dynamics of orbits which make large excursions along the r_1 or r_2 axis. In the chaotic collinear subspace these orbits are characterized by symbol sequences of form $(a0^n)$ where a stands for an arbitrary binary symbol sequence and 0^n is a succession of n 0's in a row. A summation of the form $\sum_{n=0}^{\infty} t_{a0^n}$, where t_p are the cycle weights in (35.12), and cycle expansion of indeed yield all Rydberg states up the various ionization thresholds, see ref. [35.4]. For a comprehensive overview on spectra of two-electron atoms and semiclassical treatments ref. [35.1].

Résumé

We have covered a lot of ground starting with considerations of the classical properties of a three-body Coulomb problem, and ending with the semiclassical helium spectrum. We saw that the three-body problem restricted to the dynamics on a collinear appears to be fully chaotic; this implies that traditional semiclassical methods such as *WKB*quantization will not work and that we needed the full periodic orbit theory to obtain leads to the semiclassical spectrum of helium. As a piece of unexpected luck the symbolic dynamics is simple, and the semiclassical quantization of the collinear dynamics yields an important part of the helium spectrum, including the ground state, to a reasonable accuracy. A sceptic might say: "Why bother with all the semiclassical considerations? A straightforward numerical quantum calculation achieves the same goal with better precision." While this is true, the semiclassical analysis offers new insights into the *structure* of the spectrum. We discovered that the dynamics perpendicular to the collinear plane was stable, giving rise to an additional (approximate) quantum number ℓ. We thus understood the origin of the different Rydberg series depicted in figure 35.6, a fact which is not at all obvious from a numerical solution of the quantum problem.

Having traversed the long road from the classical game of pinball all the way to a credible helium spectrum computation, we could declare victory and fold down this enterprise. Nevertheless, there is still much to think about - what about such quintessentially quantum effects as diffraction, tunnelling, ...? As we shall now see, the periodic orbit theory has still much of interest to offer.

References

[35.1] G. Tanner, J-M. Rost and K. Richter, Rev. Mod. Phys. **72**, 497 (2000).

[35.2] K. Richter, G. Tanner, and D. Wintgen, Phys. Rev. A **48**, 4182 (1993).

[35.3] Bürgers A., Wintgen D. and Rost J. M., J. Phys. B **28**, 3163 (1995).

[35.4] G. Tanner and D. Wintgen Phys. Rev. Lett. **75** 2928 (1995).

[35.5] P. Kustaanheimo and E. Stiefel, *J. Reine Angew. Math.* **218**, 204 (1965).

[35.6] E.L. Steifel and G. Scheifele, *Linear and regular celestial mechanics* (Springer, New York 1971).

[35.7] G.S. Ezra, K. Richter, G. Tanner and D. Wintgen, J. Phys. B **24**, L413 (1991).

[35.8] D. Wintgen, K. Richter and G. Tanner, CHAOS **2**, 19 (1992).

[35.9] R. Blümel and W. P. Reinhardt, *Directions in Chaos Vol 4*, eds. D. H. Feng and J.-M. Yuan (World Scientific, Hongkong), 245 (1992).

[35.10] K. Richter and D. Wintgen, J. Phys. B **24**, L565 (1991).

[35.11] D. Wintgen and K. Richter, Comments At. Mol. Phys. **29**, 261 (1994).

[35.12] P. Kustaanheimo, *Ann. Univ. Turku, Ser. AI.,* **73** (1964).

[35.13] T. Levi-Civita, *Opere mathematische* **2** (1956).

[35.14] H. Hopf, *Math. Ann.* **104** (1931).

Exercises

Exercise 35.1 **Kustaanheimo–Stiefel transformation.** *Check the Kustaanheimo–Stiefel regularization for collinear helium; derive the Hamiltonian (7.18) and the collinear helium equations of motion (7.19).*

Exercise 35.2 **Helium in the plane.** *Starting with the helium Hamiltonian in the infinite nucleus mass approximation $m_{he} = \infty$, and angular momentum $L = 0$, show that the three body problem can be written in terms of three independent coordinates only, the electron-nucleus distances r_1 and r_2 and the inter-electron angle Θ, see figure 7.1.*

Exercise 35.3 **Helium trajectories.** *Do some trial integrations of the collinear helium equations of motion (7.19). Due to the energy conservation, only three of the phase space coordinates (Q_1, Q_2, P_1, P_2) are independent. Alternatively, you can integrate in 4 dimensions and use the energy conservation as a check on the quality of your integrator.*

The dynamics can be visualized as a motion in the original configuration space (r_1, r_2), $r_i \geq 0$ quadrant, or, better still, by an appropriately chosen 2-d Poincaré section, exercise 35.4. Most trajectories will run away, do not be surprised - the classical collinear helium is unbound. Try to guess approximately the shortest cycle of figure 35.4.

Exercise 35.4 **A Poincaré section for collinear Helium.** *Construct a Poincaré section of figure 35.3b that reduces the helium flow to a map. Try to delineate regions which correspond to finite symbol sequences, i.e. initial conditions that follow the same topological itinerary in the figure 35.3a space for a finite number of bounces. Such rough partition can be used to initiate 2–dimensional Newton-Raphson method searches for helium cycles, exercise 35.5.*

Exercise 35.5 **Collinear helium cycles.** *The motion in the (r_1, r_2) plane is topologically similar to the pinball motion in a 3-disk system, except that the motion is in the Coulomb potential.*

Just as in the 3-disk system the dynamics is simplified if viewed in the fundamental domain, *in this case the region between r_1 axis and the $r_1 = r_2$ diagonal. Modify your integration routine so the trajectory bounces off the diagonal as off a mirror. Miraculously, the symbolic dynamics for the survivors again turns out to be binary, with 0 symbol signifying a bounce off the r_1 axis, and 1 symbol for a bounce off the diagonal. Just as in the 3-disk game of pinball, we thus know what cycles need to be computed for the cycle expansion (35.16).*

Guess some short cycles by requiring that topologically they correspond to sequences of bounces either returning to the same r_i axis or reflecting off the diagonal. Now either Use special symmetries of orbits such as self-retracing to find all orbits up to length 5 by a 1-dimensional Newton search.

Exercise 35.6 **Collinear helium cycle stabilities.** *Compute the eigenvalues for the cycles you found in exercise 35.5, as described in sect. 35.3. You may either integrate the reduced 2×2 matrix using equations (35.6) together with the generating function $\mathbf{l}$ given in local coordinates by (35.7) or integrate the full 4×4 Jacobian matrix, see sect. 21.1. Integration in 4 dimensions should give eigenvalues of the form $(1, 1, \Lambda_p, 1/\Lambda_p)$; The unit eigenvalues are due to the usual periodic orbit invariances; displacements along the orbit as well as perpendicular to the energy manifold are conserved; the latter one provides a check of the accuracy of your computation. Compare with table 35.3; you should get the actions and Lyapunov exponents right, but topological indices and stability angles we take on faith.*

Exercise 35.7 **Helium eigenenergies.** *Compute the lowest eigenenergies of singlet and triplet states of helium by substituting cycle data into the cycle expansion (35.16) for the symmetric and antisymmetric zeta functions (35.15). Probably the quickest way is to plot the magnitude of the zeta function as function of real energy and look for the minima. As the eigenenergies in general have a small imaginary part, a contour plot such as figure 18.1, can yield informed guesses. Better way would be to find the zeros by Newton method, sect. 18.2.3. How close are you to the cycle expansion and quantum results listed in table 35.2? You can find more quantum data in ref. [35.3].*

Chapter 36

Diffraction distraction

(N. Whelan)

Diffraction effects characteristic to scattering off wedges are incorporated into the periodic orbit theory.

36.1 Quantum eavesdropping

As noted in chapter 35, the classical mechanics of the helium atom is undefined at the instant of a triple collision. This is a common phenomenon - there is often some singularity or discontinuity in the classical mechanics of physical systems. This discontinuity can even be helpful in classifying the dynamics. The points in phase space which have a past or future at the discontinuity form manifolds which divide the phase space and provide the symbolic dynamics. The general rule is that quantum mechanics smoothes over these discontinuities in a process we interpret as diffraction. We solve the local diffraction problem quantum mechanically and then incorporate this into our global solution. By doing so, we reconfirm the central leitmotif of this treatise: think locally - act globally.

While being a well-motivated physical example, the helium atom is somewhat involved. In fact, so involved that we do not have a clue how to do it. In its place we illustrate the concept of diffractive effects with a pinball game. There are various classes of discontinuities which a billiard can have. There may be a grazing condition such that some trajectories hit a smooth surface while others are unaffected - this leads to the creeping described in chapter 33. There may be a vertex such that trajectories to one side bounce differently from those to the other side. There may be a point scatterer or a magnetic flux line such that we do not know how to continue classical mechanics through the discontinuities. In what follows, we specialize the discussion to the second example - that of vertices or wedges. To further simplify the discussion, we consider the special case of a half line which can be thought of as a wedge of angle zero.

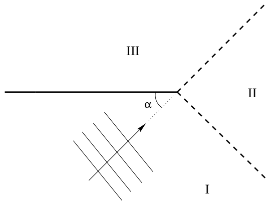

Figure 36.1: Scattering of a plane wave off a half line.

We start by solving the problem of the scattering of a plane wave off a half line (see figure 36.1). This is the local problem whose solution we will use to construct a global solution of more complicated geometries. We define the vertex to be the origin and launch a plane wave at it from an angle α. What is the total field? This is a problem solved by Sommerfeld in 1896 and our discussion closely follows his.

The total field consists of three parts - the incident field, the reflected field and the diffractive field. Ignoring the third of these for the moment, we see that the space is divided into three regions. In region I there is both an incident and a reflected wave. In region II there is only an incident field. In region III there is nothing so we call this the shadowed region. However, because of diffraction the field does enter this region. This accounts for why you can overhear a conversation if you are on the opposite side of a thick wall but with a door a few meters away. Traditionally such effects have been ignored in semiclassical calculations because they are relatively weak. However, they can be significant.

To solve this problem Sommerfeld worked by analogy with the full line case, so let us briefly consider that much simpler problem. There we know that the problem can be solved by images. An incident wave of amplitude A is of the form

$$v(r,\psi) = Ae^{-ikr\cos\psi} \tag{36.1}$$

where $\psi = \phi - \alpha$ and ϕ is the angular coordinate. The total field is then given by the method of images as

$$v_{\text{tot}} = v(r,\phi-\alpha) - v(r,\phi+\alpha), \tag{36.2}$$

where the negative sign ensures that the boundary condition of zero field on the line is satisfied.

Sommerfeld then argued that $v(r,\psi)$ can also be given a complex integral representation

$$v(r,\psi) = A\int_C d\beta f(\beta,\psi)e^{-ikr\cos\beta}. \tag{36.3}$$

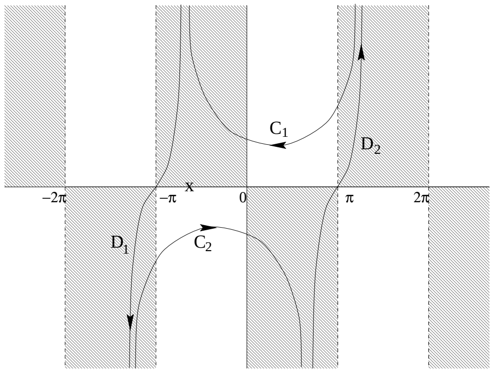

Figure 36.2: The contour in the complex β plane. The pole is at $\beta = -\psi$ (marked by $\times$ in the figure) and the integrand approaches zero in the shaded regions as the magnitude of the imaginary part of β approaches infinity.

This is certainly correct if the function $f(\beta,\psi)$ has a pole of residue $1/2\pi i$ at $\beta = -\psi$ and if the contour C encloses that pole. One choice is

$$f(\beta,\psi) = \frac{1}{2\pi}\frac{e^{i\beta}}{e^{i\beta}-e^{-i\psi}}. \tag{36.4}$$

(We choose the pole to be at $\beta = -\psi$ rather than $\beta = \psi$ for reasons discussed later.) One valid choice for the contour is shown in figure 36.2. This encloses the pole and vanishes as $|\mathrm{Im}\,\beta| \to \infty$ (as denoted by the shading). The sections D_1 and D_2 are congruent because they are displaced by 2π. However, they are traversed in an opposite sense and cancel, so our contour consists of just the sections C_1 and C_2. The motivation for expressing the solution in this complicated manner should become clear soon.

What have we done? We extended the space under consideration by a factor of two and then constructed a solution by assuming that there is also a source in the unphysical space. We superimpose the solutions from the two sources and at the end only consider the solution in the physical space to be meaningful. Furthermore, we expressed the solution as a contour integral which reflects the 2π periodicity of the problem. The half line scattering problem follows by analogy.

Whereas for the full line the field is periodic in 2π, for the half line it is periodic in 4π. This can be seen by the fact that the field can be expanded in a series of the form $\{\sin(\phi/2), \sin(\phi), \sin(3\phi/2), \cdots\}$. As above, we extend the space by thinking of it as two sheeted. The physical sheet is as shown in figure 36.1 and the unphysical sheet is congruent to it. The sheets are glued together along the half line so that a curve in the physical space which intersects the half line is continued in the unphysical space and vice-versa. The boundary conditions are that the total field is zero on both faces of the half line (which are physically distinct boundary conditions) and that as $r \to \infty$ the field is composed solely of plane waves and outgoing circular waves of the form $g(\phi)\exp(ikr)/\sqrt{kr}$. This last condition is a result of Huygens' principle.

We assume that the complete solution is also given by the method of images as

$$v_{\text{tot}} = u(r, \phi - \alpha) - u(r, \phi + \alpha). \tag{36.5}$$

where $u(r, \psi)$ is a 4π-periodic function to be determined. The second term is interpreted as an incident field from the unphysical space and the negative sign guarantees that the solution vanishes on both faces of the half line. Sommerfeld then made the ansatz that u is as given in equation (36.3) with the same contour $C_1 + C_2$ but with the 4π periodicity accounted for by replacing equation (36.4) with

$$f(\beta, \psi) = \frac{1}{4\pi}\frac{e^{i\beta/2}}{e^{i\beta/2} - e^{-i\psi/2}}. \tag{36.6}$$

(We divide by 4π rather than 2π so that the residue is properly normalized.) The integral (36.3) can be thought of as a linear superposition of an infinity of plane waves each of which satisfies the Helmholtz equation $(\nabla^2 + k^2)v = 0$, and so their combination also satisfies the Helmholtz equation. We will see that the diffracted field is an outgoing circular wave; this being a result of choosing the pole at $\beta = -\psi$ rather than $\beta = \psi$ in equation (36.4). Therefore, this ansatz is a solution of the equation and satisfies all boundary conditions and therefore constitutes a valid solution. By uniqueness this is the only solution.

In order to further understand this solution, it is useful to massage the contour. Depending on ϕ there may or may not be a pole between $\beta = -\pi$ and $\beta = \pi$. In region I, both functions $u(r, \phi \pm \alpha)$ have poles which correspond to the incident and reflected waves. In region II, only $u(r, \phi - \alpha)$ has a pole corresponding to the incident wave. In region III there are no poles because of the shadow. Once we have accounted for the geometrical waves (i.e., the poles), we extract the diffracted waves by saddle point analysis at $\beta = \pm\pi$. We do this by deforming the contours C so that they go through the saddles as shown in figure 36.2.

Contour C_1 becomes $E_2 + F$ while contour C_2 becomes $E_1 - F$ where the minus sign indicates that it is traversed in a negative sense. As a result, F has no net contribution and the contour consists of just E_1 and E_2.

As a result of these machinations, the curves E are simply the curves D of figure 36.2 but with a reversed sense. Since the integrand is no longer 2π

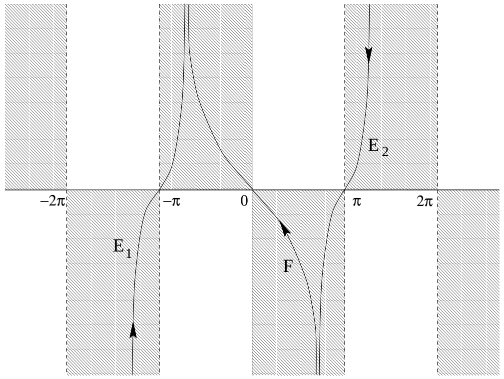

Figure 36.3: The contour used to evaluate the diffractive field after the contribution of possible poles has been explicitly evaluated. The curve F is traversed twice in opposite directions and has no net contribution.

periodic, the contributions from these curves no longer cancel. We evaluate both stationary phase integrals to obtain

$$u(r, \psi) \approx -A\frac{e^{i\pi/4}}{\sqrt{8\pi}}\sec(\psi/2)\frac{e^{ikr}}{\sqrt{kr}} \tag{36.7}$$

so that the total diffracted field is

$$v_{\text{diff}} = -A\frac{e^{i\pi/4}}{\sqrt{8\pi}}\left(\sec\left(\frac{\phi - \alpha}{2}\right) - \sec\left(\frac{\phi + \alpha}{2}\right)\right)\frac{e^{ikr}}{\sqrt{kr}}. \tag{36.8}$$

Note that this expression breaks down when $\phi \pm \alpha = \pi$. These angles correspond to the borders among the three regions of figure 36.1 and must be handled more carefully - we can not do a stationary phase integral in the vicinity of a pole. However, the integral representation (36.3) and (36.6) is uniformly valid. 36.1 page 676

We now turn to the simple task of translating this result into the language of semiclassical Green's functions. Instead of an incident plane wave, we assume a source at point x' and then compute the resulting field at the receiver position x. If x is in region I, there is both a direct term, and a reflected term, if x is in region II there is only a direct term and if x is in region III there is neither. In any event these contributions to the semiclassical Green's function are known since the free space Green's function between two points x_2 and x_1 is

$$G_{\text{f}}(x_2, x_1, k) = -\frac{i}{4}H_0^{(+)}(kd) \approx -\frac{1}{\sqrt{8\pi kd}}\exp\{i(kd + \pi/4)\}, \tag{36.9}$$

where d is the distance between the points. For a reflection, we need to multiply by -1 and the distance is the length of the path via the reflection point. Most interesting for us, there is also a diffractive contribution to the Green's function. In equation (36.8), we recognize that the coefficient A is simply the intensity at the origin if there were no scatterer. This is therefore replaced by the Green's function to go from the source to the vertex which we label x_V. Furthermore, we recognize that $\exp(ikr)/\sqrt{kr}$ is, within a proportionality constant, the semiclassical Green's function to go from the vertex to the receiver.

Collecting these facts, we say

$$G_{\text{diff}}(x, x', k) = G_{\text{f}}(x, x_V, k) d(\theta, \theta') G_{\text{f}}(x_V, x', k), \tag{36.10}$$

where, by comparison with equations (36.8) and (36.9), we have

$$d(\theta, \theta') = \sec\left(\frac{\theta - \theta'}{2}\right) - \sec\left(\frac{\theta + \theta'}{2}\right). \tag{36.11}$$

Here θ' is the angle to the source as measured from the vertex and θ is the angle to the receiver. They were denoted as α and ϕ previously. Note that there is a symmetry between the source and receiver as we expect for a time-reversal invariant process. Also the diffraction coefficient d does not depend on which face of the half line we use to measure the angles. As we will see, a very important property of G_{diff} is that it is a simple multiplicative combination of other semiclassical Green's functions.

36.2
page 676

We now recover our classical perspective by realizing that we can still think of classical trajectories. In calculating the quantum Green's function, we sum over the contributions of various paths. These include the classical trajectories which connect the points and also paths which connect the points via the vertex. These have different weights as given by equations (36.9) and (36.10) but the concept of summing over classical paths is preserved.

For completeness, we remark that there is an exact integral representation for the Green's function in the presence of a wedge of arbitrary opening angle [36.15]. It can be written as

$$G(x, x', k) = g(r, r', k, \theta' - \theta) - g(r, r', k, \theta' + \theta) \tag{36.12}$$

where (r, θ) and (r', θ') are the polar coordinates of the points x and x' as measured from the vertex and the angles are measured from either face of the wedge. The function g is given by

$$g(r, r', k, \psi) = \frac{i}{8\pi\nu} \int_{C_1 + C_2} d\beta \frac{H_0^+(k\sqrt{r^2 + r'^2 - 2rr'\cos\beta})}{1 - \exp\left(i\frac{\beta+\psi}{\nu}\right)} \tag{36.13}$$

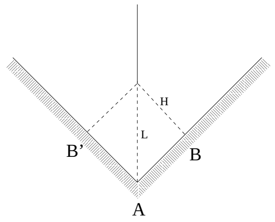

Figure 36.4: The billiard considered here. The dynamics consists of free motion followed by specular reflections off the faces. The top vertex induces diffraction while the bottom one is a right angle and induces two specular geometric reflections.

where $\nu = \gamma/\pi$ and γ is the opening angle of the wedge. (ie $\gamma = 2\pi$ in the case of the half plane). The contour $C_1 + C_2$ is the same as shown in figure 36.2.

The poles of this integral give contributions which can be identified with the geometric paths connecting x and x'. The saddle points at $\beta = \pm\pi$ give contributions which can be identified with the diffractive path connecting x and x'. The saddle point analysis allows us to identify the diffraction constant as

$$d(\theta, \theta') = -\frac{4\sin\frac{\pi}{\nu}}{\nu} \frac{\sin\frac{\theta}{\nu}\sin\frac{\theta'}{\nu}}{\left(\cos\frac{\pi}{\nu} - \cos\frac{\theta+\theta'}{\nu}\right)\left(\cos\frac{\pi}{\nu} - \cos\frac{\theta-\theta'}{\nu}\right)}, \tag{36.14}$$

which reduces to (36.11) when $\nu = 2$. Note that the diffraction coefficient vanishes identically if $\nu = 1/n$ where n is any integer. This corresponds to wedge angles of $\gamma = \pi/n$ (eg. n=1 corresponds to a full line and n=2 corresponds to a right angle). This demonstration is limited by the fact that it came from a leading order asymptotic expansion but the result is quite general. For such wedge angles, we can use the method of images (we will require $2n - 1$ images in addition to the actual source point) to obtain the Green's function and there is no diffractive contribution to any order. Classically this corresponds to the fact that for such angles, there is no discontinuity in the dynamics. Trajectories going into the vertex can be continued out of them unambiguously. This meshes with the discussion in the introduction where we argued that diffractive effects are intimately linked with classical discontinuities.

The integral representation is also useful because it allows us to consider geometries such that the angles are near the optical boundaries or the wedge angle is close to π/n. For these geometries the saddle point analysis leading to (36.14) is invalid due to the existence of a nearby pole. In that event, we require a more sophisticated asymptotic analysis of the full integral representation.

36.2 An application

Although we introduced diffraction as a correction to the purely classical effects; it is instructive to consider a system which can be quantized solely

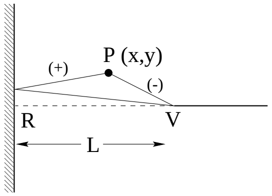

Figure 36.5: The dashed line shows a simple periodic diffractive orbit γ. Between the vertex V and a point P close to the orbit there are two geometric legs labeled $\pm$. The origin of the coordinate system is chosen to be at R.

in terms of periodic diffractive orbits. Consider the geometry shown in figure 36.4 The classical mechanics consists of free motion followed by specular reflections off faces. The upper vertex is a source of diffraction while the lower one is a right angle and induces no diffraction. This is an open system, there are no bound states - only scattering resonances. However, we can still test the effectiveness of the theory in predicting them. Formally, scattering resonances are the poles of the scattering S matrix and by an identity of Balian and Bloch are also poles of the quantum Green's function. We demonstrate this fact in chapter 33 for 2-dimensional scatterers. The poles have complex wavenumber k, as for the 3-disk problem.

Let us first consider how diffractive orbits arise in evaluating the trace of G which we call $g(k)$. Specifying the trace means that we must consider all paths which close on themselves in the configuration space while stationary phase arguments for large wavenumber k extract those which are periodic - just as for classical trajectories. In general, $g(k)$ is given by the sum over all diffractive and geometric orbits. The contribution of the simple diffractive orbit labeled γ shown in figure 36.5 to $g(k)$ is determined as follows.

We consider a point P just a little off the path and determine the semiclassical Green's function to return to P via the vertex using (36.9) and (36.10). To leading order in y the lengths of the two geometric paths connecting P and V are $d_\pm = (L \pm x) + y^2/(L \pm x)^2/2$ so that the phase factor $ik(d_+ + d_-)$ equals $2ikL + iky^2/(L^2 - x^2)$. The trace integral involves integrating over all points P and is

$$g_\gamma(k) \approx -2d_\gamma \frac{e^{i(2kL+\pi/2)}}{8\pi k} \int_0^L \frac{dx}{\sqrt{L^2-x^2}} \int_{-\infty}^{\infty} dy e^{\left(iky^2 \frac{L}{L^2-x^2}\right)} . \quad (36.15)$$

We introduced an overall negative sign to account for the reflection at the hard wall and multiplied by 2 to account for the two traversal senses, $VRPV$ and $VPRV$. In the spirit of stationary phase integrals, we have neglected the y dependence everywhere except in the exponential. The diffraction constant d_γ is the one corresponding to the diffractive periodic orbit. To evaluate the y integral, we use the identity

$$\int_{-\infty}^{\infty} d\xi e^{ia\xi^2} = e^{i\pi/4}\sqrt{\frac{\pi}{a}}, \quad (36.16)$$

and thus obtain a factor which precisely cancels the x dependence in the x

integral. This leads to the rather simple result

$$g_\gamma \approx -\frac{il_\gamma}{2k}\left\{\frac{d_\gamma}{\sqrt{8\pi k l_\gamma}}\right\} e^{i(kl_\gamma+\pi/4)} \quad (36.17)$$

where $l_\gamma = 2L$ is the length of the periodic diffractive orbit. A more sophisticated analysis of the trace integral has been done [36.6] using the integral representation (36.13). It is valid in the vicinity of an optical boundary and also for wedges with opening angles close to π/n.

Consider a periodic diffractive orbit with n_γ reflections off straight hard walls and μ_γ diffractions each with a diffraction constant $d_{\gamma,j}$. The total length of the orbit $L_\gamma = \sum l_{\gamma,j}$ is the sum of the various diffractive legs and l_γ is the length of the corresponding prime orbit. For such an orbit, (36.17) generalizes to

$$g_\gamma(k) = -\frac{il_\gamma}{2k}\left\{\prod_{j=1}^{\mu_\gamma}\frac{d_{\gamma,j}}{\sqrt{8\pi k l_{\gamma,j}}}\right\} \exp\left\{i(kL_\gamma + n_\gamma\pi - 3\mu_\gamma\pi/4)\right\}. \quad (36.18)$$

Each diffraction introduces a factor of $1/\sqrt{k}$ and multi-diffractive orbits are thereby suppressed. 36.3 page 676

If the orbit γ is prime then $L_\gamma = l_\gamma$. If γ is the r'th repeat of a prime orbit β we have $L_\gamma = rl_\beta$, $n_\gamma = rp_\beta$ and $\mu_\gamma = r\sigma_\beta$, where l_β, p_β and σ_β all refer to the prime orbit. We can then write

$$g_\gamma = g_{\beta,r} = -\frac{il_\beta}{2k} t_\beta^r \quad (36.19)$$

where

$$t_\beta = \left\{\prod_{j=1}^{\sigma_\beta}\frac{d_{\beta,j}}{\sqrt{8\pi k l_{\beta,j}}}\right\} \exp\left\{i(kl_\beta + p_\beta\pi - 3\sigma_\beta\pi/4)\right\}. \quad (36.20)$$

It then makes sense to organize the sum over diffractive orbits as a sum over the prime diffractive orbits and a sum over the repetitions

$$g_{\text{diff}}(k) = \sum_\beta \sum_{r=1}^{\infty} g_{\beta,r} = -\frac{i}{2k}\sum_\beta l_\beta \frac{t_\beta}{1-t_\beta}. \quad (36.21)$$

We cast this as a logarithmic derivative (17.7) by noting that $\frac{dt_\beta}{dk} = il_\beta t_\beta - \sigma_\beta t_\beta/2k$ and recognizing that the first term dominates in the semiclassical limit. It follows that

$$g_{\text{diff}}(k) \approx \frac{1}{2k}\frac{d}{dk}\left\{\ln \prod_\beta (1-t_\beta)\right\}. \quad (36.22)$$

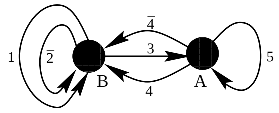

Figure 36.6: The two-node Markov graph with all the diffractive processes connecting the nodes.

In the case that there are only diffractive periodic orbits - as in the geometry of figure 36.4 - the poles of $g(k)$ are the zeros of a dynamical zeta function

$$1/\zeta(k) = \prod_{\beta}(1 - t_\beta). \tag{36.23}$$

For geometric orbits, this function would be evaluated with a cycle expansion as discussed in chapter 18. However, here we can use the multiplicative nature of the weights t_β to find a closed form representation of the function using a Markov graph, as in sect. 10.4.1. This multiplicative property of the weights follows from the fact that the diffractive Green's function (36.10) is multiplicative in segment semiclassical Green's functions, unlike the geometric case.

There is a reflection symmetry in the problem which means that all resonances can be classified as even or odd. Because of this, the dynamical zeta function factorizes as $1/\zeta = 1/\zeta_+\zeta_-$ (as explained in sects. **??** and **??**) and we determine $1/\zeta_+$ and $1/\zeta_-$ separately using the ideas of symmetry decomposition of chapter **??**.

In the Markov graph shown in figure 36.6, we enumerate all processes. We start by identifying the fundamental domain as just the right half of figure 36.4. There are two nodes which we call A and B. To get to another node from B, we can diffract (always via the vertex) in one of three directions. We can diffract back to B which we denote as process 1. We can diffract to B's image point B' and then follow this by a reflection. This process we denote as $\bar{2}$ where the bar indicates that it involves a reflection. Third, we can diffract to node A. Starting at A we can also diffract to a node in three ways. We can diffract to B which we denote as 4. We can diffract to B' followed by a reflection which we denote as $\bar{4}$. Finally, we can diffract back to A which we denote as process 5. Each of these processes has its own weight which we can determine from the earlier discussion. First though, we construct the dynamical zeta functions.

The dynamical zeta functions are determined by enumerating all closed loops which do not intersect themselves in figure 36.6. We do it first for $1/\zeta_+$ because that is simpler. In that case, the processes with bars are treated on an equal footing as the others. Appealing back to sect. **??** we find

$$\begin{aligned} 1/\zeta_+ &= 1 - t_1 - t_{\bar{2}} - t_5 - t_3t_4 - t_3t_{\bar{4}} + t_5t_1 + t_5t_{\bar{2}}\,, \\ &= 1 - (t_1 + t_{\bar{2}} + t_5) - 2t_3t_4 + t_5(t_1 + t_{\bar{2}}) \end{aligned} \tag{36.24}$$

where we have used the fact that $t_4 = t_{\bar{4}}$ by symmetry. The last term has a positive sign because it involves the product of shorter closed loops. To calculate $1/\zeta_-$, we note that the processes with bars have a relative negative sign due to the group theoretic weight. Furthermore, process 5 is a boundary orbit (see sect. **??**) and only affects the even resonances - the terms involving t_5 are absent from $1/\zeta_-$. The result is

$$\begin{aligned} 1/\zeta_- &= 1 - t_1 + t_{\bar{2}} - t_3t_4 + t_3t_{\bar{4}}\,, \\ &= 1 - (t_1 - t_{\bar{2}}). \end{aligned} \tag{36.25}$$

Note that these expressions have a finite number of terms and are not in the form of a curvature expansion, as for the 3-disk problem. 36.4 page 676

It now just remains to fix the weights. We use equation (36.20) but note that each weight involves just one diffraction constant. It is then convenient to define the quantities

$$u_A^2 = \frac{\exp\{i(2kL + 2\pi)\}}{\sqrt{16\pi kL}} \qquad u_B^2 = \frac{\exp\{i(2kH + \pi)\}}{\sqrt{16\pi kH}}. \tag{36.26}$$

The lengths L and $H = L/\sqrt{2}$ are defined in figure 36.4; we set $L = 1$ throughout. Bouncing inside the right angle at A corresponds to two specular reflections so that $p = 2$. We therefore explicitly include the factor $\exp(i2\pi)$ in (36.26) although it is trivially equal to one. Similarly, there is one specular reflection at point B giving $p = 1$ and therefore a factor of $\exp(i\pi)$. We have defined u_A and u_B because, together with some diffraction constants, they can be used to construct all of the weights. Altogether we define four diffraction coefficients: d_{AB} is the constant corresponding to diffracting from B to A and is found from (36.11) with $\theta' = 3\pi/4$ and $\theta = \pi$ and equals $2\sec(\pi/8) \approx 2.165$. With analogous notation, we have d_{AA} and $d_{BB} = d_{B'B}$ which equal 2 and $1 + \sqrt{2}$ respectively. $d_{ij} = d_{ji}$ due to the Green's function symmetry between source and receiver referred to earlier. Finally, there is the diffractive phase factor $s = \exp(-i3\pi/4)$ each time there is a diffraction. The weights are then as follows:

$$\begin{aligned} t_1 = sd_{BB}u_B^2 \quad t_{\bar{2}} &= sd_{B'B}u_B^2 \quad t_3 = t_4 = t_{\bar{4}} = sd_{AB}u_Au_B \\ t_5 &= sd_{AA}u_A^2. \end{aligned} \tag{36.27}$$

Each weight involves two u's and one d. The u's represent the contribution to the weight from the paths connecting the nodes to the vertex and the d gives the diffraction constant connecting the two paths.

The equality of d_{BB} and $d_{B'B}$ implies that $t_1 = t_{\bar{2}}$. From (36.25) this means that there are no odd resonances because 1 can never equal 0. For the even resonances equation (36.24) is an implicit equation for k which has zeros shown in figure 36.7.

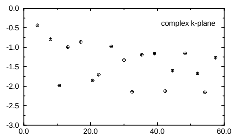

Figure 36.7: The even resonances of the wedge scatterer of figure 36.4 plotted in the complex $k-$plane, with $L = 1$. The exact resonances are represented as circles and their semiclassical approximations as crosses.

For comparison we also show the result from an exact quantum calculation. The agreement is very good right down to the ground state - as is so often the case with semiclassical calculations. In addition we can use our dynamical zeta function to find arbitrarily high resonances and the results actually improve in that limit. In the same limit, the exact numerical solution becomes more difficult to find so the dynamical zeta function approximation is particularly useful in that case.

36.5
page 676

In general a system will consist of both geometric and diffractive orbits. In that case, the full dynamical zeta function is the product of the geometric zeta function and the diffractive one. The diffractive weights are typically smaller by order $O(1/\sqrt{k})$ but for small k they can be numerically competitive so that there is a significant diffractive effect on the low-lying spectrum. It might be expected that higher in the spectrum, the effect of diffraction is weaker due to the decreasing weights. However, it should be pointed out that an analysis of the situation for creeping diffraction [36.7] concluded that the diffraction is actually *more* important higher in the spectrum due to the fact that an ever greater fraction of the orbits need to be corrected for diffractive effects. The equivalent analysis has not been done for edge diffraction but a similar conclusion can probably be expected.

To conclude this chapter, we return to the opening paragraph and discuss the possibility of doing such an analysis for helium. The important point which allowed us to successfully analyze the geometry of figure 36.4 is that when a trajectory is near the vertex, we can extract its diffraction constant without reference to the other facets of the problem. We say, therefore, that this is a "local" analysis for the purposes of which we have "turned off" the other aspects of the problem, namely sides AB and AB'. By analogy, for helium, we would look for some simpler description of the problem which applies near the three body collision. However, there is nothing to "turn off". The local problem is just as difficult as the global one since they are precisely the same problem, just related by scaling. Therefore, it is not at all clear that such an analysis is possible for helium.

Commentary

Remark 36.1 Classical discontinuities. Various classes of discontinuities for billiard and potential problems discussed in the literature:

- a grazing condition such that some trajectories hit a smooth surface while others are unaffected, refs. [36.1, 36.2, 36.3, 36.7]

- a vertex such that trajectories to one side bounce differently from those to the other side, refs. [36.2, 36.4, 36.5, 36.8, 36.9].
- a point scatterer [36.10, 36.11] or a magnetic flux line [36.12, 36.13] such that we do not know how to continue classical mechanics through the discontinuities.

Remark 36.2 Geometrical theory of diffraction. In the above discussion we borrowed heavily from the ideas of Keller who was interested in extending the geometrical ray picture of optics to cases where there is a discontinuity. He maintained that we could hang onto that ray-tracing picture by allowing rays to strike the vertex and then leave at any angle with amplitude (36.8). Both he and Sommerfeld were thinking of optics and not quantum mechanics and they did not phrase the results in terms of semiclassical Green's functions but the essential idea is the same.

Remark 36.3 Generalizations Consider the effect of replacing our half line by a wedge of angle γ_1 and the right angle by an arbitrary angle γ_2. If $\gamma_2 > \gamma_1$ and $\gamma_2 \geq \pi/2$ this is an open problem whose solution is given by equations (36.24) and (36.25) (there will then be odd resonances) but with modified weights reflecting the changed geometry [36.8]. (For $\gamma_2 < \pi/2$, more diffractive periodic orbits appear and the dynamical zeta functions are more complicated but can be calculated with the same machinery.) When $\gamma_2 = \gamma_1$, the problem in fact has bound states [36.21, 36.22]. This last case has been of interest in studying electron transport in mesoscopic devices and in microwave waveguides. However we can not use our formalism as it stands because the diffractive periodic orbits for this geometry lie right on the border between illuminated and shadowed regions so that equation (36.7) is invalid. Even the more uniform derivation of [36.6] fails for that particular geometry, the problem being that the diffractive orbit actually lives on the edge of a family of geometric orbits and this makes the analysis still more difficult.

Remark 36.4 Diffractive Green's functions. The result (36.17) is proportional to the length of the orbit times the semiclassical Green's function (36.9) to go from the vertex back to itself along the classical path. The multi-diffractive formula (36.18) is proportional to the total length of the orbit times the product of the semiclassical Green's functions to go from one vertex to the next along classical paths. This result generalizes to any system — either a pinball or a potential — which contains point singularities such that we can define a diffraction constant as above. The contribution to the trace of the semiclassical Green's function coming from a diffractive orbit which hits the singularities is proportional to the total length (or period) of the orbit times the product of semiclassical Green's functions in going from one singularity to the next. This result first appeared in reference [36.2] and a derivation can be found in reference [36.9]. A similar structure also exists for creeping [36.2].

Remark 36.5 Diffractive orbits for hydrogenic atoms. An analysis in terms of diffractive orbits has been made in a different atomic physics system, the response of hydrogenic atoms to strong magnetic fields [36.23]. In these systems, a single electron is highly excited and takes long traversals far from the nucleus. Upon returning to a hydrogen nucleus, it is re-ejected with the reversed momentum as discussed in chapter 35. However, if the atom is not hydrogen but sodium or some other atom with one valence electron, the returning electron feels the charge distribution of the core electrons and not just the charge of the nucleus. This so-called quantum defect induces scattering in addition to the classical re-ejection present in the hydrogen atom. (In this case the local analysis consists of neglecting the magnetic field when the trajectory is near the nucleus.) This is formally similar to the vertex which causes both specular reflection and diffraction. There is then additional structure in the Fourier transform of the quantum spectrum corresponding to the induced diffractive orbits, and this has been observed experimentally [36.24].

Résumé

In this chapter we have discovered new types of periodic orbits contributing to the semiclassical traces and determinants. Unlike the periodic orbits we had seen so far, these are not true classical orbits. They are generated by singularities of the scattering potential. In these singular points the classical dynamics has no unique definition, and the classical orbits hitting the singularities can be continued in many different directions. While the classical mechanics does not know which way to go, quantum mechanics solves the dilemma by allowing us to continue in all possible directions. The likelihoods of different paths are given by the quantum mechanical weights called diffraction constants. The total contribution to a trace from such orbit is given by the product of transmission amplitudes between singularities and diffraction constants of singularities. The weights of diffractive periodic orbits are at least of order $1/\sqrt{k}$ weaker than the weights associated with classically realizable orbits, and their contribution at large energies is therefore negligible. Nevertheless, they can strongly influence the low lying resonances or energy levels. In some systems, such as the N disk scattering the diffraction effects do not only perturb semiclassical resonances, but can also create new low energy resonances. Therefore it is always important to include the contributions of diffractive periodic orbits when semiclassical methods are applied at low energies.

References

[36.1] A. Wirzba, CHAOS **2**, 77 (1992);

[36.2] G. Vattay, A. Wirzba and P. E. Rosenqvist, Phys. Rev. Lett. **73**, 2304 (1994); G. Vattay, A. Wirzba and P. E. Rosenqvist in *Proceedings of the International Conference on Dynamical Systems and Chaos: vol. 2*, edited by Y.Aizawa, S.Saito and K.Shiraiwa (World Scientific, Singapore, 1994).

[36.3] H. Primack, H. Schanz, U. Smilansky and I. Ussishkin, Phys. Rev. Lett. **76**, 1615 (1996).

[36.4] N. D. Whelan, Phys. Rev. E **51**, 3778 (1995).

[36.5] N. Pavloff and C. Schmit, Phys. Rev. Lett. **75**, 61 (1995).

[36.6] M. Sieber, N. Pavloff, C. Schmit, Phys. Rev. E **55**, 2279 (1997).

[36.7] H. Primack et. al., J. Phys. A **30**, 6693 (1997).

[36.8] N. D. Whelan, Phys. Rev. Lett. **76**, 2605 (1996).

[36.9] H. Bruus and N. D. Whelan, Nonlinearity, **9**, 1 (1996).

[36.10] P. Seba, Phys. Rev. Lett. **64**, 1855 (1990).

[36.11] P. E. Rosenqvist, N. D. Whelan and A. Wirzba, J. Phys. A **29**, 5441 (1996).

[36.12] M. Brack et. al., Chaos **5**, 317 (1995).

[36.13] S. M. Reimann et. al., Phys. Rev. A **53**, 39 (1996).

[36.14] A. Sommerfeld, Mathem. Ann. **47**, 317 (1896); *Optics* (Academic Press, New York 1954).

[36.15] H. S. Carslaw, Proc. London Math. Soc. (Ser. 1) **30**, 121 (1989); H. S. Carslaw, Proc. London Math. Soc. (Ser. 2) **18**, 291 (1920).

[36.16] J. B. Keller, J. Appl. Phys. **28**, 426 (1957).

[36.17] A. Voros, J. Phys. A **21**. 685 (1988).

[36.18] see for example, D. Ruelle, *Statistical Mechanics, Thermodynamic Formalism* (Addison-Wesley, Reading MA, 1978).

[36.19] see for example, P. Grassberger, Z. Naturforsch. **43a**, 671 (1988).

[36.20] P. Cvitanović and B. Eckhardt, Nonlinearity **6**, 277 (1993).

[36.21] P. Exner, P. Seba and P. Stovicek, Czech J. Phys **B39**, 1181 (1989).

[36.22] Hua Wu and D. W. L. Sprung, J. Appl. Phys. **72**, 151 (1992).

[36.23] P. A. Dando, T. S. Monteiro, D. Delande and K. T. Taylor, Phys. Rev. Lett. **74**, 1099 (1995). P. A. Dando, T. S. Monteiro and S. M. Owen, preprint (1997).

[36.24] D. Delande et. al., J. Phys. B **27**, 2771 (1994); G. Raithel et. al., J. Phys. B **27**, 2849 (1994); M. Courtney et. al., Phys. Rev. Lett., **73**, 1340 (1994).

Exercises

(N. Whelan)

Exercise 36.1 Stationary phase integral. *Evaluate the two stationary phase integrals corresponding to contours E_1 and E_2 of figure 36.3 and thereby verify (36.7).*

Exercise 36.2 Scattering from a small disk *Imagine that instead of a wedge, we have a disk whose radius a is much smaller than the typical wavelengths we are considering. In that limit, solve the quantum scattering problem - find the scattered wave which result from an incident plane wave. You can do this by the method of partial waves - the analogous three dimensional problem is discussed in most quantum textbooks. You should find that only the $m = 0$ partial wave contributes for small a. Following the discussion above, show that the diffraction constant is*

$$d = \frac{2\pi}{\log\left(\frac{2}{ka}\right) - \gamma_e + i\frac{\pi}{2}} \tag{36.28}$$

where $\gamma_e = 0.577\cdots$ is Euler's constant. Note that in this limit d depends weakly on k but not on the scattering angle.

Exercise 36.3 Several diffractive legs. *Derive equation (36.18). The calculation involves considering slight variations of the diffractive orbit as in the simple case discussed above. Here it is more complicated because there are more diffractive arcs - however you should convince yourself that a slight variation of the diffractive orbit only affects one leg at a time.*

Exercise 36.4 Unsymmetrized dynamical zeta function. *Assume you know nothing about symmetry decomposition. Construct the three node Markov diagram for figure 36.1 by considering A, B and B' to be physically distinct. Write down the corresponding dynamical zeta function and check explicitly that for $B = B'$ it factorizes into the product of the the even and odd dynamical zeta functions. Why is there no term $t_{\bar{2}}$ in the full dynamical zeta function?*

Exercise 36.5 Three point scatterers. *Consider the limiting case of the three disk game of pinball of figure 1.3 where the disks are very much smaller than their spacing R. Use the results of exercise 36.2 to construct the desymmetrized dynamical zeta functions, as in sect. ??. You should find $1/\zeta_{A_1} = 1 - 2t$ where $t = de^{i(kR-3\pi/4)}/\sqrt{8\pi kR}$. Compare this formula with that from chapter 10. By assuming that the real part of k is much greater than the imaginary part show that the positions of the resonances are $k_nR = \alpha_n - i\beta_n$ where $\alpha_n = 2\pi n + 3\pi/4$, $\beta_n = \log\left(\sqrt{2\pi\alpha_n}/d\right)$ and n is a non-negative integer. (See also reference [36.11].)*

Epilogue

> Nowadays, whatever the truth of the matter may be (and we will probably never know), the simplest solution is no longer emotionally satisfying. Everything we know about the world militates against it. The concepts of indeterminacy and chaos have filtered down to us from the higher sciences to confirm our nagging suspicions.
>
> —L. Sante, "Review of 'American Tabloid' by James Ellroy", *New York Review of Books* (May 11, 1995)

A motion on a strange attractor can be approximated by shadowing long orbits by sequences of nearby shorter periodic orbits. This notion has here been made precise by approximating orbits by prime cycles, and evaluating associated curvatures. A curvature measures the deviation of a long cycle from its approximation by shorter cycles; the smoothness of the dynamical system implies exponential fall-off for (almost) all curvatures. We propose that the theoretical and experimental non–wandering sets be expressed in terms of the symbol sequences of short cycles (a topological characterization of the spatial layout of the non–wandering set) and their eigenvalues (metric structure)

Cycles as the skeleton of chaos

We wind down this all-too-long treatise by asking: why cycle?

We tend to think of a dynamical system as a smooth system whose evolution can be followed by integrating a set of differential equations. Traditionally one used integrable motions as zeroth-order approximations to physical systems, and accounted for weak nonlinearities perturbatively. However, when the evolution is actually followed through to asymptotic times, one discovers that the strongly nonlinear systems show an amazingly rich structure which is not at all apparent in their formulation in terms of differential equations. In particular, the periodic orbits are important because they form the *skeleton* onto which all trajectories trapped for long times cling. This was already appreciated century ago by H. Poincaré, who, describing in *Les méthodes nouvelles de la méchanique céleste* his discovery of homoclinic tangles, mused that "the complexity of this figure will be striking, and I shall not even try to draw it". Today such drawings are cheap and plentiful; but Poincaré went a step further and, noting that hidden in this apparent chaos is a rigid skeleton, a tree of *cycles* (periodic orbits) of increasing lengths and self-similar structure, suggested that the cycles should be the key to chaotic dynamics.

The zeroth-order approximations to harshly chaotic dynamics are very different from those for the nearly integrable systems: a good starting approximation here is the stretching and kneading of a baker's map, rather than the winding of a harmonic oscillator.

For low dimensional deterministic dynamical systems description in terms of cycles has many virtues:

1. cycle symbol sequences are *topological* invariants: they give the spatial layout of a non–wandering set
2. cycle eigenvalues are *metric* invariants: they give the scale of each piece of a non–wandering set
3. cycles are *dense* on the asymptotic non–wandering set
4. cycles are ordered *hierarchically*: short cycles give good approximations to a non–wandering set, longer cycles only refinements. Errors due to neglecting long cycles can be bounded, and typically fall off exponentially or super-exponentially with the cutoff cycle length
5. cycles are *structurally robust*: for smooth flows eigenvalues of short cycles vary slowly with smooth parameter changes
6. asymptotic averages (such as correlations, escape rates, quantum mechanical eigenstates and other "thermodynamic" averages) can be efficiently computed from short cycles by means of *cycle expansions*

Points 1, 2: That the cycle topology and eigenvalues are invariant properties of dynamical systems follows from elementary considerations. If the same dynamics is given by a map f in one set of coordinates, and a map g in the next, then f and g (or any other good representation) are related by a reparametrization and a coordinate transformation $f = h^{-1} \circ g \circ h$. As both f and g are arbitrary representations of the dynamical system, the explicit form of the conjugacy h is of no interest, only the properties invariant under any transformation h are of general import. The most obvious invariant properties are topological; a fixed point must be a fixed point in any representation, a trajectory which exactly returns to the initial point (a cycle) must do so in any representation. Furthermore, a good representation should not mutilate the data; h must be a smooth transformation which maps nearby cycle points of f into nearby cycle points of g. This smoothness guarantees that the cycles are not only topological invariants, but that their linearized neighborhoods are also

metrically invariant. In particular, the cycle eigenvalues (eigenvalues of the fundamental matrixs $df^n(x)/dx$ of periodic orbits $f^n(x) = x$) are invariant.

Point 5: An important virtue of cycles is their *structural robustness*. Many quantities customarily associated with dynamical systems depend on the notion of "structural stability", i.e., robustness of non–wandering set to small parameter variations.

Still, the sufficiently short unstable cycles are structurally robust in the sense that they are only slightly distorted by such parameter changes, and averages computed using them as a skeleton are insensitive to small deformations of the non–wandering set. In contrast, lack of structural stability wreaks havoc with long time averages such as Lyapunov exponents, for which there is no guarantee that they converge to the correct asymptotic value in any finite time numerical computation.

The main recent theoretical advance is **point 4:** we now know how to control the errors due to neglecting longer cycles. As we seen above, even though the number of invariants is infinite (unlike, for example, the number of Casimir invariants for a compact Lie group) the dynamics can be well approximated to any finite accuracy by a small finite set of invariants. The origin of this convergence is geometrical, as we shall see in appendix I.1.2, and for smooth flows the convergence of cycle expansions can even be super-exponential.

The cycle expansions such as (18.7) outperform the pedestrian methods such as extrapolations from the finite cover sums (19.2) for a number of reasons. The cycle expansion is a better averaging procedure than the naive box counting algorithms because the strange attractor is here pieced together in a topologically invariant way from neighborhoods ("space average") rather than explored by a long ergodic trajectory ("time average"). The cycle expansion is co-ordinate and reparametrization invariant - a finite nth level sum (19.2) is not. Cycles are of finite period but infinite duration, so the cycle eigenvalues are already evaluated in the $n \to \infty$ limit, but for the sum (19.2) the limit has to be estimated by numerical extrapolations. And, crucially, the higher terms in the cycle expansion (18.7) are deviations of longer prime cycles from their approximations by shorter cycles. Such combinations vanish exactly in piecewise linear approximations and fall off exponentially for smooth dynamical flows.

In the above we have reviewed the general properties of the cycle expansions; those have been applied to a series of examples of low-dimensional chaos: 1-d strange attractors, the period-doubling repeller, the Hénon-type maps and the mode locking intervals for circle maps. The cycle expansions have also been applied to the irrational windings set of critical circle maps, to the Hamiltonian period-doubling repeller, to a Hamiltonian three-disk game of pinball, to the three-disk quantum scattering resonances and to the extraction of correlation exponents, Feasibility of analysis of experimental non–wandering set in terms of cycles is discussed in ref. [18.1].

Homework assignment

> "Lo! thy dread empire Chaos is restor'd, Light dies before thy uncreating word; Thy hand, great Anarch, lets the curtain fall, And universal darkness buries all."
>
> —Alexander Pope, *The Dunciad*

We conclude cautiously with a homework assignment posed May 22, 1990 (the original due date was May 22, 2000, but alas...):

1. **Topology** Develop optimal sequences ("continued fraction approximants") of finite subshift approximations to generic dynamical systems. Apply to (a) the Hénon map, (b) the Lorenz flow and (c) the Hamiltonian standard map.

2. **Non-hyperbolicity** Incorporate power–law (marginal stability orbits,"intermittency" corrections into cycle expansions. Apply to long-time tails in the Hamiltonian diffusion problem.

3. **Phenomenology** Carry through a convincing analysis of a genuine experimentally extracted data set in terms of periodic orbits.

4. **Invariants** Prove that the scaling functions, or the cycles, or the spectrum of a transfer operator are the maximal set of invariants of an (physically interesting) dynamically generated non–wandering set.

5. **Field theory** Develop a periodic orbit theory of systems with many unstable degrees of freedom. Apply to (a) coupled lattices, (b) cellular automata, (c) neural networks.

6. **Tunneling** Add complex time orbits to quantum mechanical cycle expansions (WKB theory for chaotic systems).

7. **Unitarity** Evaluate corrections to the Gutzwiller semiclassical periodic orbit sums. (a) Show that the zeros (energy eigenvalues) of the appropriate Selberg products are real. (b) Find physically realistic systems for which the "semiclassical" periodic orbit expansions yield the exact quantization.

8. **Atomic spectra** Compute the helium spectrum from periodic orbit expansions (already accomplished by Wintgen and Tanner!).

9. **Symmetries** Include fermions, gauge fields into the periodic orbit theory.

10. **Quantum field theory** Develop quantum theory of systems with infinitely many classically unstable degrees of freedom. Apply to (a) quark confinement (b) early universe (c) the brain.

Conclusion

> Good-bye. I am leaving because I am bored.
>
> —George Saunders' dying words

> Nadie puede escribir un libro. Para Que un libro sea verdaderamente, Se requieren la aurora y el poniente Siglos, armas y el mar que une y separa.
>
> —Jorge Luis Borges El Hacedor, *Ariosto y los arabes*

The buttler did it.

Index